MICROCOPY RESOLUTION TEST CHART
NATIONAL BUREAU OF STANDARDS-1963-A

ACCELERATOR DEVELOPMENT IN SUPPORT
OF THE NRL BEAM DYNAMIC PROGRAM

FINAL REPORT

PSI-FR-21-129

JULY 1984

BY

P.D.'A. CHAMPNEY, R.G. ALTES, S.D. PUTNAM, I.D. SMITH
P.W. SPENCE, W.N. WESELOH, C.B. EICHENBERGER, K.E. NIELSEN

DTIC
ELECTE
SEP 2 6 1984

A

PREPARED BY

ψpsi **PULSE SCIENCES INC.**

14796 Wicks Blvd. • San Leandro, CA 94577
Tel: (415) 895-2984

84 08 17 088

REPORT DOCUMENTATION PAGE

READ INSTRUCTIONS
BEFORE COMPLETING FORM

1. REPORT NUMBER	2. GOVT ACCESSION NO.	3. RECIPIENT'S CATALOG NUMBER
	AD-A145976	

4. TITLE (and Subtitle)	5. TYPE OF REPORT & PERIOD COVERED
Accelerator Development in Support of the NRL Beam Dynamics Program	Final Report 23 March 1981 to 29 Feb. 1984
	6. PERFORMING ORG. REPORT NUMBER PSI-FR-21-129

7. AUTHOR(s)	8. CONTRACT OR GRANT NUMBER(s)
P. Champney, R. Altes, S. Putnam, I. Smith, P. Spence, W. Weseloh, C. Eichenberger, K. Nielsen	N00014-81-C-2191

9. PERFORMING ORGANIZATION NAME AND ADDRESS	10. PROGRAM ELEMENT, PROJECT, TASK AREA & WORK UNIT NUMBERS
Pulse Sciences, Inc. 14796 Wicks Blvd. San Leandro, Ca. 94577	P.R. 47-2311-81

11. CONTROLLING OFFICE NAME AND ADDRESS	12. REPORT DATE
Contracting Officer Naval Research Laboratory Washington, D.C. 20375	July 1984
	13. NUMBER OF PAGES 191

14. MONITORING AGENCY NAME & ADDRESS(If different from Controlling Office)	15. SECURITY CLASS (of this report)
	Unclassified
	15a. DECLASSIFICATION/DOWNGRADING SCHEDULE

16. DISTRIBUTION STATEMENT (of this Report)

This document has been approved for public release and sale; its distribution is unlimited.

17. DISTRIBUTION STATEMENT (of the abstract entered in Block 20, if different from Report)

18. SUPPLEMENTARY NOTES

19. KEY WORDS (Continue on reverse side if necessary and identify by block number)

Modified betatron accelerator
Linear induction accelerator
Accelerating gaps
Beam injector

20. ABSTRACT (Continue on reverse side if necessary and identify by block number)

Electrical and mechanical designs, design packages, and supporting analyses are given and described in detail for: (1) new insulators and accelerating gaps for the NBS linear induction accelerator (LIA) to withstand voltages $\geq$ 250 KV; (2) nine new LIA module and power supplies with specifications of (a) 500 KV, 0.5 μsec, (b) 1 MV, 0.5 μsec, and (c) 500 KV, 2 μsec; (3) power supplies for the toroidal, vertical, capture, and image compensation field coils, for the modified betatron accelerator (MBA) at the conceptual design

DD $_{1\ JAN\ 73}^{FORM}$ 1473   EDITION OF 1 NOV 68 IS OBSOLETE

20. cont.

level; (4) the preliminary design package for the power supply of the toroidal field coil; and (5) the power transport system from the external electron beam accelerator to the internal betatron diode. Also included are mechanical design recommendations for the MBA structural frame including the coil and vacuum chamber mountings, and discussion of material issues for the vacuum vessel and coil bus connections.

FOREWARD

Accelerator development support was provided by Pulse Sciences Inc. (PSI) to the Naval Research Laboratory (NRL) during the period March 1981 through February 1984. The work involved supporting the NRL Free Electron Laser and Modified Betatron Development programs. PSI would like to thank Dr. Chris Kapetanakos of NRL and his staff; Dr. Chuck Roberson (now with the Office of Naval Research), Dr. Jeff Golden, Dr. John Pasour, and Mr. Ken McDonald for the help received in executing this program. PSI would also like to acknowledge assistance from Dr. Donald Kerst, Dr. Andy Faltens (Lawrence Berkeley Laboratory), and Mr. David Cummings (Lawrence Livermore National Laboratory) who acted as consultants to PSI at various times throughout the contract.

i

TABLE OF CONTENTS

TABLE OF CONTENTS (Continued)

LIST OF FIGURES

LIST OF FIGURES (Continued)

LIST OF FIGURES (Continued)

INTRODUCTION

This report covers work performed by Pulse Sciences Inc. (PSI) for the
Naval Research Laboratory (NRL) under contract N00014-81-C-2191 during the
period March 1981 through February 1984. PSI has provided mechanical and
electrical design support to the Free Electron Laser (FEL) program and to the
Modified Betatron Accelerator (MBA) program.

In the area of FEL support PSI has redesigned the NBS linear induction
accelerator (LIA) accelerating gaps to accommodate higher voltages (>250 kV
per gap) and designed a new 500 kV, 0.5 μs LIA to operate in conjunction with
an upgraded version of the present injector/LIA. PSI has also examined the
impact on the new LIA design to obtain a 0.25 μs to 0.5 μs 1 MV accelerating
voltage, or extend the 500 kV accelerating voltage to 2 μs duration. A novel
alternative to the present injector and dual accelerator approach has been
identified by PSI, consisting of a compact 2 MeV, 3.6 kA electron beam
accelerator with continously adjustable pulse width up to 2 μs.

The work related to FEL support is contained in Section 2 of this report.
Appendices 2A through 2R pertain to Section 2.

In the area of MBA support PSI determined an optimum structural frame
including coil and vacuum chamber mountings to withstand the electromagnetic
and atmospheric forces. The scheme recommended by PSI is now in fabrication.
PSI also assisted in mechanical design and materials issues related to the
vacuum vessel and coil bus connections.

1

Following design studies by PSI covering a range of Betatron field coil requirements, PSI provided NRL with conceptual design packages for the power supplies to drive the vertical (VF) and toroidal (TF) magnetic field coils, and the capture (CF) and image compensation (ICF) magnetic field coils. The design of the TF power supply has been taken through preliminary design by PSI.

PSI has assisted NRL in designs of power systems that transport the electron beam from the 3 MeV injector accelerator to the cathode of ⸗ injector that is located inside the MBA. PSI has also generated a ʌceptual design of a 5 MeV injector accelerator capable of providing a bursι ⸗ four pulses in about 1 second.

The work related to the MBA support is presented in Section 3 of this report. Appendices 3A through 3M apply to Section 3.

SECTION 2
PRELIMINARY DESIGN OF THE ACCELERATING MODULE
AND POWER SUPPLY FOR THE UPGRADED INDUCTION LINAC

2.1 Introduction

This section initially describes work performed by PSI to provide
electrical and mechanical designs for new insulators and accelerator gaps for
the existing NBS/LIA induction modules, with the objective of achieving
accelerating voltages of approximately 250 kV/module.

The preliminary design of a new induction module and associated power
supplies is presented, compatible with integration with a 5 MV racetrack
accelerator and the existing NBS/LIA. PSI was asked to develop a design
including a) use of the technology of the NBS Induction Linac, incorporating
experience gained and, if possible, actual components; b) flexibility to
reduce the pulse duration to approximately 0.5 μsec, while increasing the
accelerating voltage to about 500 kV consistent with using the full VT
(Voltage x Time) product of two existing module cores.

The section continues with a description of core fabrication and cost issues, and summarizes experiments which were performed to evaluate the various options.

Section 2 concludes with a discussion of the implications of core options and module specification changes to the final module design. Also addressed in this conclusion is the option of a single module potentially capable of fulfilling the combined role of the existing injector, the existing NBS/LIA, and the new module.

2.2 Induction Linac Accelerating Gaps

2.2.1 General

Included in this section are descriptions of the electrical and mechanical aspects of the accelerating gap design. The description is presented chronologically and includes critical design criteria, design issues and documentation assembled during the project.

Pertinent documents generated by PSI during the work are included as Appendices. These documents include mechanical design packages sent to NRL for conceptual, preliminary, and final design reviews (Appendices 2A, 2B, 2E, and 2J). Also included are summaries for ceramic materials and vendor search (Appendix 2D), accelerating gap manufacturing cost (Appendix 2A), and documentation for several design revisions (Appendices 2H and 2I), which occurred prior to the final design transmittal (Appendix 2J).

The following sections are detailed discussions of the electrical and mechanical design of the accelerating gaps.

2.2.2 Accelerator Gap Electrical Design

A schematic of the 3-stage linear induction accelerator is shown in Figure 2.2.1. The injector provides a 0.8 MeV, 1 kA, 2 μsec electron beam. Two additional stages of acceleration are provided by a positive 2 μsec output modulator driving an acclerating gap via a four core set, followed by a second negative 2 μsec output modulator driving an identical inverted accelerating gap via a five core set.

Without the electron beam present electrical breakdown occurs in the four core and five core accelerating gaps at approximately 155 kV and 175 kV, respectively. With the electron beam present breakdown is observed to take place at about 130 kV and 150 kV in the four core and five core accelerating gaps, respectively.

The objective of this task was to redesign the induction linac accelerating gaps to withstand the higher voltages of the upgraded linear induction accelerators. The individual accelerating gap voltage was anticipated to be in the range 250 to 500 kV, but with a reduced pulse duration of about 250 to 500 μsec. In addition, the new design was to include current and voltage monitors.

Figure 2.2.2 shows a half section drawing of the accelerating gap. The drawing shows the accelerating gap region, the cylindrical ceramic insulators,

5
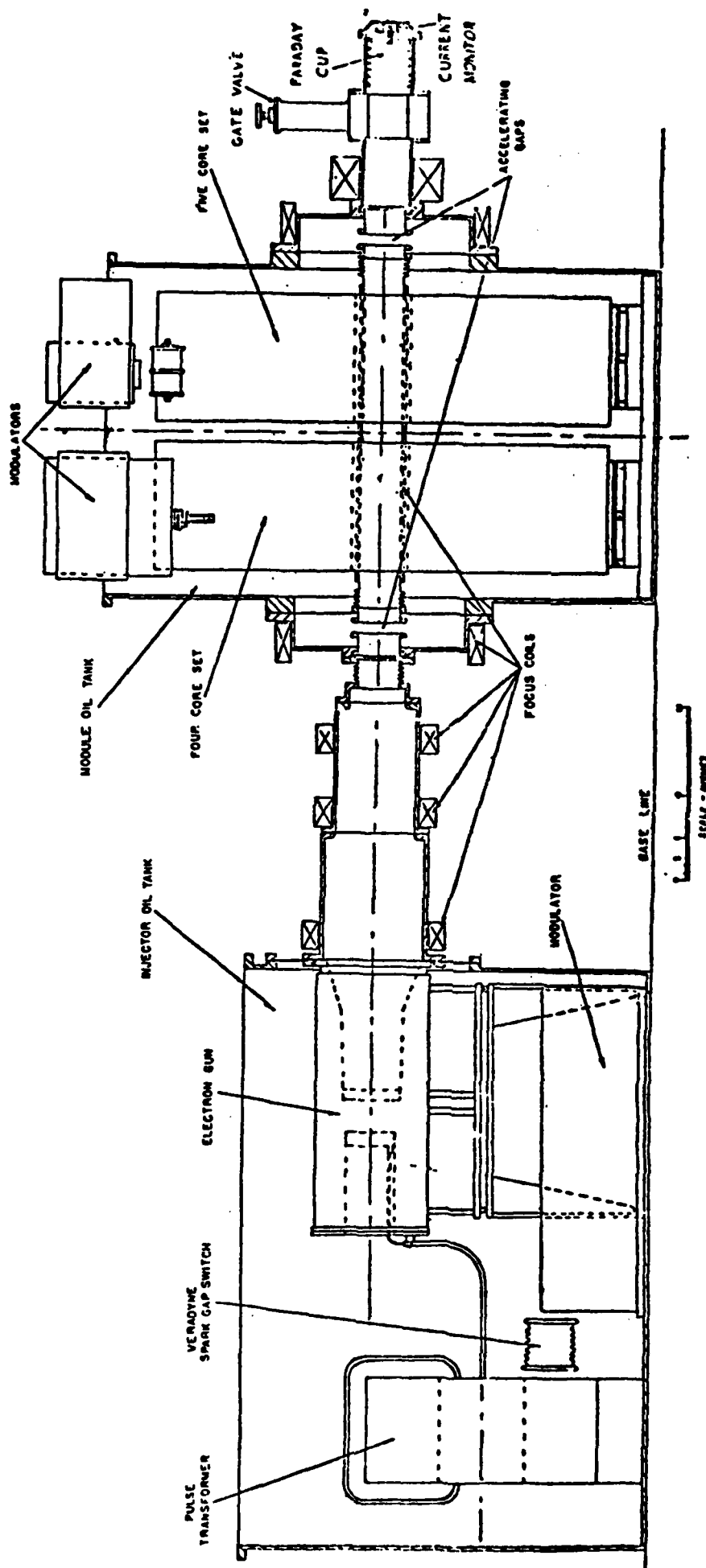
Figure 2.2.1 Schematic of 3-stage accelerator

XXX Shows areas of most involvement in arcing along curvature of 4-core electrodes.

••• Shows areas of 5-core gap breakdown.
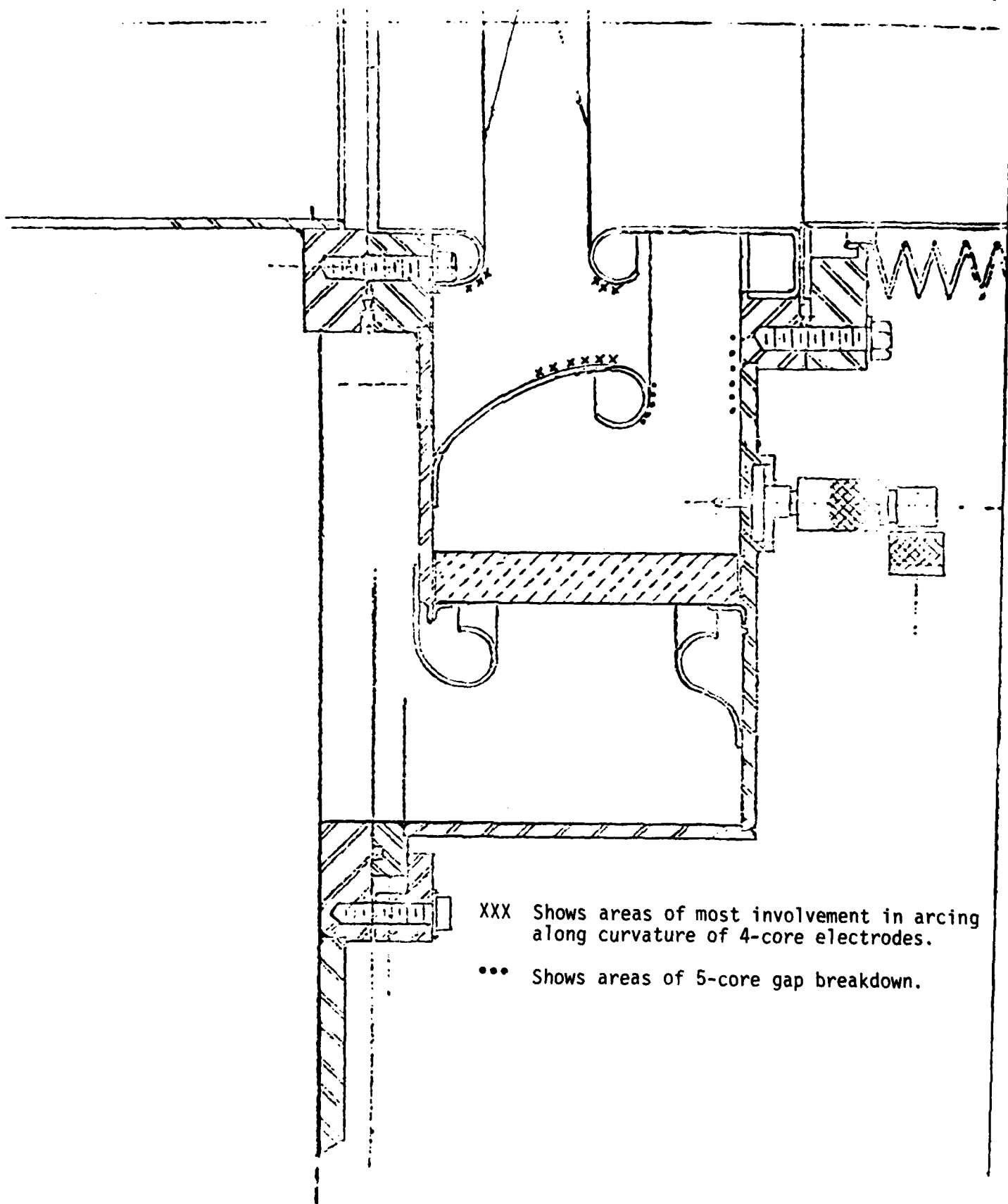
Figure 2.2.2 Half-section of gap electrodes

and the field shaping electrodes in the vacuum and insulating oil. Also indicated on the drawing are the areas involving arcing for both accelerating gap configurations.

Figures 2.2.3 and 2.2.4 show equipotential plots of the accelerating gap with and without the field shaping electrode in the vacuum. Apart from the high electric fields on the surfaces of the negatively charged electrodes in the vacuum, of particular concern is the magnitude of the electric field across the ceramic insulator/vacuum interface and the angle of that field with respect to the interface. In the accelerating gap case where the vacuum field shaping electrode is negative, the interface electric field actually directs electrons into the ceramic at a shallow angle. This sets up the worst possible conditions: accelerating free electrons before driving them into the ceramic to produce secondaries and a resultant electron avalanche. Removing the negatively charged vacuum field shaping electrode improves somewhat the electric field angles, and reduces the magnitude of the electric field; however, the geometry remains far from optimum.

The equipotential plot in Figure 2.2.5 shows a redesigned ceramic insulator and vacuum electrode structure. For a positive voltage applied to the vacuum field shaping electrode it can be seen that the electric field directs electrons away from the insulator surface at angles mostly in the optimum 50 to 60 degree range.

The ceramic/vacuum interface electric field parallel to the surface varies from a low of 13 kV/cm at the positive triple point to a high of 25 kV/cm at the negative triple point for an applied voltage of 250 kV. Peak

8
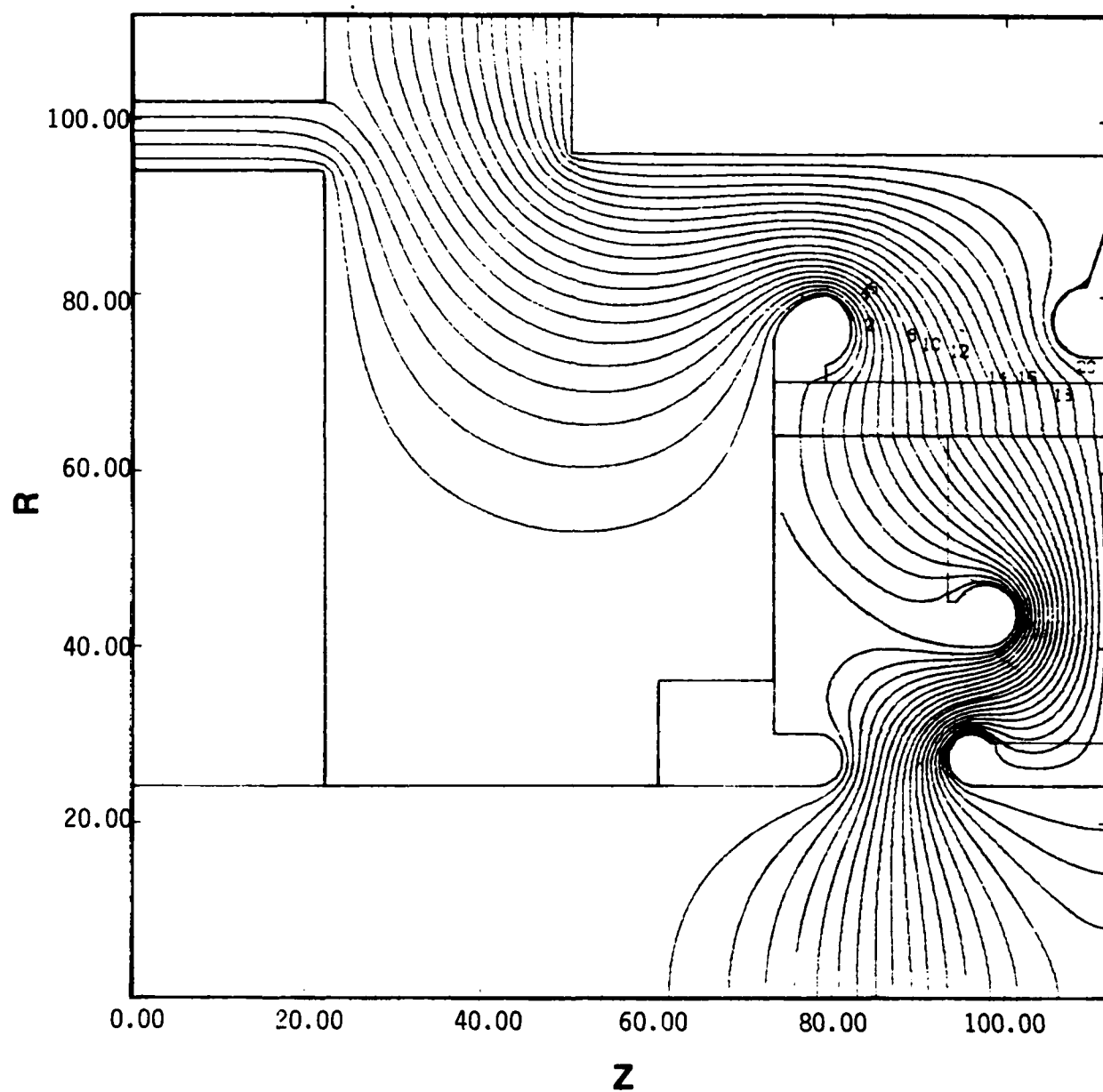
Figure 2.2.3   Original accelerating gap with vacuum field shaping electrode
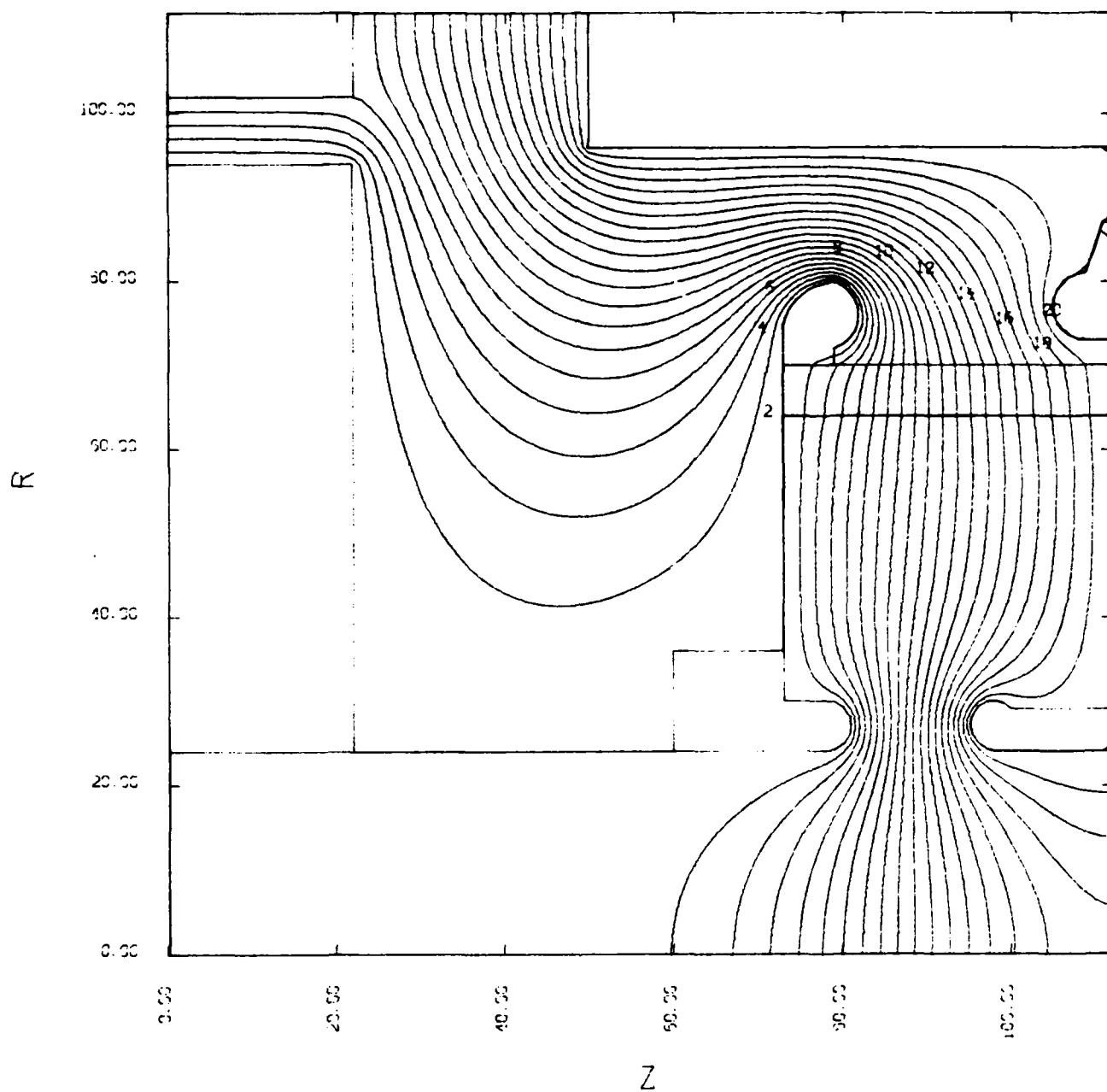
Figure 2.2.4   Original accelerating gap without vacuum field shaping electrode

10
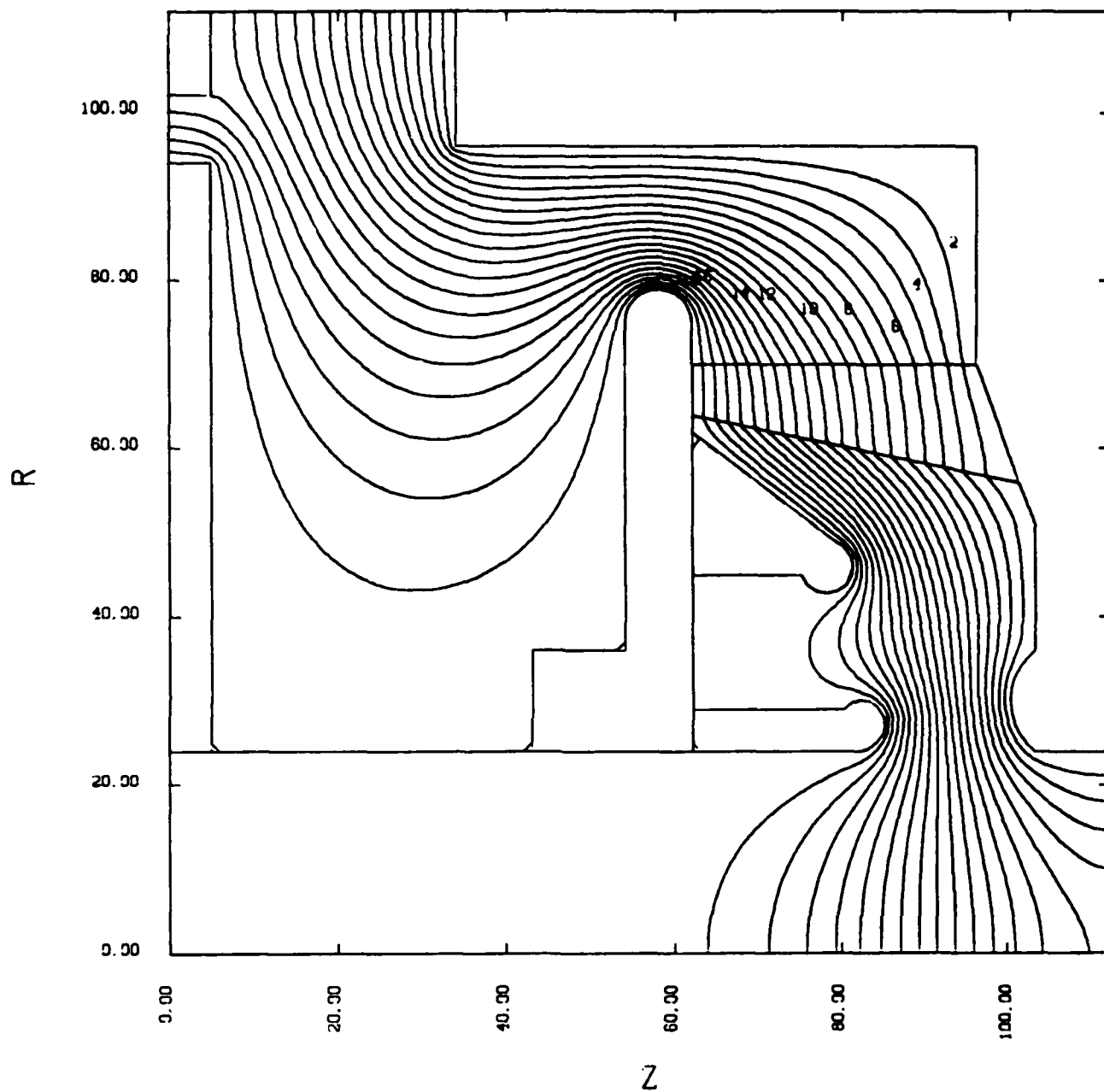
Figure 2.2.5   Redesigned accelerating gap –
positive applied voltage

11

electric fields on the electrode surfaces in the vacuum are 58 kV/cm, 79 kV/cm and 77 kV/cm for the negative and positive accelerating gap electrodes and field shaping electrode respectively for an applied voltage of 250 kV. The peak sideways electric field in the insulating oil on the positive electrode is 93 kV/cm.

The following oil breakdown and vacuum interface flashover formulations are used in analyzing the electrical capabilities of the design.

OIL:

$$F \times t_{eff}^{0.33} \times A^{0.073} = 0.48$$

Where F is the electric field in kV/cm, t_{eff} is the effective time that the voltage exceeds 63% of the peak voltage, and A is the electrode area in cm^2, stressed at more than 0.9 F.

The electric fields in the oil around the accelerator gap region are substantially below breakdown for voltages and times of the order of 250 kV, and 500 ns.

VACUUM:

$$F \times t_{eff}^{0.31} \times A^{0.18} = K$$

Where F is the electric field across the insulator in kV/cm, t is the effective time in sec that the voltage exceeds 63% of the peak voltage, and A is the insulator interface area in cm^2. K, the vacuum breakdown constant, has been determined to be 0.22 for pulse durations over the range

12

0.01 to 0.1 μsec. Data taken by Sandia National Laboratories, Albuquerque (SNLA), with pulse durations in the range 0.5 to 1.5 μsec and with a poorly electrically graded segmented insulator indicated the power law dependence coincided with previous SNLA short-pulse data. The breakdown voltage however, was less than one-half that predicted for short-pulse (K=0.09).

For the proposed design with stressed insulator area of 1495 cm^2, a pulse duration of 0.25 sec, and effective insulator length of 12.5 cm, and using the pessimistic SNLA breakdown constant of 0.09, the insulator breakdown voltage is given by 464 kV. For an effective time of 0.5 μsec the anticipated breakdown voltage is reduced to about 370 kV).

Recent data obtained by PSI in testing a segmented insulator assembly electrically graded to be uniform to better than 20%, indicated a breakdown constant, K, of greater than or equal to 0.2. The assembly consisted of 12 insulators, each 4.45 cm thick, with an effective stressed area of 1.37 x 10^4 cm^2. An applied voltage of 1 MV rising in about 0.1 μsec and decaying with an e-folding constant of 19 μsec, corresponding to a t_{eff} of 8 μsec did not cause the assembly to flashover. The PSI data implies a breakdown voltage of the proposed accelerating gap insulator of greater than 1 MV and 825 kV for pulse duration of 0.25 μsec and 0.5 μsec, respectively.

Data has also been obtained by PSI as a result of applying long duration (greater than 1 μsec) pulses to a cathode stalk in a cylindrical geometry, with the cathode stalk designed to provide a non-emitting electrostatic grading structure. The cathode consisted of a 14 cm diameter aluminum cylinder terminating in a hemisphere. The aluminum was hard anodized per

13

MIC-A-8625C Type III to a thickness of between 0.0025 and 0.005 cm. Electric fields of up to 220 kV/cm were reliably held without emission for microsecond time scales. When the pulse generator was not crowbarred and allowed to decay with an e-fold time constant of about 20 μ sec, some emission was observed.

These data indicate that the peak electric fields on the electrode surfaces in the vacuum in the revised accelerator gap design will allow operation in excess of 500 kV for microsecond type pulse durations.

Figure 2.2.6 shows the equipotential plot of the optimized design for the reverse charged accelerating gap. The insulator and electrode structure is a mirror image of the accelerating gap of Figure 2.2.5, utilizing the same insulator and electrodes simply reversed. This clearly has many fabrication advantages and was made possible by iteration of the normal and reverse charged accelerator gap designs.

For a negative voltage applied to the vacuum field shaping electrode, the electric field directs electrons away from the insulator surface at angles ranging from 52 to 56 degrees, except for the cathode triple point where the angles drop to 37 degrees (still acceptable). Peak electric fields on the electrode surfaces in the vacuum are 55 kV/cm, 79 kV/cm, and 54 kV/cm for the negative and positive accelerating gap electrodes, and field vacuum shaping electrode respectively, for an applied voltage of 250 kV. The peak sideways electric field in the insulating oil on the negative electrode is 103 kV/cm.

14
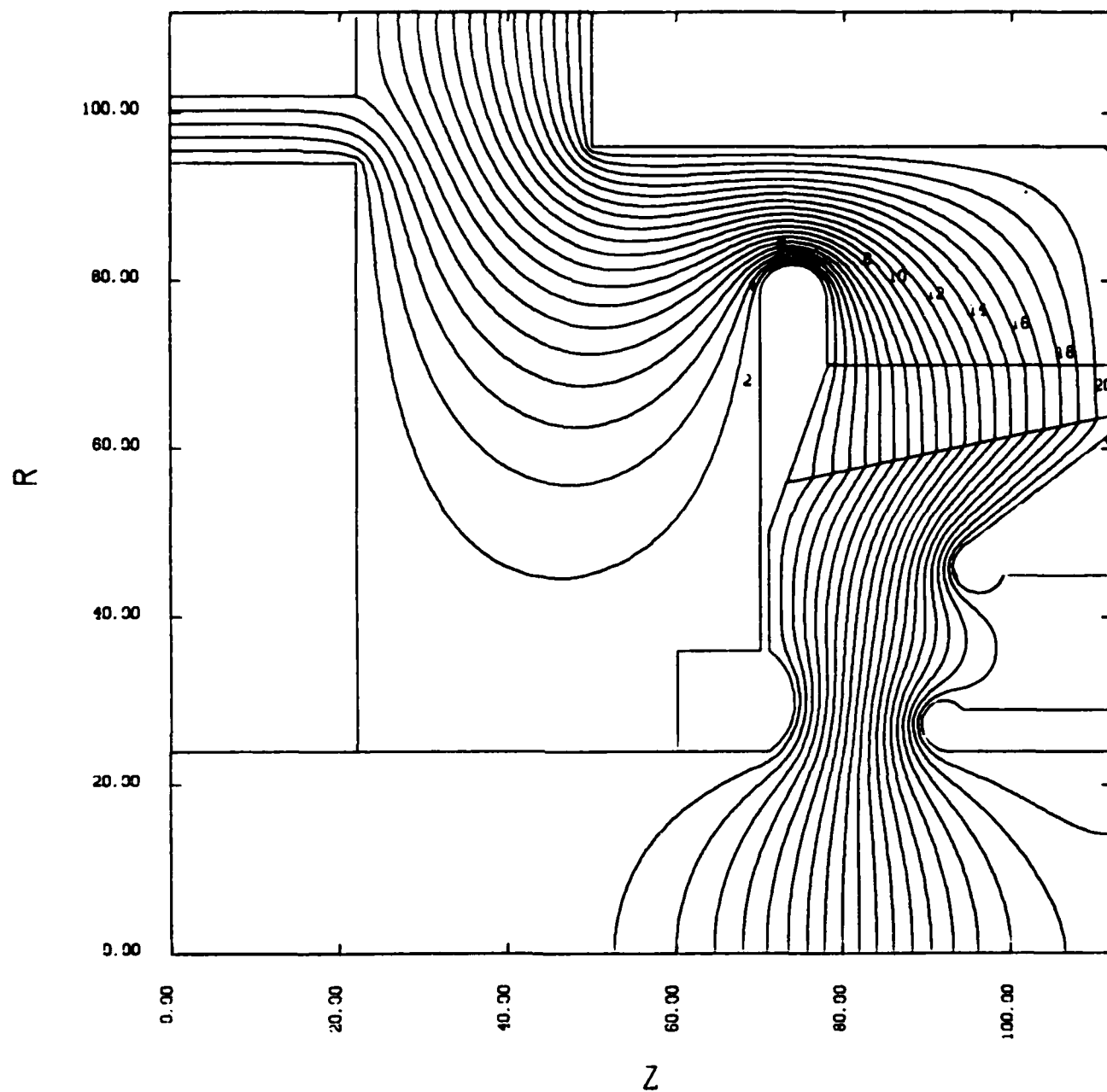
Figure 2.2.6 Redesigned accelerating gap – negative applied voltage

2.2.3 Accelerating Gap Mechanical Design

2.2.3.1 Conceptual Design

The conceptual design of the accelerating gaps using a trapezoidal insulator shown in Appendix 2A, was completed June 1981. The accelerating gaps were designed to fit the existing NBS linac, one gap assembly was designed for the injector side of the accelerating module and the other for the beam exit side of the accelerating module. The accelerating module has two sets of cores, each composed of concentric core sub-assemblies with the axis of the assembly mounted horizontally. The core assemblies are not the same since one is made of four sub-assemblies and the other of five sub-assemblies. The core assembly with four core sub-assemblies is installed in the injector side of the induction module: consequently, the injector side gap assembly was named the four core side accelerating gap assembly and the beam exit gap assembly named the five core side accelerating gap assembly.

The design for each of the accelerating gaps consists of a stainless steel enclosure weldment, a stainless steel endplate, a ceramic insulator, copper accelerating gap electrodes, a copper vacuum field shaping electrode, nylon tie rods, and appropriate nuts and miscellaneous fasteners. The gap materials were selected to ensure the capability of better than 10^{-6} mm Hg vacuum, enabling operation of a hot cathode injector.

The endplate is fastened to the enclosure weldment by nylon tie rods located around the outside of the insulator in the region filled with oil. The tie rods pass through clearance holes in the enclosure weldment and

16

endplate. A seal washer is installed on the enclosure end of the tie rod and nuts are installed on both ends for tensioning. "O" ring grooves are located on the inside surface of the enclosure weldment and endplate, providing a vacuum/oil interface seal when the insulators are installed and the O rings are compressed. The copper accelerating gap electrodes are manufactured to be a tight fit in the enclosure and endplate. The vacuum field shaping electrode is fastened to the endplate with screws.

The outside face of the enclosure weldment and the endplate are machined to be compatible with metal seals (conflat flanges) which are used on the mating beam pipe components.

General issues raised during the conceptual design were: 1) could ceramic rings the size required for the accelerating gaps be manufactured, and 2) could metal seals be used at the ceramic metal interfaces in place of elastomer seals to provide a system which could operate at a lower vacuum than with a system with elastomer seals.

In order to answer the question of feasiblity of manufacturing large ceramic rings, PSI was asked to contact vendors with the capability to supply NRL with the rings machined to print. Numerous vendors were contacted and the information assembled in a summary document. The results of the PSI search for ceramic insulator material and manufacturers for the accelerating gaps is included as Appendix 2D. Information on cylindrical ceramic insulators to be used as replacements in the existing NBS designed accelerating gap assemblies, and trapezoidal ceramic insulators for the new PSI designed accelerating gaps was obtained and summarized in the ceramic search document. Vendors were

17

located who could produce both insulator configurations to the required specifications.

The feasibility of using metal seals at insulator-metal interfaces was studied. The force necessary to compress the metal seals was approximately two to three times the force necessary to compress the elastomer O-rings. The additional tensile load in the nylon tie rods would require substantially more and/or larger tie rods than included in the conceptual design. The increase in required cross-section was judged to be impractical for the present design and the decision was made to use elastomer O-rings.

2.2.3.2 Preliminary Design

The preliminary design of the accelerating gaps and a lifting fixture were completed in July, 1981. The basic design concept is the same as the conceptual design, although the details have been refined and a lifting fixture designed to handle the gap assemblies during installation and removal for maintenance.

The tie bolts which are used to compress the O-rings at the ceramic metal interface and hold the enclosure weldment and endplate in alignment are threaded into the endplate rather than passing through the endplate with nuts installed on the back side. Shoulders previously shown on the tie rods were removed to eliminate potential stack up problems with the insulator.

The plates either side of the insulator are thick to minimize deflection of the plates when the interior of the acelerating gap assembly is evacuated.

18

If the plates were thin with large deflections, the vacuum load would be carried on the unsupported tip of the ceramic ring cross section, risking fracture of the ceramic. The plate thickness is also compatible with comflat flange requirements on both the enclosure weldment and endplate and is sufficiently thick to meet electrical radius constraints on the outside of the endplate.

in the preliminary design, the surface of the plates adjacent to the sharp point of the insulator cross section is contoured to diminish the steel, insulator and vacuum triple point electric field vacuum.

A summary of all calculations performed for the accelerating gaps and lifting fixture were sent to NRL as part of the preliminary design review package. The calculations are included in Appendix 2B.

General issues were identified for action during the preliminary design review. The PSI response to these issues is included in Appendix 2C.

2.2.3.3 Final Design and Fabrication Cost

The final design of the accelerating gaps was completed and prints for final design review sent to NRL September, 1981. The prints sent to NRL are listed in Appendix 2E. Following the review of the drawings by NRL the sepias for the drawing package were transmitted to NRL on 3 December 1981. A copy of this letter is given in Appendix F.

Near the completion of the final design, PSI was asked to provide NRL with the cost for manufacturing and assembling the accelerating gap assemblies and the lifting fixture. Table 2-1 is a summary of the estimated loaded costs, through fee, to fabricate one four core side and one five core side accelerating gap in addition to the lifting fixture for handling the gap assemblies. The cost of insulators is not included as requested by NRL, however, the as-quoted cost for ceramic insulators can be found in the Appendix 2D ceramic search.

TABLE 2-1

ESTIMATED FABRICATION AND ASSEMBLY COSTS
FOR TWO ACCELERATING GAPS PLUS LIFTING FIXTURE

Cost is for one each, four core, one each, five side accelerating gap, and one each, lifting fixture.

Cost does not include gap insulator.

Fabricated Components

Materials, etc.	$ 24,561	
Labor (coordination, inspection & packing for shipment)	5,725	
		$ 30,286
As-Built Drawings		852
Assembly		
Misc. materials & leak testing	1,006	
Labor	1,828	
		2,834
TOTAL		$ 33,472

The materials include: the machined and spun pieces for the gap assemblies, the parts for the lifting fixture, vacuum leak testing, prints,

20

crates for shipping component parts to NRL, and cost of local transportation accumulated while coordinating with machine shops during the fabrication. Labor costs include: vendor liaison during the final bid cycle, fabrication coordination, and inspection and packing parts for shipment.

The as-built drawing cost is a rough estimate of labor required to document the as-fabricated configuration of components. This is particularly important in the event that replacement parts are required at a later date.

The assembly material and labor costs are for incidental materials, outside services, and labor required to assemble the accelerating gaps and perform leak testing prior to shipping the final assemblies.

Backup for the costs in Table 2-1 are included in Appendix 2G.

Early in 1982 NRL requested PSI to revise the accelerating gap design to include the following:

1. Voltage monitors

2. Current monitors

3. The ability to order gap assemblies with either ceramic or acrylic insulators.

4. The ability to order gap assemblies with either copper or anodized aluminum electrodes.

21

A detailed description of the revisions, including assembly drawings of the revised assemblies is shown in Appendix 2H. The revised design was delivered to NRL May 1982.

A second revision to the accelerating gap diagnostics was made in January 1983. The electrical description of the operating characteristics of the diagnostics is included in the following section 2.2.4. A copy of a letter sent to NRL in January 1983, describing the operating characteristics of the diagnostics is included in Appendix 2I. Drawings showing the final configuration of the accelerating gap assemblies with revised diagnostics are also included in Appendix 2I.

A list of drawings for the final revised accelerating gap design and the final letter of transmittal for the accelerating gap project is included in Appendix 2J.

2.2.4 Accelerating Gap Diagnostics

The current and voltage sensors were chosen to be of the differential types in order to maximize the signal sent to the diagnostic screen room. Operating conditions for the accelerating gap were taken as:

(1) Current pulses as long as 2 μs and low as 500 A peak.

(2) Voltage pulses of 250 kV for 2 μs or 500 kV for 500 ns.

(2) Current and voltage will typically rise to peak in 200 ns.

The current sensor is a non-integrating Rogowski coil fabricated as a 50 ohm transmission line with termination. Reflections and ringing are thereby minimized. Calibration is performed on a test bench. The response will be independent of uniformity of current density. The coil has a minor mean radius of 0.95 cm, a major mean radius of 29 cm, and 70 turns. For 500 A rising in 200 ns

$$(d\phi/dt) \simeq [(\mu o)(Na^2)/2r]\ (dI/dt) = 34\ \text{volts}.$$

A 50 ohm termination built into the sensor, resulting in a signal of about 17 volts being sent to the screen room. If the signal cable is terminated in 50 ohms and a 20 μs integrator used at the oscilloscope, a peak near 170 mV will be recorded.

The voltage monitor senses changes in the magnitude of the electric field. This sensor is less subject to electrical stress failure than a resistive monitor. It is also mechanically more stable than a larger area capacitive monitor. However, because of the fringing electric fields, it is necessary to calibrate this monitor in position. An approximation to the capacitance between the pick-off plate and the high voltage electrode is 0.2 pF. Therefore, the output for 250 kV rising in 200 ns is given by

$$V_o = iR = CR\ dV/dt = (0.2\ \text{pF}) \times (50\,\Omega) \times 250\ \text{kV}/200\ \text{ns} = 12\ \text{V}.$$

Using a 50 ohm termination and 20 μs integrator at the oscilloscope will yield approximately 120 mV.

23

2.3 Free Electron Laser Accelerator Module Preliminary Design

2.3.1 General

A long pulse induction linac was built at the National Bureau of Standards (Leiss, et al., 1980) and is currently in operation at NRL. Figure 2.3.1 is a schematic of the long pulse induction linac. The accelerator consists of two major components; (1) an injector and (2) an induction accelerator module.

Electrons are accelerated in the gun through a series of annular electrodes, spaced by ceramic insulator rings. The gun has been used with both cold and thermionic cathodes.

The electron gun is immersed in an oil filled tank. The gun voltage is fed from a pulse line driving a 12:1 step up transformer. The injector typically produces a 0.8 kA, 2 μs beam pulse of 400 keV. The electron beam is transported to the induction accelerator module via a series of focusing coils.

The induction accelerator module consists of two core sets, each driven by a Type E pulse forming network (PFN). One of the core sets give a 4:1 step up voltage and the other a 5:1 step up. The cores are wound with 0.001 inch mild steel foil, separated by 0.00025 inch Mylar sheets. An accelerating voltage of up to about 200 kV can be delivered to each accelerating gap.
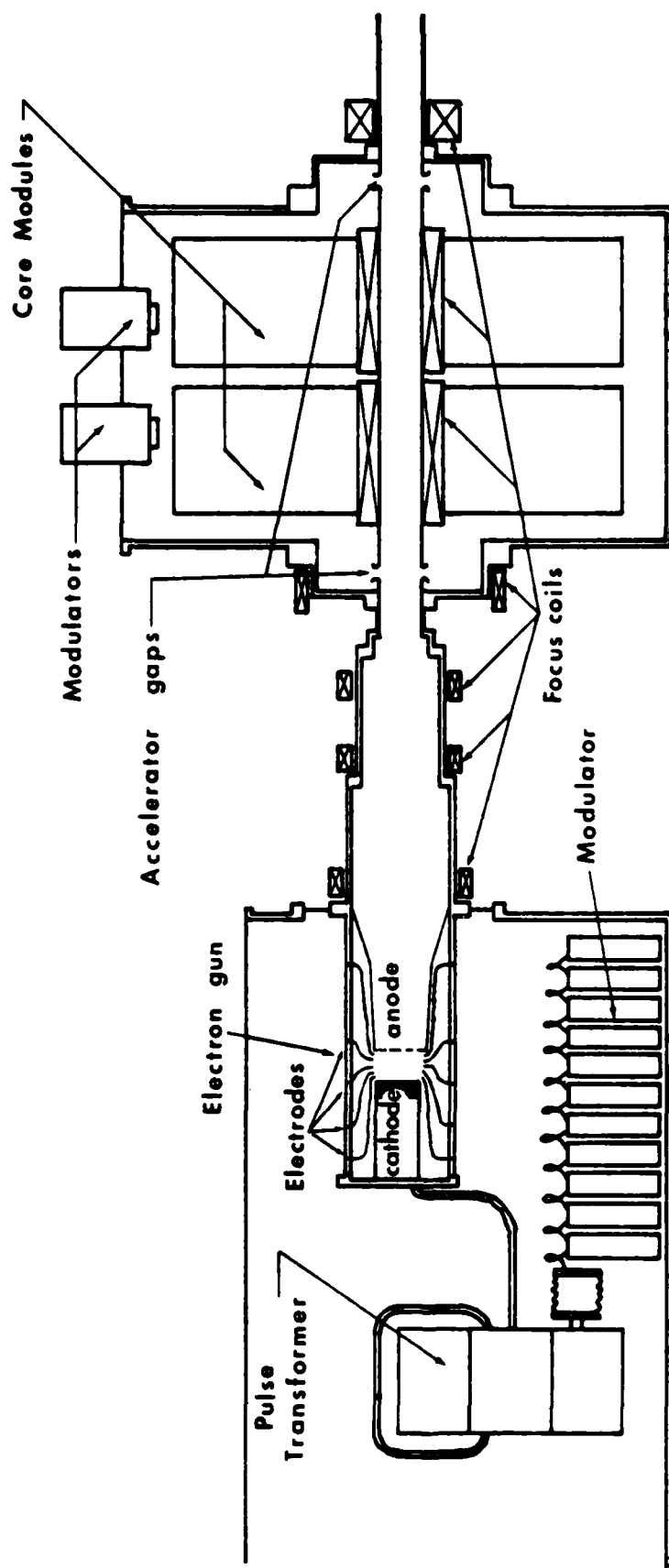
Figure 2.3.1 Schematic of existing injector and induction linear accelerator

Core Modules

Modulators

Accelerator gaps

Focus coils

Modulator

Electron gun

anode

cathode

Electrodes

Pulse Transformer

25

Typically, the output energy of the electron beam generated by the linac is 0.6 to 0.8 MeV, the current approximately 0.8 kA, and the pulse length 2 µs.

2.3.2 Conceptual Design

Conceptual design of the new induction module commenced with assessments of total induction core current, assuming the injector to be upgraded to produce 2 kA of beam current, and two NBS induction modules upgraded with each of the new accelerating gaps driven at 250 kV. Dr. Andy Faltens of Lawrence Berkeley Laboratory assisted PSI in making these assessments. Dr. Chuck Roberson of NRL assisted in performing experiments to aid this assessment. It was determined that for a 2 kA beam current, and including core losses associated with a 2 mil SiFe/Mylar core, the effective load current for an accelerating gap driven at 250 kV for 500 ns will rise from 4 to 6 kA.

Initially, modulators consisting of Marxed Type E PFN's were examined, with 10 to 15 sections per PFN. Waveshaping to a specific load impedance profile was achieved by tuning the individual section inductors. As this design approach was pursued and resistive elements introduced to protect the PFN capacitors against a variety of fault modes (which may be expected to occur in an experimental apparatus, such as load arcing, absence of beam load, etc.) the complexity of the design increased to a point where alternate approaches were examined. Of the alternate approaches considered, such as PFN/transformers, combination Type A/Type C PFN's, and various forms of Marx run-down circuits; the latter offered the simplest, cheapest, and most versatile approach.

26

The choice was made, therefore, to use two Marx run-down circuits (modulators), one to drive each induction core. Each modulator consists of a 4-stage Marx generator capable of being charged to a maximum of plus and minus 50 kV dc.

The 500 ns pulse duration is obtained by crowbarring the voltage across each induction core. Each of the two crowbars is triggered from a separate trigger generator. To achieve adequate voltage flatness, shaping and compensator circuits are used in the output of each modulator. Within the bounds of allowable voltage flatness, a variable trigger delay between the trigger signal to the two modulators and the trigger signals to the two crowbars can provide an adjustable accelerating pulse width.

Induction core reset circuits are provided, and relay interlocks integrate the small module with the facility operation.

The cores are separately supported via nylon straps attached to lifting frames, enabling assembly and removal of individual cores with the aid of the overhead crane. Similarly the two modulators are separately supported via nylon straps to the lifting frames. Modulator maintenance is affected by removal of the modulator from the oil tank to a maintenance area (adjacent to the tank) again with the aid of the overhead crane.

An umbilical cord comprising power, command and control, monitoring and safety feature cables enables low voltage testing of the modulator when removed from the tank. The two power supplies for the modulators and the

27

power supply for the modulator trigger generator are located external to the oil tank. The accelerator gaps are mounted as in the case of the existing NBS module, between the beam pipe and the outside walls of the oil tank.

The Interface Control Document and The Conceptual Design Package (attached in Appendix 2K) were completed in August 1981. A Conceptual Design Review (CDR) was held at NRL in September 1981, and a letter was prepared documenting the various issues raised and responses given following the CDR. A copy of this letter is presented in Appendix 2L. A revised Interface Control Document was then issued, and is attached in Appendix 2M. The final part of the conceptual design effort was the preparation of fabrication cost estimates; these estimates are given in Appendix 2N.

2.3.3 Preliminary Design

The preliminary design of the new small module proceeded under the following ground rules:

1. Acceleration of the injected beam by 500 kV over a period of $0.5\,\mu s$ through the use of the existing "Recirculating Core" and a new core.

2. Complete integration of the 500 kV, $0.5\,\mu s$ accelerator module with the NRL building layout and system command and control system.

3. The introduction of two additional new cores for future racetrack accelerator testing without structural changes to the module tank or component electrical layout.

4. The use of the existing support platform.

5.   Access to the beam pipe and focus coils by means of lateral movement of the tank/platform on rails.

6.   Removal of the core assemblies via the overhead crane.

7.   Removal of the modulators via the overhead crane.

The preliminary design package was completed early November 1981. A copy of this package is included in Appendix 20.

The preliminary design electrical approach is to use two Marx run-down modulators, one to drive each induction core. Each modulator consists of a 4-stage Marx generator charged to about plus and minus 42 kV. The Marxes are electrically identical and physically mirror images of each other producing plus 250 kV and minus 250 kV, for a total accelerating voltage of 500 kV. The two Marxes are charged from independent power supplies and discharged from a common trigger generator. The 0.5 μs pulse duration is obtained by crowbarring the voltage across each Marx. Each crowbar is triggered from a separate trigger generator.

To achieve adequate voltage flatness, pulse shaping and damping circuits are located in the output of each modulator. Within the bounds of available volt-seconds in the cores, a variable trigger delay between the trigger signal to the two modulators and the trigger signal to the two crowbars provides an adjustable accelerating pulse width. Reset circuits are operated prior to each firing to reset the induction cores.

The 500 kV, 0.5 µs accelerator module control rack design is integrated with that of the main facility controls. Operation of this control rack centers around the control panel.

A typical operating sequence for the 500 kV module is as follows. Turn on the sulphur hexafluoride gas supply and the circuit breakers on all individual panels. When the oil level in the tank and the tank cover interlocks are satisfied, the control panel "Interlocks" will light. When the "Facility Ready" lights, the 500 kV module operation can continue.

The operator checks all gas pressures then pushes "Pressure OK", which then lights. The operator then pushes "Core Reset" and observes the core reset voltage meter rising. After a time controlled by a delay relay, opposite core reset voltages are applied in turn to the two cores and the "Core Reset" indicator lights. The operator then presses the "Trigger Test" button which lights after automatically turning on the trigger power supplies. The operator observes the modulator trigger voltmeter, and when it reaches 70 kV, presses the manual trigger button on the delay generator panel. Only after output signals are received at the control panel from the modulator trigger generator and the two crowbar trigger circuits does the "Module Ready" indicator light (the trigger power supplies do not recharge).

When the module ready indicator lights, a contact closure sends the Module Ready information to the facility. A signal from the facility closes command charge contacts; the "Start Charge" indicator lights and the trigger and modulator power supplies are automatically turned on. At this point a 5-minute limit-timer starts; this limits the time the modulator and trigger

capacitors are subjected to high voltage; if it times out, the control chain is opened. The modulator power supplies detect when charging is complete, turn on the "Charge Complete" indicator light, and by contact closure send this information to the facility. The facility then sends a fire command pulse to the delay generator which initiates the triggering sequence.

The modulator power supplies detect the voltage discharge, light the "Fire Complete" indicator, and turn off the control chain. The control chain is reset when the "Facility Ready" contacts open or when the "Abort" button is pressed.

A representation of the electrical circuit of one half of the 500 kV is shown in Figure 2.3.2. The Marx has a nominal capacitance of $0.125\mu F$ and an inductance estimated at $2\mu H$ including the external current paths. The resistor $R(t)$ represents the time-varying core current, and R is a parallel resistive load whose value is chosen at will. The stray core capacitance that must be charged to the accelerating voltage is represented as $C(s)$. The values of L and Z in the filter may also be chosen at will. $I(t)$ is the beam current, which may be turned on at an arbitrary time relative to Marx erection, but whose waveform is not controllable. The crowbar is represented by an inductance of $1\mu H$ and a switch that may be closed at an arbitrary time relative to Marx erection.

The principle of the circuit is that the Marx capacitance is initially charged to a higher voltage (about 350 kV) than the desired accelerating voltage V (250 kV), and the filter resistance Z is chosen so that the initial current $V/R(o) + V/R + I(o)$ causes the voltage difference to be dropped across

31
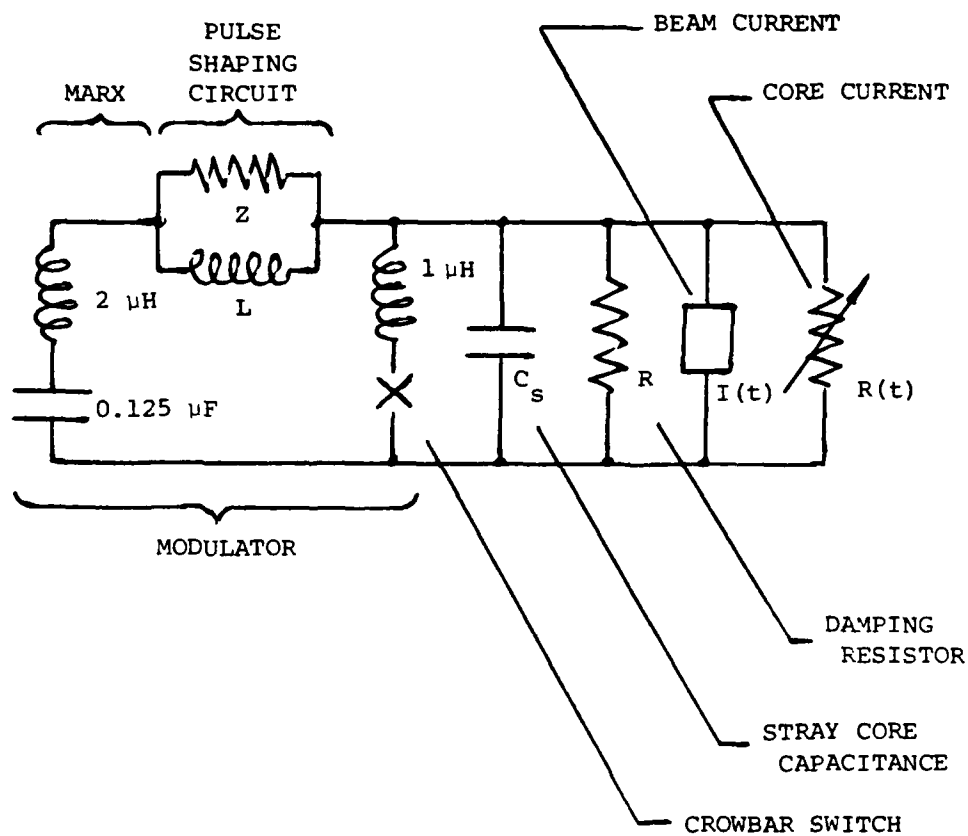
Figure 2.3.2 Circuit model of one modulator (half module, 250 kV acceleration)

Z. As the Marx discharges and R(t) falls, the filter inductance shunts the filter resistor to appropriately reduce the voltage drop across the filter. Calculations in which the total current is represented by an R(t) term (with stray capacitance ignored) show that the voltage flatness is controlled mainly by the relative change in current $I/\bar{I}$ during the pulse, and is roughly plus/minus $4(\Delta I/\bar{I}^2 + 0.2 \ (\bar{I}/10 \ kA)^2$ percent. It is expected that the ΔI produced by the cores will be about 2 kA.

The stray capacitance C(s), together with the inductance of the Marx and filter can generate an oscillation on the rise of the pulse, delaying the time for which the voltage is flat until the oscillation has damped sufficiently. Damping is most effectively provided by the parallel resistors R(t) and R. The stray capacitance of a shield large enough to house two cores is estimated as 0.4 nF. A shunt load resistance R = 50 ohms damps the oscillation adequately for Cs = 0.4 nF (even Cs = 0.6 nF) with the voltage entering the specified flatness (plus/minus 2%) at 130 ns; after 170 ns the voltage becomes flat within less than plus/minus 1% for a time greater than 1,000 ns. This is illustrated in Figure 2.3.3, which shows the accelerating voltage with no beam loading. Note: the computer printout gives numeric data considerably more accurate than the plot shown in Figure 2.3.3. The pulse flatness information was derived from the numeric printout data.

The 50-ohm shunt resistor is also useful in reducing the beam deceleration if the beam is turned on early, which may be desirable because of its rather long risetime. The effect of adding the beam and firing the crowbar is shown in Figure 2.3.4. The injected beam was assumed to have a 150 ns ramp rise to 2 kA, have a flat top of 1,300 ns, and a ramp fall of

33

PLOT OF VCS VS TIME
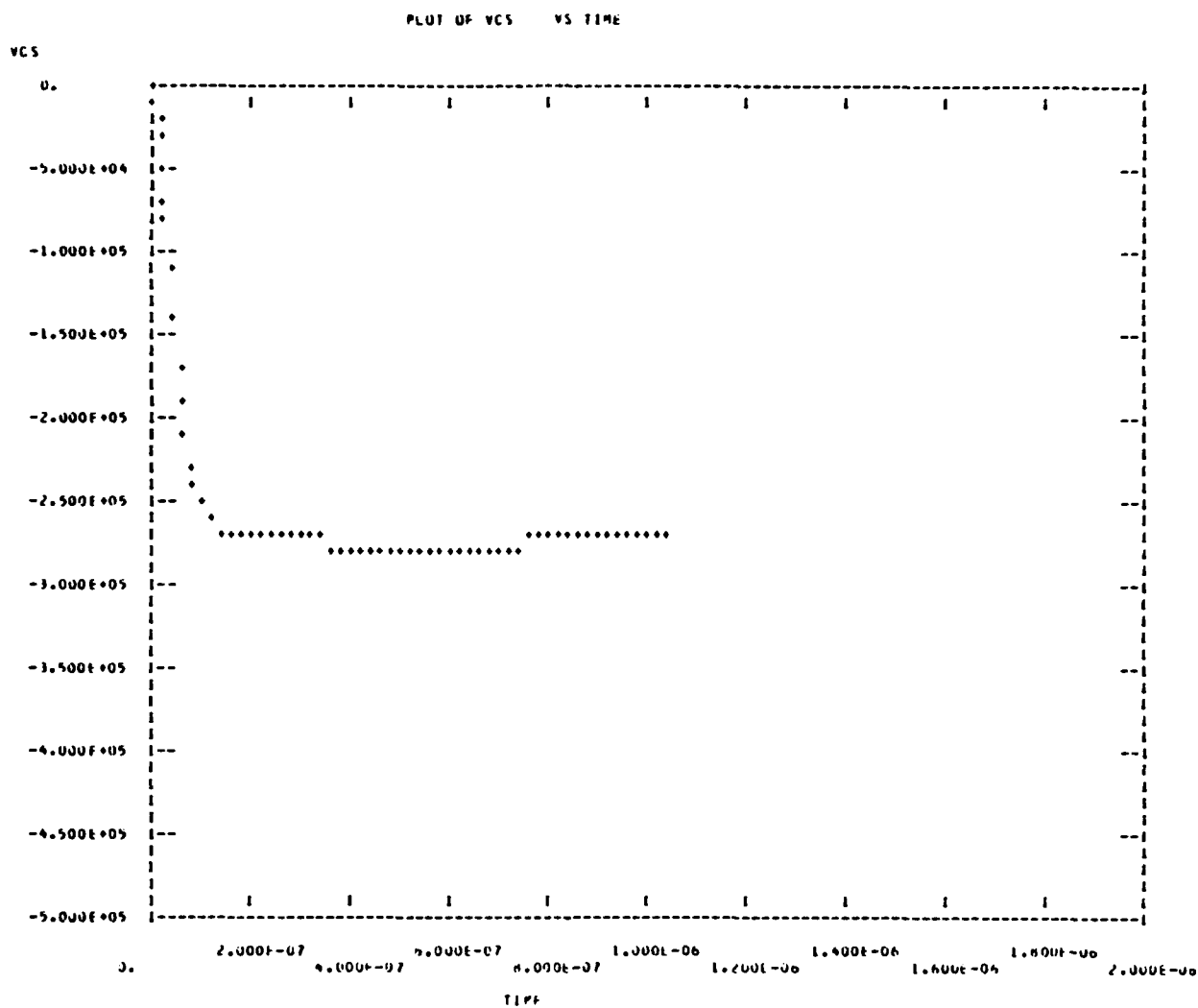
Figure 2.3.3   Half module accelerating voltage
(no injected beam, no crowbar)
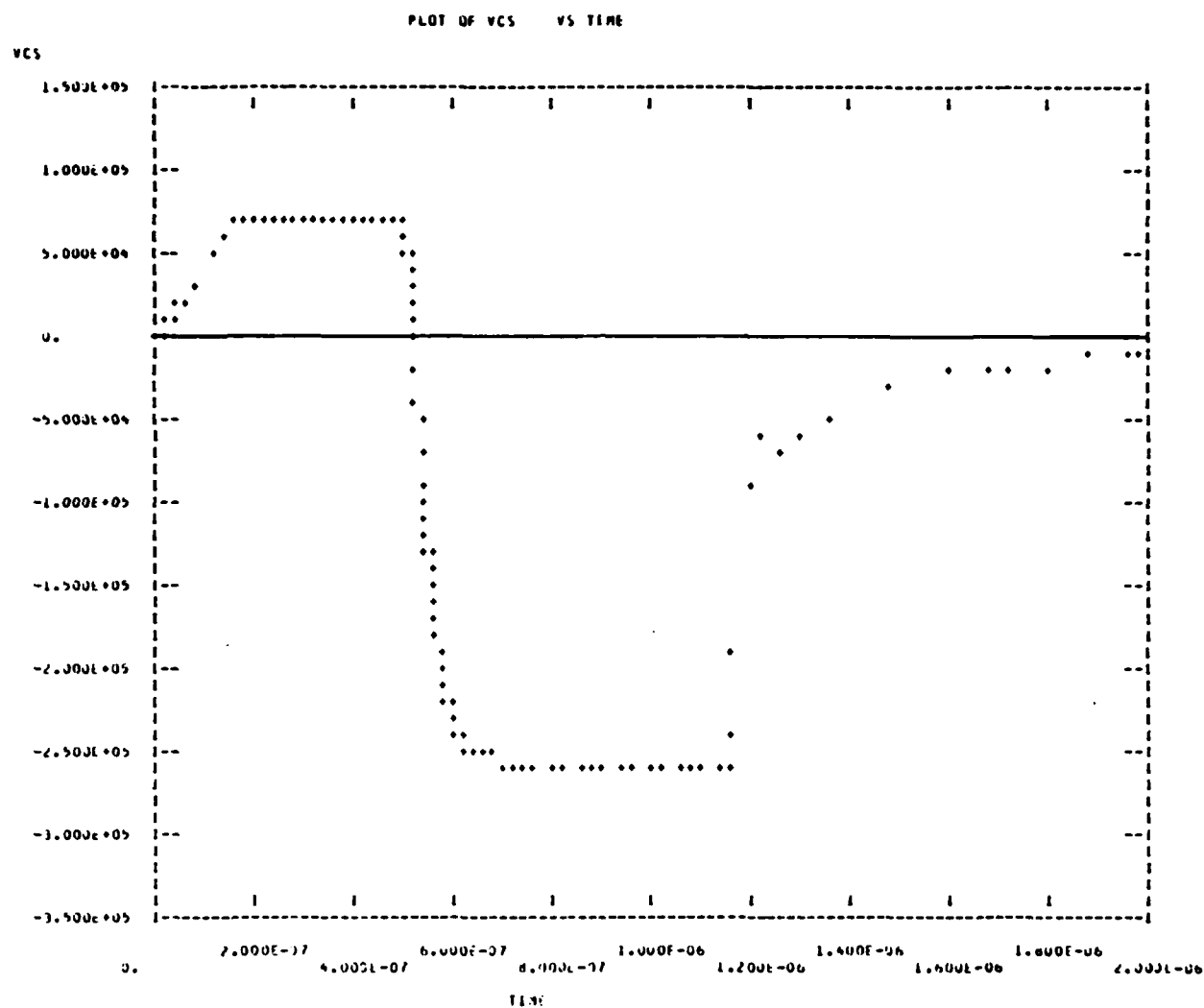
Figure 2.3.4   Half module accelerating voltage
(with injected beam and crowbar)

300 ns. The modulator was fired arbitrarily 500 ns after the arrival of the injected beam, and the crowbar triggered 650 ns after the Marx. The accelerating voltage is shown by the computer numeric printout to be within plus/minus 2% between 640 ns and the crowbar time of 1,150 ns, giving 510 ns of "in-spec" pulse at 260 kV.

Because of the perturbing effect of stray capacitance, it is desirable to keep the core shield length to a minimum in the single pass mode where voltage flatness is of concern, rather than building each shield along enough to house the additional core for the racetrack recirculating mode.

The crowbar and shunt resistor are placed well away from the accelerating gap with minimal loop area to the Marx in order to reduce stray magnetic fields "seen" by the beam.

To minimize the effects of the beam return current on the beam trajectory, the Marx current is fed to the core shield at two points, distant from the accelerating gap. This allows the beam return current to diverge symmetrically from the beam axis. The Marx ground return is similarly attached to the tank wall at two points, and to further preserve symmetry these points are made diametrically opposite to the high voltage shield connections.

The underlying design philosophy adopted at the start of the module assembly layout required a) providing space for two additional cores, and b) enabling the module assembly to be moved laterally out of the beam line for removal of the beam pipe and focus coils. Lateral movement of the new module

also permits removal of the beam pipe from the existing NBS module should this be required.

The present NRL 8' x 8' tank support platform is used; the present casters are replaced with rigid V-groove casters. The casters run on tracks positioned at right angles to the beam line and fastened to the laboratory floor.

A summary of pertinent mechanical specifications for the module is listed below:

Overall Dimensions of Accelerating Module

Height: 93 inches

Length: 109 inches (tank support platform with screw jack brackets)
: 106.25 inches (overall with new accelerating gaps installed)

Width: 109.5 inches (tank upper flanges)

Required Floor Space: 108 x 109.5 inches (based on tank without accelerating gaps) = 82 square feet

Approximate Weight of Module Assembly

Item	Weight
1 Assembly	2,712
Core 2 Assembly	2,935
Modulators 2 @ 1180	2,360
Miscellaneous Electrical Hardware	590
Gaps 2 @ 300	600
Beam Pipe and Focus Coils	800
Tank	4,900
Structural Spacer	3,000
Air Pallet	800
Platform 8' x 8' existing	3,000
	21,697 lb
Transformer Oil 1850 Gal.	13,407 lb
Total Module Weight	35,104 lb

Floor Loading

Based on Floor Space: 428 lb. per sq. ft.

Under 4 inch diameter Screw Jack Pads:

Load per Screw Jack: 5,850 lb.
   (5 ton gap E.A.)

Pad Area, (4 in. diameter): 12.57 sq. in.

Floor Load: 465 lb. per sq. in.

Tank Dimensions

Length: (measured along beam line)

Outside Maximum: 94 in.
Flange face to flange face: 92.5 in. (for new accelerating gaps)

Inside: 88.5 in.

Width:

Outside Maximum: 109.5 inc.

Inside: 102 in.

Height:

Outside: 57.5 in. (60-1/2 proposed for final design)

Inside: 57 in. (60 proposed for final design)

Access Limit: 72 in. x 94.25 (Interface Control Document ICD-115-21-A)

Gross Internal Volume: 287.3 cu. ft. (2,149 Gal.)

Cores:

Core No. 1 (Existing Recirculator)

Dimensions:
    I.D.: 12.5 in.
    O.D.: 32 in.
    Width: 14 in.
    Weight: 2,233 lb. (calculated)

Core No. 2 (New)

Dimensions:
    I.D.: 12.5 in.
    O.D.: 35 in.
    Width: 11.5 in.
    Weight: 2,456 lb. (calculated)

Modulators

Capacitors:
    Manufacturer: Aerovox
    Type: PX210D26
    Capacitance: 1.0 µF nominal
    Voltage: 50,000 VDC
    Individual Weight: 95 lb. plus/minus 5%
    Number/Modulator: 8
    Modulator: Overall Dim. (including support structure)
        Length: 51 in.
        Width: 24 in.
        Height: 55 in.

Calculated total weight of each modulator: 1,180 lb. (including support structure).

The 500 kV, 0.5 µsec Accelerator Module consists of the following mechanical subassemblies as shown on the layout drawings.

1. Tank containing the Accelerator Module electrical components.

2. Structural spacer located under the tank.

3. Air pallet between the structural spacer and the tank support platform.

4. Existing tank support platform.

39

The tank for the Accelerator Module is freestanding, rectangular in plan, measuring 94 in. long (measured along the beam lines), 109 in. wide, and 57-1/2 in. high as shown on the preliminary layouts. It may be desirable to increase the height of the tank allowing a final design of 60 inches to permit the installation of a flat lid.

The tank is fabricated with sides of flat plate stiffened with standard structural steel channels to minimize deflections of side panels to approximately 1/8 inch when the tank is filled with oil.

Machined flanges of the same design as on the NBS module are welded to the sides of the tank for attachment of the accelerating gaps.

Structural members for supporting major electrical components inside the tank are bolted to brackets (welded to the tank) to permit removal of the components and support structures.

The core assemblies (including shields) occupy approximately 1/2 of the tank. The other half of the tank is for the two modulators and other electrical circuit components. The layout allows sufficient space between the two modulators for entry into this portion of the tank (when drained of oil) for servicing electrical system components.

The cores and Marx generators are suspended on nylon straps from structural members secured near the top of the tank. This system permits removal of core assembly 1 or 2 (after beam pipe removal) and Marx generator 1 or 2 using the overhead crane.

40

Access for moving the tank through the building into the laboratory will most likely be through the 12 foot rollup door in the west end of the building, and via corridors leading to the door of room Number 3 (Ref. NRL Y & D Drawing Number F1029138, sheet 12 of 95). As presently drawn, the tank will pass through the door into room Number 3 with approximately 1/4 inches clearance at the top of the tank, with the 94 inch tank "length" oriented vertically. The tank will probably have to be pulled through the door using come-alongs with the tank cribbed on steel plates on the floor.

Tank dimensions were minimized consistent with electrical breakdown considerations requiring a 4 in. minimum standoff between electrical components and the tank structure. The distance between the beam centerline and the inside bottom of the tank is approximately 26 inches. To satisfy the 60 inch beam height interface dimension, the bottom of the tank is raised approximately 33.5 inches from the floor. This space is partially taken up by the 8' x 8' tank support platform and an air pallet system. The air pallet system enables final beam pipe alignment through relative motion of the tank on the support platform. The remainder of the space is taken up by a structural spacer.

The spacer will be fabricated from steel plate and standard structural steel shapes. The spacer is a separate structure, not permanently fastened to the tank. As presently shown, the spacer is also independent of the air pallet; however, the air pallet and structural spacer could be combined into one structure. The air pallet has been shown on top of the 8' x 8' tank support platform. Various manufacturers market individual air pads which

41

could be incorporated into the pallet design or a custom pallet could be ordered.

The support platform shown on the layout drawings is the existing platform at NRL as called for in the interface contract document, with the exception of using rigid V-groove casters in place of the existing casters. This change enables the module assembly to be rolled out of the beam line on tracks for removal of accelerating gaps, beam pipe, focus coils, and cores. The tracks will allow repositioning of the module with a minimum of realignment after disassembly, assembly, and re-installation in the beam line. Once in position, the platform will be raised on the screw jacks to avoid overload of the casters when the tank is full of oil.

Installation and assembly of the module will begin with laying out the position of the tracks in the floor using a transit. The tracks will then be bolted to the floor and the platform installed on the tracks and fixed in place. The air pallet, structural spacer, and tank will then be positioned and fastened together. The structural beam across the tank which forms one of the internal component support surfaces is then installed.

There are four major subassemblies to be installed in the tank. These are: two core assemblies and two modulator assemblies. Each of these subassemblies can be assembled out of the tank on the floor and/or by using assembly fixtures. Once assembled, the four subassemblies can be installed or removed from the tank independently.

The first time the module is assembled, it may be advisable to install the modulators and all the associated circuitry before the core assemblies. This will allow increased access during installation. The core assemblies would be the last components to be lowered into the tank.

When the mechanical assembly of the module has been completed, the tank will be moved into position on the tracks and position adjustment of the tank and cores made.

The position of the cores in the module can be adjusted normal to and along the beam line. The adjustment of the position of the beam centerline through the core relative to the tank flanges is accomplished by:

1. Movement of the core mandrel strap hangers on the core support cross beams.

2. Raising or lowering the core assembly support structure by shimming under the support frame at the support structure/tank interface.

Adjustment of the core position along the beam axis is achieved by moving the core support structure along the support brackets within the limit of the slotted holes in the support structure.

At this point the beam pipe assembly is installed and accelerating gaps bolted in place. The module assembly is positioned in the beam line by moving the assembly along the tracks and locking it in place.

43

Adjustment of the location of the accelerating module so that the centerline of the module beam line coincides with the beam axis is accomplished by:

1. Lateral and height movement of the tank support platform.

2. Movement of the air pads on the support platform laterally and along the beam axis.

2.4 Free Electron Laser Accelerator Module Final Design

2.4.1 General

Following NRL approval of the preliminary design package, PSI was scheduled to generate the final design for the 500 kV, 500 ns accelerator module and power supply for the augmented NBS/LIA and/or racetrack accelerator. During the Preliminary Design Review (PDR) held at NRL in February 1982, however, discussions were commenced regarding the possible doubling of the new module accelerating voltage to 1 MV (500 kV per module/accelerating gap), and halving the pulse duration to 250 ns. A summary of these interactions is contained in Appendix 2P.

The 1 MV, 250 ns can be accomplished by doubling the stage voltage in each of the two modulators from approximately plus/minus 42 kV to plus/minus 84 kV with minimal impact upon the general layout of the module components. The capacitor manufacturer, Aerovox, has been contacted and a standard capacitor selected, having the same capacitance and double the rated voltage.

The height of the capacitor is the same. The width and length of each capacitor is 52 percent and 67 percent larger respectively. The capacitor weight is 2.6 times heavier. The higher operating voltage will require the individual spark gaps to be lengthened.

The design of the crowbar and core reset circuitry is not anticipated to require change. The working voltage of the two modulator power supplies and electromechanical safety shorting systems will now be specified at plus/minus 100 kV.

The overall impact on the tank size appears to be to lengthen the tank in the beam axis by approximately 1-1/4 ft., and to increase the width of the tank by approximately 2 ft.

In April 1982, PSI was asked to look into the technical feasibility of increasing the Accelerator Module Specification from the original 500 kV, to 1 MV, 500 ns. The following subsections address these alternate specifications and the impact on the module core design, core fabrication options and performance limitations. Experiments are described which were performed to assist in evaluating various fabrication techniques. The subsection concludes the examination of alternate accelerating concepts in view of the trend toward larger accelerating voltages and longer pulse durations.

45

2.4.2 Technical Feasiblity of Increasing the Accelerator Module Specifications to 1 MV, 500 ns

The 1 MV, 250 ns mode addressed at the end of the Preliminary Design effort requires the individual modulators supply twice the voltage and saturate the core in half the time. Assuming the rise time increases from 100 to 150 ns when supplying the additional current, approximately one-third extra core material is required (150 ns + 250 ns = 400 ns x 500 kV versus 100 ns + 500 ns = 600 ns x 250 kV). Similarly, only two thirds of the Marx capacitance is required

$$(C = (2 \times I \times 400)/2V = (I \times 400)/V \text{ versus } C' = (I \times 600)/V).$$

As PSI considered there to be about a one third core reserve, it did not seem necessary to increase the proposed core size. In order to change from one operating mode to the other, it seemed prudent to retain the full Marx capacitance rather than reduce the individual capacitance values by one third. Retaining the original value would improve pulse flatness, but leave more energy to be crowbarred.

In the case of the 1 MV, 500 ns specification, the individual modulators are required to supply twice the voltage and saturate the cores in the original time, i.e., supply the same current and charge. Thus, double the core material is required (100 ns + 500 ns = 600 ns x 500 kV versus 100 ns + 500 ns = 600 x 250 kV). Similarly, only one half of the Marx capacitance is required

$$(C = (I \times 600)/2V = (I \times 300)/V \text{ versus } C' = (I \times 600)/V)$$

46

Thus, the individual capacitor capacitance values are decreased to 0.5 F from the 1 μF proposed for the 250 ns pulse. By using the same technique proposed in March 1982, of doubling the capacitor stage voltage to double the modulator output voltage, the working voltage of each capacitor is doubled in going from the preliminary 500 kV, 500 ns design to the 1 MV 500 ns design.

The new 1 MV, 500 ns specifications require a) the use of fourcores (the space for which was allowed in the preliminary design, and b) the use of 0.5 μF, 100 kV Marx capacitors. Assuming the same capacitor case size as for the 1 μF, 100 kV Aerovox capacitor, the increased tank dimensions associated with the larger capacitors documented in March, 1982 are applicable. However, twice the voltage for the original time will require the oil spacings to be opened up for adequate insulation.

The overall impact on the tank size in increasing the specification to plus/minus 500 kV rather than plus/minus 250 kV, appears to lengthen the tank in the beam axis by approximately 2-1/2 ft., and to increase the width of the tank by approximately 3-1/2 ft.

The modulator filter capacitor and mechanical crowbars become larger and hence more space must be allowed for them. Similarly, a re-examination of the core reset circuitry will be required to ensure adequate voltage standoff distances for the 500 kV, 500 ns output pulses. The layout of the region between the opposing core shields will require particular attention to accomodate the high voltage connections, ground return pipes, and support the plus/minus 500 kV, i.e., 1 MV. All these changes seem feasible within the new

47

tank dimensions; however, considerable attention will need to be paid to the layout of components in this region -- particularly with respect to adequate oil breakdown clearances and the avoidance of ground loops by careful routing of charging, command and control, and diagnostic cables.

The letter transmitted to NRL in April 1982, summarizing this technical information and containing cost estimates for the 500 kV, 500 ns and 1 MV, 500 ns modules, is reproduced in Appendix 2Q.

The impact of the plus/minus 500 kV, 500 ns specification on the core insulation design, core to core configuration, and core shield design is complex.

The proposed new cores are wound on a 13 inch I.D. mandrel out of 11-1/2 inch wide , 1/4 ml Mylar, and 11 inch wide, 2 mil SiFe. The O.D. of the cores is 32", which, assuming an 80 percent packing factor, results in approximately 3,400 turns. The weight of such an assembly is estimated to be about 2,500 lbs.

The preliminary plus/minus 250 kV, 500 ns design incorporated three of the new cores, and the existing recirculated core (being 13" I.D., 32" O.D. and 14" wide). In the preliminary design the cores are housed in shields 42" diameter, allowing 3-1/2" of radial clearances between the outer core winding and the shield. The minimum clearance between the shields and the oil containment tank was set at 4".

Longitudinal distances of new core to shield was 4" and existing core to shield was 5". Inter-core longitudinal separation was 3-1/2". The inter-shield separation was 8".

The plus/minus 500 kV, 500 ns specification requires re-evaluation of the distribution of potentials and the resultant radial and longitudinal electric fields. These fields are strongly influenced by the relative locations of the cores and shields.

Very little data existed on the limiting radial and longitudinal electric stresses for cores of this type. No data existed that PSI could determine for such limiting stresses as a function of the core manufacturing process, i.e., dry wound/oil immersed, dry wound/oil, acetate, or epoxy impregnated, or wet wound with acetate or epoxy.

PSI and Dr. A. Faltens developed a tentative core and shield layout using all new cores. This layout was made compatible with the beam pipe length increase dictated by the proposed Marx generator changes. The shield diameter is increased to 46', giving 7" of radial clearance between the outer core winding and the shield. The radial clearance between the shields and the oil containment tank is set at 8" and the longitudinal clearance in the accelerating gap region is set as 8". Longitudinal distance of the cores to the shields inboard of the accelerating gap is 4" and in the region near the center of the module is 8". Inter-core longitudinal separations are 7", and the intershield separation is 18-1/2" (this space must hold off 1 MV for 500 ns and have grounding connections and support plates pass through the center).

49

The larger core shields and increased shield to tank spacings requires the tank height to be increased.

Resistors (300-500 ohms) positioned between each shield and the tank tapped at the R/4 and 3R/4 points are proposed to establish equal voltages on the cores. Assuming equal voltage distribution along the edges of the cores (125 kV on each edge), the turn to turn voltage is extremely low. Longitudinal fields are higher and the limiting fields are significantly influenced by the quality of the core winding impregnation.

Electrical testing of various winding and impregnation methods was considered vital to determining the best winding techniques and allowable operating stresses. In making the cost estimations in Appendix 2Q, PSI used an escalated price of $17,500 per core (the escalated price quotes discussed in Appendix R ranged from $11K dry wound to $37K wet wound). As the cores are the highest cost item (4 x $17,500 = $70,000 or $148,000 in the case of the highest bid from Ogalala Electronics), and the highest risk item, PSI recommended that NRL support an experimental test effort to assess allowable operating electric fields and an optimum manufacturing technique.

A compact 500 kV Marx generator was designed and fabricated by PSI capable of replicating the anticipated core waveform by means of series inductance/shunt capacitance, and a triggered gas crowbar switch. By this means, flat-top pulses could be obtained with representative risetime and falltime, with adjustable pulse width in the microsecond regime.

As presently conceived, the cores in the new induction module utilize 0.002" thick silicon steel and are required to operate at radial and longitudinal electric fields (in the dielectric) of approximately 50 kV/cm and 19 kV/cm, respectively. Impregnation of the silicon steel and interturn insulation with a dielectric is essential to achieve high radial and longitudinal electrostatic operating fields. Previous attempts by others to epoxy impregnate magnetic cores with polymerized resin have been reported to result in shrinkage upon curing which has degraded the magnetic properties of the core material. In addition, the epoxy has not adhered well to the typical interturn Mylar dielectric. Liquid dielectric impregnants have also been used. However, solid dielectric sealing barriers have typically been provided to allow the core to be easily transported and to operate in an environment of differing dielectric (such as oil or water).

Test cores, having a comparable aspect ratio to the proposed module cores, were wound on a 3" diameter, 2" wide mandrel. Approximately 1000 turns of silicon steel (2" wide) and Mylar or paper (2.5" wide) were wound on the mandrel to an outside diameter of 8.38".

Core testing involved stressing the core with a voltage pulse (50-400 kV) rising in about 100 ns (10 -90%) and decaying uncrowbarred in roughly 20 μsec (e-fold). This corresponds to radial fields in the dielectric in the range of approximately 45 to 360 kV/cm. The triggered crowbar switch enabled the cores to be stressed for times of 1 to 2 μsec for output voltages in the range of 150 to 400 kV. At output voltages below 150 kV, an attenuated version of the exponentially decaying voltage was applied across the test core, with a decay time constant of about 1.2 μsec.

51

The inner metallic mandrel and outer connecting metallic sleeve form, in
effect, two shorted turns. Thus, detection of dielectric breakdown in the
inner or outermost turns is difficult using only voltage diagnostics. A test
procedure was developed to commence at the new module core proposed design
stress level of 52 kV/cm radial field and 18.5 kV/cm longitudinal fields,
referred to as the nominal stress of X1. The test core was pulsed a number of
times at progressively higher stresses (for example, X1.5, X2.0, X2.5, etc.)
where the ratio of the radial to longitudinal field was kept the same. After
each test run at an elevated field, a repeat run was made at the X1 nominal
stress. By using a current viewing resistor to determine the peak current
flowing in the core, a correlation was found between a significant increase in
the peak current at an elevated stress level and a peak current increase when
returning to the nominal stress. At progressively higher stresses, the effect
was accentuated. While this technique indicates that an irreversible ahange
had mccurred someuhere within the core, it is not clear what this implies
concerning the magnetic properties of the core. The magnetic properties were
not investigated. It is conceivable that this change would not significantly
affect the core's performance. It is also possible that breakdowns which
could slightly affect the core's performance occur at lower stresses and
escape detection by this technique.

Two test cores were commercially fabricated for PSI by Ogalala using a
1/4 mil Mylar and a polyester wet winding technique. The test cores
fabricated by Ogalala for PSI appeared to contain many air pockets. The first
core showed signs of breakdown at levels below the X1 nominal stress. The
second core was vacuum impregnated with transformer oil in an attempt to fill

52

the air pockets. This technique appeared to increase the breakdown level to X2.4. The cores in use in the NBS 2 μsec LIA at NRL were fabricated by Ogalala using this same technique.

The peak core test stresses of the NBS LIA have been less than 2/3 of the new module nominal design stress. Operational electrical core stresses are thought to be even less than the 2/3 nominal level, and may explain how it has been possible to operate with cores using this fabrication technique.

Tests were performed using three PSI cores fabricated with 1/4 mil Mylar and transformer oil impregnated under vacuum. These cores showed a breakdown condition at levels of about 2.3, 2.5, and >3.0.

Another PSI core utilized two layers of 0.4 mil Kraft paper vacuum impregnated with transformer oil. The advantage of the Kraft paper is that impregnation is much easier due to the "wicking" action of the paper. To drive absorbed water out of the paper, the core was heated under vacuum to 135° for 48 hours, enabling a base pressure of less than 500 microns before impregnation with degassed transformer oil. The technique used to heat the core was somewhat novel in that approximately 100 volts AC was applied directly across the core (the core measured roughly 70 ohm DC). The core temperature was measured with a thermocouple and the temperature was controlled by a rheostat limiting the core current to about 1 amp. When tested, this core showed signs of breakdown at approximately X2.3.

As part of an Engineering Effectiveness Program, PSI developed a proprietary technique enabling the encapsulation of the core in epoxy, a

method which should not degrade the magnetic properties of the core material. In this program two cores were fabricated and tested by PSI. Each was fabricated with two layers of 0.4 mil Kraft paper: one was impregnated with unpolymerized polyester resin, the other with unpolymerized epoxy resin. In these two cases, the cores were not heated to drive the water out of the paper, but rather, a longer pumping time was used resulting in a comparable base pressure and a simplified procedure. In the case of the polyester, the resin was of sufficiently low viscosity that it was used at room temperature. However, the epoxy resin was degassed and poured at a temperature of 40° C to reduce the viscosity.

After impregnation, the polyester core was let up to atmospheric pressure and polymerized resin was poured onto one face and allowed to set. The process was then repeated on the second face. An important point in this procedure is that the surface of the unpolymerized resin is a few mm beneath the edges of the paper. Thus, the polymerized resin adheres to the edges of the paper forming a strong structure. When tested, this core gave indications of breakdown at the X2.8 - X2.9 level.

The unpolymerized epoxy resin impregnated paper core was encapsulated with catalyzed resin in a similar manner to the polyester one.

500 shots were initially performed at the level of 52 kV/cm radial electricl field and 19 kV/cm longitudinal electric field inthe dielectric. Thereafter 100 shots each were performed at the x1, x1.5, x2, x2.5,x3, x4, x5, and x6 levels. After each 100 shot sequence, a repeat run of 6 shots was made at the x1 nominal stress. As with the previous cores each sequence of the

54

peak core currents were averaged and the average peak current plotted versus
the test stress level which preceded that sequence. By way of example the
test data is shown plotted in Figure 2.4.1. Figure 2.4.1 was interpreted to
indicate breakdown at an electric stress level at the x5-x6 level. This
represents the highest stress level achieved. The fact that this high stress
level was achieved after a total of over 1,000 shots using encapsulated core
(compatible with easy storage and transportation) makes this core fabrication
technique very attractive.

In summary, the Ogalala Electronics wet wound polyester test core did not
operate satisfactorily at the new module proposed electric field stress levels
of 52 kV/cm and 19 kV/cm radial and longitudinal fields respectively in the
core dielectric. Other test cores utilizing various alternate dielectrics and
impregnation techniques did not show signs of electrostatic failure until
stress levels ranging from x2-3 to x6. The test core operating at the highest
electric field was an unpolymerized epoxy resin impregnated paper,
encapsulated in epoxy.

Before cost versus performance trade-off analyses were made on the
different core dielectric and fabrication options, PSI was asked by NRL to
examine the feasibility of a reliable 500 kV, 2 μs accelerating module. These
specifications were examined briefly and determined to require double the
number of cores.

Using four cores within each of two longer core shields results in the
length of the module tank (in the beam axis) increasing from approximately

55
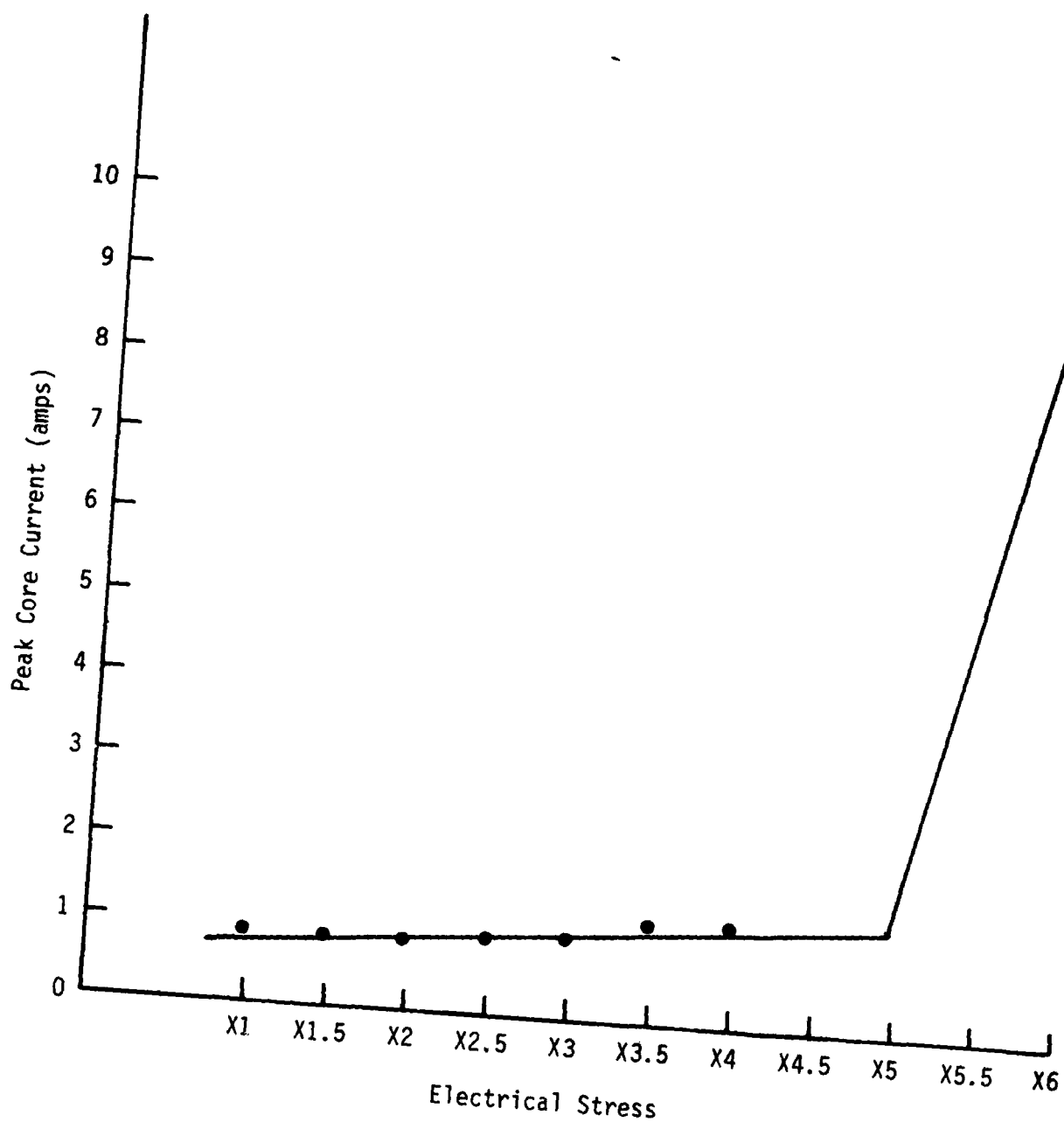
Figure 2.4.1 Core current vs. electric stress for an unpolymerized epoxy resin impregnated, Kraft paper dielectric, encapsulated test core

56

118.5 in. to about 145 in. At this point PSI reviewed alternate approaches to satisfy the current NRL specifications.

Assuming (a) the present injector is upgraded from the present 400 keV, 0.8 kA, 2 μs to 400 keV, 2 kA, 2 μs, (b) the existing linear induction accelerator is upgraded from the present 300 keV, 2 kA, 2 μs to 500 keV, 2 kA, 2 μs, and (c) a new module is designed and built providing 500 keV, 2 kA, 2 μs, the final output beam would be 1.4 MeV, 2 kA, 2 μs. A beam of this type could conceivably be produced by a single compact accelerator for a cost comparable to or less than that of the new module.

Recently PSI designed and built an electron beam generator for the University of Michigan consisting of an oil-insulated modified Marx run-down circuit, a command crowbar circuit, plus an oil/vacuum interface and diode region. In its present form the generator is capable of producing a 1 MeV, 10 kA electron beam of adjustable pulse length between 0.1 to 1.0 μs.

In this circuit a conventional Marx is placed in series with one or more "Ringing Stages" i.e. capacitors charged with reverse voltage. Inversion of the reverse charged stage/s during the pulse boosts the output voltage, which would otherwise droop due to the impedance decay of the diode load, compounded by the RC decay of the Marx into the load. By this means energy can be delivered from a Marx generator into a fixed or time varying load resistance with much increased efficiency and with an output voltage flatness of a few percent.

57

PSI chose this approach after examining and rejecting the available alternatives including the normal Marx rundown circuit and Guilleman Type E pulse forming networks (PFNs). Diode impedance decay and output pulse flatness specifications made these impractical, for reasons described below.

First, consider the PFN approach to the University of Michigan requirement. This might use a 2 MV Marx in which each stage is a Type E network. The output voltage into a matching impedance is then 1 MV. To compensate for a 6:1 impedance decay, the inductances of the L-C sections would decrease with distance from the switches. It is unclear whether an impedance change of 300 to 50 ohms can be accommodated in this way while maintaining $\pm$5% flatness in output voltage; but supposing that it can, then ten or more L-C sections would be needed in each PFN to give the voltage precision required. For a given impedance-time history, each inductance would need to be accurately calculated and set, or tuned. Whenever the time-history changed, for example because the diode was altered, new inductance values would have to be determined, and then each section of every Marx stage would need to be adjusted accordingly. This approach is obviously not practical in a pulser that is to be used for a variety of purposes in a research program.

Consider next a Marx rundown circuit to the University of Michigan requirment. Allow first of all that to limit capacitive voltage drop the Marx will store five times the energy required at the diode, or 50 kJ. This makes the capacitance 0.1 μF if the peak voltage is 1 MV. Extracting a charge of 10 mCb in order to deliver 10 kJ at 1 MV reduces the voltage by 100 kV, which is a drop of 10%. Additional voltage droop results from the increase in inductive voltage drop as the current increases during the pulse. If we

58

assume that the diode impedance is decaying exponentially with time (Z ≈ 300 exp - 1.8t to give a fall from 300 ohms at t=0 to 50 ohms at t=1 μs), then we find that di/dt increases from about 6 kA/μs at t=0 to about 36 kA/μs at t=1 μs. For a Marx and beam tube with a combined inductance of 3 μH, the increase in L di/dt throughout the pulse is about 100 kV. The total voltage droop is thus about 200 kV, or more than twice the University of Michigan specification.

To reduce the capacitive voltage drop, the Marx energy could be increased, but this would greatly increase the cost and the space required. To reduce the inductive drop, a very low inductance Marx (or parallel Marxes) could be employed; again the cost would increase greatly, and moreover the low driving inductance would make the crowbar circuit that terminates the pulse ineffective. Thus it is impractical to reduce droop by a factor of two by these means. Furthermore, studies at PSI have shown that effects other than capacitive droop and inductive droop also spoil the voltage flatness, namely (1) parasitic oscillations, (2) charge delivered to circuits introduced to damp parasitic oscillations, and (3) the increase of Marx resistive drop because of impedance decay.

Therefore what is required is a positive means of correcting the voltage droop, that is, a compensating mechanism that tends to increase the voltage during the pulse. The reverse-charged stage droop-compensating scheme was found to be very effective, mainly because it gives a rate of compensation that increases with time, matching the effect of impedance decay. The technique also has the great advantage that it can be tuned to a great extent by changes that are made quickly at the control panel - charging the inverted

59

Marx stage to a different voltage, or firing it at a different time relative to the remainder of the Marx.

This circuit has been studied for laser applications ("Pulse Power for 0.3-0.5 μs Durations", UCID 18318, Ian Smith, written under contract to Lawrence Livermore Laboratory, October 1979). However, to PSI's knowledge it had not been applied or investigated in practice in the U.S. Therefore PSI devised and carried out an Engineering Effectiveness Program to test the ability of the technique to improve the droop of a Marx rundown circuit.

The verification experiments were performed using the same stage Marx generator used for the core tests. One stage was modified for reverse-charge and inverted by a parallel spark gap and inductor. All stages were charged to 50 kV total ($\pm$ 25 kV). The erected Marx capacitance was 6.86 nF. The load was a 323 ohm resistor, giving a 2 μs e-folding decay time. The droop in the first 1 μs is therefore about 40% without compensation. The inverted stage was designed to give a 1 μs pulse with an approximately flat top. Figure 2.4.2 shows oscilloscope waveforms of the unmodified and modified Marx (one reverse-charged stage) firing into the fixed load described above. Figure 2.4.3 shows the modified Marx waveform on an expanded scale. The peak-to-peak voltage deviation is about 4.6 percent.

In this circuit the crowbar resistor was positioned in series with the load with the crowbar switch in shunt with the load, producing the rapid pulse falltime. The experiments showed that the approach worked in accordance with expectations. No difficulties were encountered. Where the shape of the

60
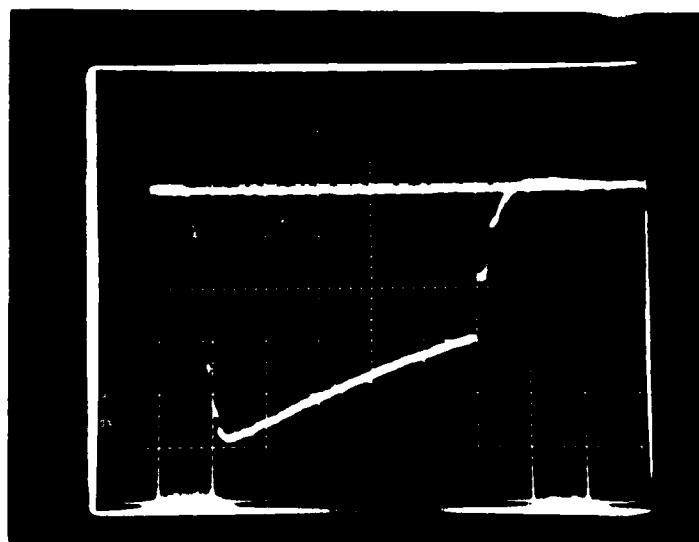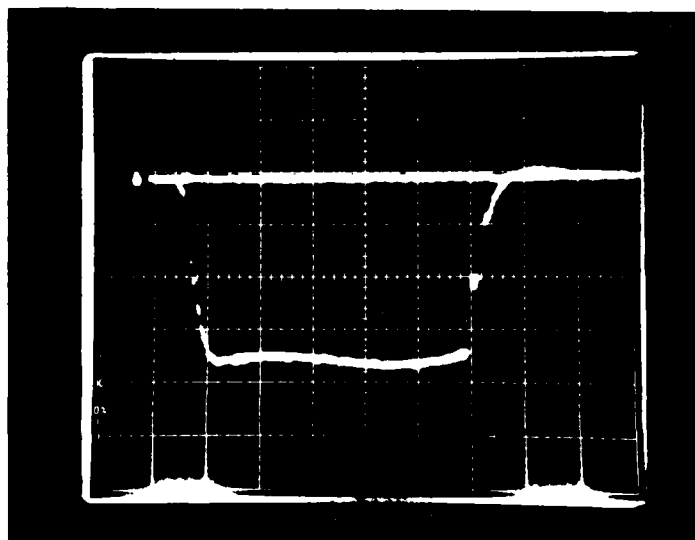
a)   69.4 kV/div

b)   69.4 kV/div
                                                                   200 ns/div

Figure 2.4.2   Unmodified and modified Marx waveforms

61
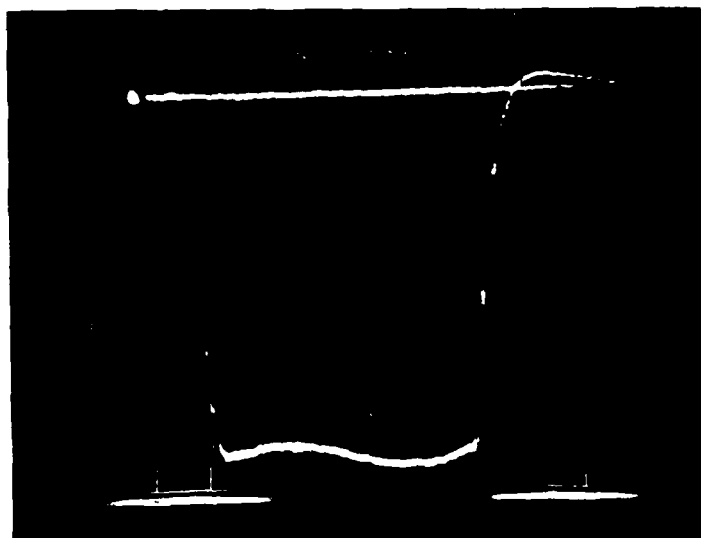
34.7 kV/div
200 ns/div

Figure 2.4.3   Modified Marx waveform - expanded scale

pulsetop could be compared with a simple circuit calculation, agreement was very good.

The 1 MeV, 10 kA, 1 μs electron beam accelerator for the University of Michigan is presently undergoing checkout prior to acceptance tests. Figure 2.4.4 shows a typical 1 MV, 1 μsec output pulse into a fixed 225 ohm load. The "knee" on the rise of the output pulse is due to coupling of Marx erection transients to the load via the capacitance of unfired Marx stages. The early time oscillations on the top of the pulse are caused by stray load capacitance and can be diminished in amplitude and duration at the expense of a longer output pulse risetime. The reduction in the oscillations is achieved by means of a capacitor and series resistor in shunt with the load.

In February 1984 PSI examined briefly the possibility of producing a 2 MeV, 3 kA, 2 μs electron beam accelerator using the Modified Marx run-down circuit concept.

A Childs Law diode load was assumed by PSI having a cathode area of 200 cm^2 an anode cathode spacing of about 221 cm, and a resultant plasma closure velocity of 1 cm/μs. This was based upon work performed by J.A. Pasour et al at NRL using the 2 μs NBS Linear Induction Accelerator.

Computations were performed using the diode load described above in combination with a Modified Marx run-down circuit consisting of a 14 stage Marx in series with 2 reverse-charged stages. In the test circuit each of the 28 capacitors comprising the 14 stage Marx were rated at 0.55 μF, 100 kV and were charged in the computation to 95 kV. The reverse-charged stages were

63
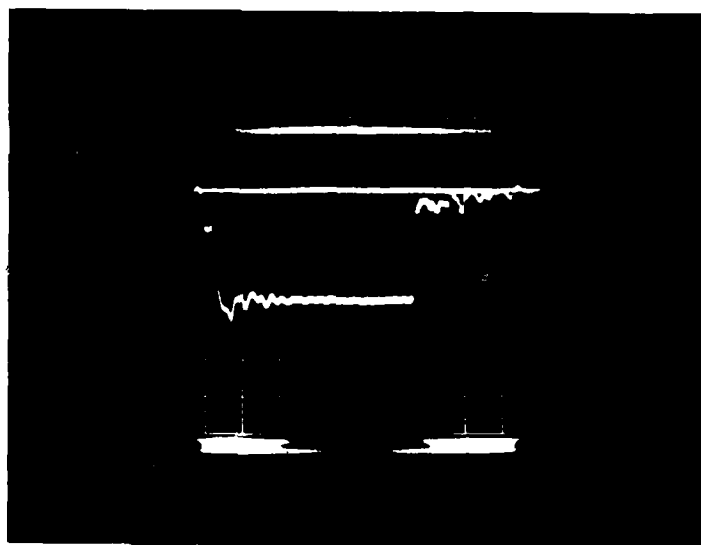
328 kV/div
200 ns/div

Figure 2.4.4   Electron beam accelerator output
voltage produced by a modified
Marx run-down circuit

rated at 0.4 µF, 100 kV and were charged in the computation to 90 kV. This corresponds to a total stored energy of 76 kJ.

Figure 2.4.5 shows a computer generated waveform resulting from the above circuit conditions. A Marx inductance of 7.8 µH was used, and a filter circuit of 6 nF and 240 ohms incorporated. Figure 2.4.5 shows a mean output voltage of 2 MeV $\pm$ 1.9% for 2.1 µs. In this flat top region the diode impedance is falling from 625 to 510 ohms while the current is increasing from 3.3 to 3.8 kA (a mean current of 3.55 kA). The peak amplitude of the voltage overshooot is 2.3 MV (17%). The energy delivered with $\pm$ 1.9% voltage flatness is a little over 14 kJ, resulting in a useful energy transfer efficiency approaching 20%.

At the present time size and cost analyses of this approach have not been made. However, providing a low-emittance electron beam can be generated at 2 MeV, the Modified Marx run-down circuit would seem to offer a compact, cost effective method of generating a 2 MeV, 3.6 kA beam having a voltage flatness better than $\pm$ 2% over a pulse duration continously adjustable up to 2 µs. The 2 MV Marx run-down circuit approach avoids the need for cores, reset circuits, separate modulators, multiple accelerating gaps, and numerous focus coils. This is to be compared to upgrading the injector to comparable current levels, upgrading the existing induction module to 500 kV, completing the final design and fabricating the new 500 kV, 2 µs induction module, and then only having a 1.4 MeV beam and pulse width control over the last 500 kV of beam acceleration.
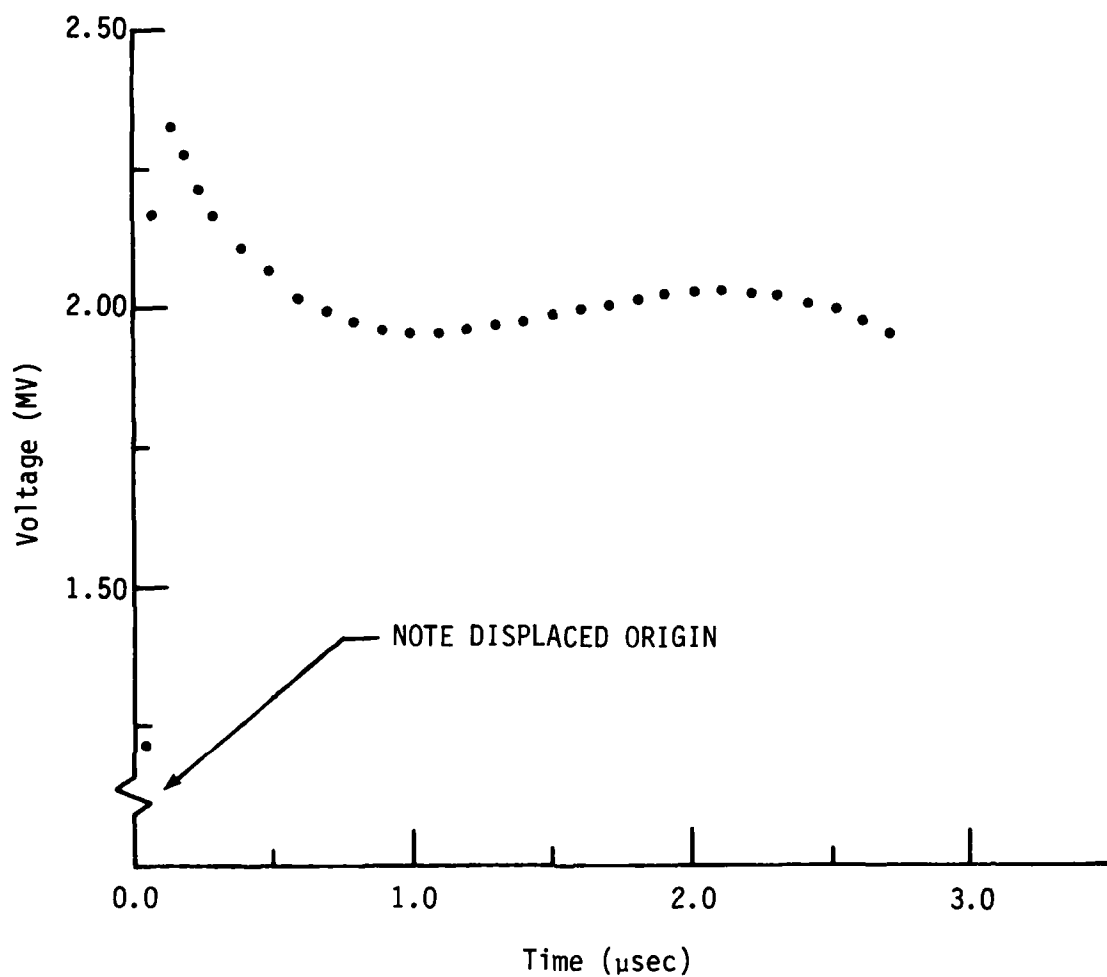
Figure 2.4.5   Computer generated, modified Marx
run-down circuit output voltage across
time varying diode load

SECTION 3
MODIFIED BETATRON ACCELERATOR

3.1 General

The principal subsystems of the NRL Modified Betatron Accelerator (MBA) include the air-core magnets, the mechanical structure, the vacuum system, the injector accelerator, and the pulse power capacitor banks. The preliminary MBA design parameters are an electron injection energy of 1-3 MeV, a circulating beam current of 1-5 kA, and an orbit radius of 1 m. The post-acceleration energy is 50 MeV.

The MBA concept uses an applied toroidal magnetic field (2-5 kG) to improve the stability and confinement of the multi-kiloamp E-beam. Twelve rectangular toroidal field (TF) coils are equally spaced azimuthally about the major (vertical, Z) axis. The TF coils are series connected to keep the current per single turn coil less than 1/4 MA. Eighteen circular vertical field (VF) coils are located within the TF coils. The VF coils accelerate the E-beam and provide the correct field and index at the orbit and satisfy the betatron flux condition. Each coil is connected to a coaxial lead that is

series connected to the VF buswork. In addition to the main VF coils, there are three single turn trimmer coils in parallel with the VF coil circuit. One trimmer is located on the midplane and primarily effects a few percent change in the flux within the orbit. The other two trimmers are located directly above and below the torus minor axis. The purpose of these two coils to change the field index.

The final choice of about 3 ms as the MBA acceleration time was based upon a compromise between a) a short acceleration to reduce the time available for instability growth, and b) a larger acceleration to obtain low field and index errors by permitting penetration of magnetic fields through the chamber walls.

Two auxiliary magnetic field coil systems are employed in addition to the VF and TF coils. These are the capture field (CF) and image compensation field (ICF) coils. The CF coils produce a B_z field inside the torus to move the beam equilibrium position away from the injector during the first poloidal bounce period. The ICF coils compensate for the self-field diffusion associated with the decay of the beam image currents.

PSI was tasked with generating initial designs of a) MBA injector options, b) connections between the MBA TF coils and corresponding buslines, c) vacuum chamber joints, d) the optimum structural frame including coil and vacuum chamber mountings capable of withstanding the electromagnetic and atmospheric forces, and e) the power supplies for the TF, VF, CF, and ICF coils.

A conceptual design review was held at NRL in December 1982, at which time the results of PSI's conceptual design efforts were presented to both NRL staff and an independent review panel. Following this review meeting PSI was asked to support an MBA demonstration experiment wherein an externally generated kiloampere electron beam will be injected into the toroidal chamber with an existing toroidal field level of about one kilogauss and a vertical field of about 60 gauss. The experiment is designed to test beam capture and stability over periods of the order of the magnetic diffusion time of the conducting chamber wall (few μsecs) and will not attempt acceleration of the beam to higher energies using the induced fields from a rising vertical field. After successful demonstration of beam capture, NRL plans to proceed with construction of the full scale betatron device, and acceleration of the electron beam to 50 MeV kinetic energy.

The reduced objectives of the demonstration experiment require only about one quarter of the full TF bank energy, a modest power supply for the VF coils (to be designed and constructed by NRl) as opposed to the 1 MJ energy of the full VF bank, and a power supply for the CF coils. PSI was tasked however, with designing the full energy (~3 MJ) TF bank in anticipation of the upgrade after the demonstration experiments. Thus, the TF bank is to be amenable to operation at the one quarter energy level, with a full energy capability through the simple addition of capacitors and associated electrical components.

NRL is currently developing revised specifications for the ICF and CF coils. The revised specifications will be used by PSI to perform detailed

69

modeling of the circuits and of the mutual inductances between the coils including the boundaries.

The mechanical support given by PSI to the MBA support structure is given in subsection 3.2. The design of the MBA power supplies and associated hardware is presented in subsection 3.3. Subsection 3.3.3 describes the conceptual design of the TF, VF, CF, and ICF power supplies. In subsection 3.3.4 the preliminary design of the TF supply is documented. Subsection 3.4 describes work performed by PSI in support of the MBA E-beam injection task.

3.2 Mechanical Engineering Support For the Modified Betatron

3.2.1 General

PSI provided Mechanical Engineering support for the following portions of the Modified Betatron: a) the Betatron structure, b) the vacuum vessel, and c) the coaxial coil connections. The work included conceptual design, material and vendor searches, and design of prototype assemblies. The following subsections discuss the work performed in each area. The discussions are supplemented by documents in the appendices which were developed and sent to NRL during the course of the work.

3.2.2 Structure

PSI provided a conceptual design for the modified Betatron support structure. The conceptual design was in the form of simple sketches and

supported by rudimentary backup calculations. Appendix 3A is a letter report summarizing the structure conceptual design effort.

One of the main design issues was to provide a structure that would be stiff enough to keep deflections to a minimum during toroidal and vertical field coil operation without unnecessarily restricting access for installation, maintenance, and repair of system components required inside the overall machine envelope.

General alternate designs were examined for the structure as discussed in Appendix 3A. The preferred candidate is a triangular shaped structure (when viewed from the top) as shown in attachment 110 of Appendix 3A.

The design consists of triangular top and bottom structural platforms separated by columns at each apex of the triangular platform. A center tubular structure passes through and is fastened to the top and bottom structures. The entire assembly rests on a base which could include provisions for rotation of the assembly about a central vertical axis or translation along tracks on the floor. Toroidal field coils, vertical field coils, and the vacuum vessel are installed between the top and bottom structure in the sequence also discussed in Appendix 3A.

Two alternate top and bottom structure designs were examined in some detail. Both structures are of box type construction to provide stiff, relatively light structural assemblies. One consists of an aluminum and fiberglass re-inforced plastic assembly, the other an all-welded aluminum alloy structure.

71

Either a composite plastic or all aluminum structure could be used, however, for a specific allowable deflection, the composite structure would require a larger cross section to provide the stiffness equivalent to an all-aluminum structure. The lower modulus of elasticity for the composite material has to be compensated by a larger moment of inertia of a given structural element to achieve the same stiffness. Magnetic field requirements may be the determining factor as to which material is permitted in the top and bottom structures. Unlike tokamak structures, the conceptual design of the modified Betatron does not have diagonal braces between the top and bottom structures. Recognizing the fact that the torsion between the top and bottom structures is lower than in a tokamak, an effort was made to design a structure with adequate stiffness in torsion without resorting to diagonal braces which severely limit access to the vacuum vessel region. Initial calculations included in Appendix 3A indicate that the stiffness of the three columns shown in the conceptual design can adequately resist expected torsion loads. The size of the columns will depend, for a given torsional load, upon their radius from the center of the machine, the distance between the top and bottom structure, and the allowable space for the cross section of the column. In any event, if the columns cannot be designed to resist the full torsion load, additional shear panels can be added as discussed in Appendix 3A.

The center tube serves several functions. First, it helps resist axial forces which tend to force the top and bottom structures apart. Second, it provides a fixed surface for positioning the inner leg of the toroidal field coils.

The toroidal field coils, vertical field coils, and vacuum vessel are supported and held in place as shown in the conceptual sketches in Appendix 3A.

3.2.3 Vacuum Vessel Materials and Joints

PSI also assisted NRL in the selection of materials and conceptual design of the vacuum vessel for the modified Betatron. The major radius of the vacuum vessel is one meter with a minor inside radius of between four inches and eight inches. Ideally, the material would be magnetically transparent and be capable of withstanding a bakeout temperature of 200° C. This specification was later revised downward to 150° C, with a two-atmosphere pressure differential. Any joint or seal material would also have to meet these requirements.

PSI efforts were directed toward investigating non-metallic vessel materials with the exception of metal "C" seals and a stainless steel low eddy current loss flange design.

The materials reviewed by PSI included ceramics, polysil, and fused silica. The primary goals of the review were: 1) to determine if reliable pieces of the desired configuration could be produced practically by industry, and 2) if the pieces could be assembled to provide a vacuum vessel capable of operating in the high vacuum range.

Vacuum vessels using ceramic pieces of several configurations were considered. The configurations are: 1) toroidal segments of approxmately 40°

73

each, and 2) short, straight sleeves with beveled faces which would be used in quantity to form the torus.

Some of the 40° toroidal segments would be tee pieces with a port through the center circumference to accomodate beam injection and extraction and a part for diagnostic penetrations into the torus. At present, plans call for three tee segments with the side port -- and three plain toroidal segments.

Vendor contacts were made to determine the feasibility of each configuration. Notes from these vendor contacts are included in Appendix 3E, along with notes from discussions with knowledgeable people in specific fields of interest relevant to the vacuum vessel materials and joint design study.

As a result of the inquiry, it is apparent that ceramic tees of the quality required are impractical to manufacture by present fabrication techniques. Short sleeves, on the one hand, are practical to fabricate and could be assembled into a torus by first brazing thin, compliant cuffs to both faces of the sleeve and joining the cuffs by Heliarc welding. The cuffs would be braze assembled to the ceramic sleeves using a sandwich seal design and conventional braze assembly procedures for ceramic to metal joints. These procedures are discussed in sections 402 and 404 of Appendix 3E.

The cuffed rings could also be joined by using a small cross section, low eddy current loss metal-to-metal joint as shown in Appendix 3B. The flange shown uses a Helicoflex "C" seal and a "V" band retainer ring to provide adequate compression in the seal and connect the cuffs of two adjacent rings together.

74

Two contacts who were very helpful and knowledgeable about ceramics and ceramic-to-metal seals were Harry Bell of Wesgo and John Richter of Eimac. The notes from conversations with both are included as items 402 and 404 respectively in Appendix 3E.

Polysil was considered as a possible alternative to ceramic as a material for fabrication of the vessel segments. From conversations with several people who have had experience with the material, additional development work would be required to arrive at a formulation which would provide consistent material properties. Additionally, the material would probably not meet the bakeout requirement specified earlier.

Fused silica was the most recent material considered for the vacuum vessel segments. Of primary interest were the questions: 1) "Would it be possible to make toroidal shaped segments, and if so, who were the vendors who have the capability to produce them?" and 2) "What type of flanged joints and seals could be used between the segments?"

A letter report, Appendix 3D, sent to NRL November 1982, summarizes initial efforts to locate vendors of fused silica segments. The letter report also discusses some possible joint configurations which could be used to join segments of the torus together.

Additional effort was expended to locate vendors who have the capability and interest in producing fused silica toroidal vessel segments. A list of all vendors contacted and notes from discussions with company representatives

75

is included in Appendix 3E. Four potential vendors were located. They are 1) Haeraeus Amersel, Thermal American, Toshiba, and U.S. Quartz Fluorocarbon.

RFQ's were prepared and sent to the vendors at NRL's request. Haeraeus Amersil and Thermal American were to be contacted by Ross Trieman and Toshiba and U.S. Quartz Fluorocarbon were contacted by PSI. Copies of letters sent to Toshiba and U.S. Quartz Fluorocarbon are included in sections 428 and 444 respectively, of Appendix 3E.

Toshiba in particular has had experience manufacturing a fused silica torus previously as shown on the print in section 428 of Appendix 3E.

Of the two RFQ's sent by PSI, U.S. Quartz responded with a no bid. Toshiba has not responded beyond initial pre-RFQ communications.

It appears that the most practical way to build a torus at this point in time would be to use short ceramic rings with short metal cuffs attached on both faces as described earlier. The metal cuffs would then be connected mechanically by bolted on "V"-band retainers or Heliarc welded.

Any of the alternate ways to fabricate and assemble torus segments will require more design, analysis and prototype work before a practical, reliable alternate can be identified.

3.2.4 Coaxial Connectors for Vertical Field Coil Bus

PSI assisted NRL in the design of the vertical field Coil Bus Work Tee connector. The effort was to include 1) the review of the NRL designed connector including the bolted joint at each end of the Tee, 2) selection of a potting compound for the connector, and 3) location of vendors who have the capability to assemble and pot NRL supplied prototype components and manufacture complete coax connectors after prototype evaluation.

The NRL coaxial connector design was reviewed and comments made regarding provisions for bolting the connector into the bus work. Analysis revealed that the designs with two bolts per joint would probably mechanically fail in operation, so the design was changed to a 4 bolt pattern.

A number of vendors were contacted regarding various types of potting compounds for the coaxial connector. Douglas Engineering Company of Rockaway, New Jersey has a number of proprietary filled epoxies used to spot high voltage electrical feedthroughs for vacuum and high temperature applications. Several discussions were held with their Western Regional sales representative regarding potting of NRL supplied components and fabrication of complete coaxial connectors. The sales representative expressed lots of enthusiasm for the project however the company responded with a no bid to a request for quotation (RFQ) sent to them in September 1982. A copy of the RFQ and other notes relevant to coax connector potting are included in a progress report, Appendix 3C, sent to Dr. Jeff Golden in October 1982.

77

Isolation Design, a Sunnyvale, California company recommended by the Douglas Engineering Western Regional salesman, was contacted regarding potting compounds, potting, and coax connector manufacturing. Isolation Design and an affiliate company, Isolation Products, manufactures a variety of high voltage feedthroughs and connectors. Information on representative products is included in Appendix 3C.

Potting and manufacturing the NRL designed coaxial connector were discussed with Isolation Design on several occasions. Polyurethane and epoxy compounds were discussed as potential compounds to use in the connector with epoxy being the preferred material specifically a Hysol product EZ4183/HD3485. Notes from discussions with Jim Chron of Isolation Design are included in the Appendix 3-C progress report.

An RFQ was sent to Isolation Design for potting NRL supplied components and for manufacturing complete coax connectors. Isolation Design responded with a letter which included: 1) a summary of their understanding of the electrical requirements of the connector, 2) comments on potting materials relavent to the NRL designed coax connector, and 3) a proposal to build two prototype coaxial connectors of different design. Isolation Design felt the alternate design would be easier to purchase, stronger and have low impedance. The letter proposal including the alternate conceptual design are included in the Appendix 3C progress report.

3.3 MBA Power Supplies

3.3.1 Initial Design Efforts

In April 1982, PSI was asked to provide conceptual designs and rough cost comparisons for TF power supplies driving two different types of coil configuration: a) discreet coils (12) and b) a single coil - cylindrical shell with separate returns. For a maximum field of 5 KG, with chamber major and minor radii of 100 cm and 10 cm respectively, the magnetic field energy (E), approximately the same for both cases, is about 1.5 MJ. For the twelve turn coil the peak coil current (I) is about 210 kA and the circuit inductance (1) about 70 μH. For the single turn coil, the peak current is 2.5 MA and the circuit inductance about 0.5 μH.

For a time to peak current (T pk) of 20 msec, the voltage (V) on a capacitor bank driving the coils would need to be

$$V \approx (\pi/2) \times (L/T\ pk)$$

For case a) $V \approx 1.1$ kV, and for case b) $V \approx 100$ V. Using the relationship

$$C \gtrsim 2E/V^2$$

For case a) C 2.5 F, and for case b) C 300 F.

The 100 V (case b) operating level for the capacitor bank was ruled impractical due to switching and contact resistance problems. The use of astep-down transformer in conjunction with a higher operating voltage capacitor bank was considered. For example, high energy electrolytic capacitor banks have been designed and operated by both Lawrence Berkeley Laboratories (LBL) and Lawrence Livermore National Laboratories (LLNL). In 1961, a 0.08 F, 5kV, 1MJ electrolytic capacitor bank was designed and fabricated by LBL.

Electrolytic capacitors have unique properties. During the manufacturing of an electrolytic capacitor, the final process is usually that of "forming-in" the capacitor. The capacitor is charged to a voltage somewhat higher than its rated operating voltage over an extended period of time. This creates the aluminum oxide dielectric, whose thickness is dependent upon the voltage rating of the capacitor. The surface of the electrolyte-impregnated paper serves as an electrode. The presence of the electrolyte subsequently allows a certain measure of self-healing, should minute internal punctures of the dielectric take place.

When a dielectric puncture occurs during the forming-in of the larger capacitors, where 10 to 100 joules may be stored, an audible "tick" is produced. Empirically, it has been determined that the capacitor will heal itself if the energy delivered to the puncture is less than 100 to 200 joules. This is probably one reason why industry has limited the size of the largest units to that corresponding to a stored energy of about 100 joules. Should the energy delivered to the puncture (from paralleled capacitors, say) exceed 200 joules, the chances are high that the capacitors will remain permanently

80

shorted. This points out the need for current-limiting resistors, inductors, or fuses in banks where large numbers of capacitors are simply parallelled.

When a capacitor is discharged into an inductor, the voltage and current during the first quarter-cycle are both, say, positive. During the second quarter-cycle, the voltage goes negative while the current remains positive. During the third quarter-cycle both the current and voltage are negative. A fourth regime exists during the charging period when the voltage is positive and the current is negative. Electrolytic capacitors operate reliably in the first and fourth regimes. Note that in the second regime the polarities are the same ones (voltage -, current +) that exist if one tries to charge the capacitor in the reverse direction. Even though the capacitor would be destroyed under dc conditions, the Berkeley banks have demonstrated that short but frequent excursions into this second regime can be tolerated indefinitely with no apparent adverse effects. The Berkeley switches (ignitrons) open at the end of the second regime, when the current is zero and the capacitor voltage is maximum negative. This permits avoiding the third regime, about which there is little information. The negative voltage left on the capacitor is found to decay in a time of the order of one second, dissipating the energy internally in the form of heat. Several factors indicate that the effective capacitance, when the voltage is reversed, is frequently doubled or tripled, and that there is a shunt internal resistance of 100 to 500 ohm for the 1000 μF 450 volt units used in the LBL banks.

This ability to "ring negative" for a quarter-cycle can result in significant operational benefits and cost savings. First: high-coulomb crowbars to short the bank at zero voltage are no longer necessary. Second:

81

diodes paralleling the capacitors, sometimes used as brute-force protection against reverse voltage, are no longer necessary. Third: the bulk of the energy is returned to the capacitors where it can be removed by simple air cooling. The cooling requirements on the load inductance are thus vastly simplified.

Present electrolyte impedances are responsible for a minimum R-C discharge time (into a short circuit) of about 70 μsec for the units mentioned above. The high currents generated in this type of discharge create magnetic forces which generally cause the output tabs to break or pull loose from the foils after a limited number of discharges. Experimentally, it has been round that the minimum discharge time compatible with long life is about 200 sec. This corresponds to a peak discharge current of about 3500A.

In the second regime, hydrogen gas is normally evolved. The vent plug in the end cap allows this to diffuse out at a rate sufficient to prevent excessive pressure buildup.

For reasonable temperatures, the 1000-μF 450-V units should be operated with an average input power of 5 watts or less. The leakage current can vary from 1 to 12 mA, depending on how well they have been formed-in. The thermal time constant, without the usual paper jacket, is about 45 minutes.

To date, the LBL high-voltage electrolytic banks have been built in 5 kV 12.5 kJ modules. Each module is made up of a 12 by 12 series parallel array of 1000 μF 450 V capacitors. One size-A welding ignitron (type 5550) is included in each module to switch the shorter, higher currents. These tubes

82

are rated for 20 to 30 coulombs, but pass less than 5 coulombs in this application. To permit inclusion of a fault-sensing circuit (later discarded as unnecessary), one bank was built with the capacitors cross-paralleled with nichrome wire. This caused large capacitor losses during forming-in and was eliminated. The 12 series strings of capacitors are now parallel only at each end. Very reliable operation has resulted. A 2-W resistor was placed in parallel with each capacitor to aid in equal voltage division down the series string. These conduct about 2.5 mA at full capacitor voltage.

The LBL 5 kV megajoule bank consists of 80 modular drawers, each having its own charging supply, firing circuitry, and switching ignitrons. Even with a common variable ac primary charging supply, the individual module power supplies permit variations in voltage between drawers of up to 100 to 200 volts. Analysis indicates that in order to reliably fire all drawers a long pulse, or burst of pulses, is required at the ignitron ignitors. A 1.2 msec ignitor pulse is supplied to the ignitrons in the megajoule bank. This reliably fires all drawers, providing the bank is well formed-in.

The switching ignitrons and the power supply transformers provide complete isolation between the modules until the instant of firing. Ignitron prefires are virtually nonexistent.

The output cabling arrangement is such that the total current is always divided into five pairs of cables, regardless of the bank portion used. This divides the intercable forces by 25 and permits the use of easily manageable output cabling. Sufficient inductance is provided in the module-to-bus panel

cables to limit minimum discharge times to 200 sec or higher, should a fault occur at the bus panel.

In practice, it has been found that the time required for adequate forming-in for operation at the maximum rating of 5 kV is intolerably long (of order of 2 or more hours daily). Accompanying capacitor losses are high. For this reason, LBL considers the bank probably should have a practical rating of 4.5 kV, 800 kJ. For a true megajoule rating, it is felt that a 13 by 13 array of 450 V capacitors should be provided for each module, rather than the existing 12 by 12 array.

A 7.5 MJ electrolytic capacitor bank was built at LLNL in 1983. The bank delivers a peak current of 1 MA rising in 10 msec, and comprises 450 V capacitors operating plus/minus to give a 900 V output via SCR switching. The total cost of the bank in 1973 was about $1.5 M, or 20¢ per stored joule (with no loading added to the raw labor and material costs).

A design for example, consisting of 13 series 1000 μF electrolytic capacitors combined with a circuit of 13 parallel limbs would provide 1000 μF, 5 kV modules similar to the LBL design, A combination of 120 such modules (20,280 electrolytic capacitors) would provide the requisite 1.5 MJ, ignoring circuit losses. The 5 kV, 50 kA bank output would then be transformed down in voltage to the 1.1 kV, 210 kA or 100 V, 2.4 MA level to drive the TF coils.

Discussions were conducted with Stanganese, a specialty transformer manufacturing house in the Bay Area, with respect to achieving a 1.1 kV, 210 kA output, or a 100 V, 2.4 MA output from a transformer driven by an

84

electrolytic capacitor bank at the 450 V to 5 kV input level. The 100 V, 2.5 MA output for 20 msec time scales was ruled out as being entirely impractical. The 1.1 kV, 210 kA case was deemed viable, with certain caveats. Stanganese thought the transformer was likely to occupy about 80 cubic feet, weigh about 15,000 lb, and cost roughly $50 K. The transformer would have a secondary resistance of about 1.7 mΩ and a leakage inductance of about 60 μsec. The load time constant would be about 8 msec, requiring the TF bank time to peak specification to be reduced significantly from 20 msec.

This general design approach was discontinued when in June 1982, NRL revised the TF power supply time to peak current down from 20 msec into the region of 3-5 msec to reduce beam resonances in the MBA.

3.3.2 Capacitor Bank Design Philosophy

As of June 1982, the TF capacitor bank was required to a) store 1.4 MJ with a margin of safety of 400 kJ (1.8 MJ total), and b) deliver a peak current of 210 kA in 3-10 msec through a load inductance of 65 M (exclusive of buss and capacitor bank inductance). The VF capacitor bank, on the other hand, was required to a) store 650 kJ with a margin of safety of 200 kJ (850 kJ total), and b) deliver a peak current of 45 kA in 3-5 msec through a load inductance of 625 μH (exclusive of buss and capacitor bank inductance).

For the TF capacitor bank the above specifications required a bank capacitance and maximum charge voltage of 516.5 mF, 2.64 kV and 46.5 mF, 8.8 kV for times to peak current of 10 msec and 3 msec respectively. For the VF capacitor bank the above specifications required a bank capacitance and

85

maximum charging voltage of 21.8 mF, 8.84 kV and 7.87 mF, 14.7 kV for times to peak current of 5 msec and 3 msec respectively. It can be seen that the revised specification had the effect of raising the range of charging voltage to between 2.64 and 14.7 kV.

In this voltage range a caster oil impregnated paper capacitor was chosen as the preferred energy storage component design for both capacitor banks. These capacitors are a mature product and have been used in numerous capacitor banks over a period of 35 years. They are preferred over other types of capacitors because o) their reliability and cost. The mean time between failure (MTBF) requirement is a trade-off between capital and operational costs. The approach used was to design to the lowest cost with an MTBF acceptable to system operation.

Increased energy density lowers the capacitor MTBF and the capital cost. For a given capacitor size, the increased energy density minimizes the number of cases and bushings, and hence capacitor production costs. In addition, a reduced number of capacitors simplifies the electrical interconnects and mechanical support hardware.

Over the years large capacitor banks have evolved from being built out of 3 kJ units with lifetimes of > 1 x 10^6 shots, costing 18 cents per joule at 1.2 joules/cubic inch, through 5 kJ units with lifeimes of > 5 x 10^5 shots, costing 12 cents per joule, at 2 joules/cu in, to 12.5 kJ units with lifetimes of > 2 x 10^5 shots, costing 4 cents per joule at 4 joules/cubic inch. More recently, experimental units have been developed storing 25 kJ with lifetimes of > 1 x 10^4 shots, costing about 5 cents per joule at 6 joules/cubic inch.

86

On the basis that capacitor bank systems can be designed so that individual capacitor failures have negligible effect on system performance and do not require immediate replacement, the conceptual design of the TF and VF capacitor banks uas pursued on the basis of a 25 kJ capacitor unit design.

Additional features incorporated into the conceptual design were a) the use of a single rack structure to serve as both the capacitor case bus, the mechanical support for the capacitors, and be insulated from ground, b) all capacitors to be individually fused and protected against a bank short circuit with individual capacitor current limiting resistors -- in the event of a bank or bus short circuit all fuses to survive, in the event of a capacitor failure, only the fuse associated with the failed capacitor to blow, c) the fuses and current limiting resistors to be sized such that the maximum energy deposited in the failed capacitor not exceed the maximum charge voltage energy by more than 10% (assuming a 1 mΩ resistive short in the failed capacitor), d) ignitrons to be used as the output and crowbar switching elements -- ignitrons to be sized such that no damage is to result from a short circuit discharge of the capacitor bank, or from failure of a parallel switching element to fire, e) dual independent safety dump circuits enabling emergency discharge of the energy stored in the capacitors in internal dump resistors, either at the operator's discretion or automatically in the event of a power failure or interlock opening, f) the entire capacitor bank, switching, and dump circuitry operate in an ambient air environment, and g) the capacitor bank be coupled to the inductive load by up to 250 ft. of transmission line.
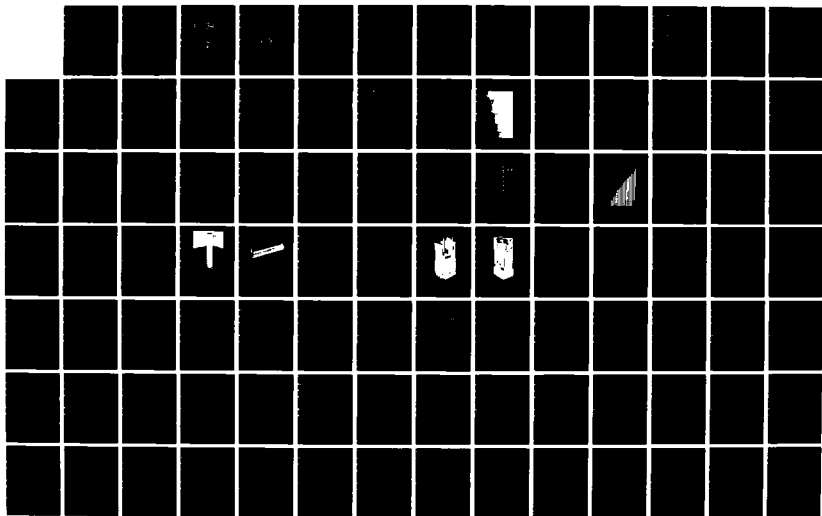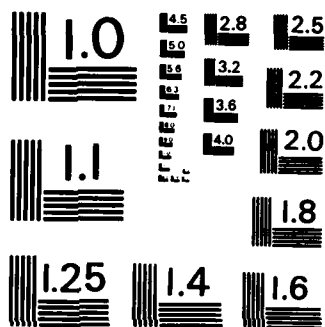
MICROCOPY RESOLUTION TEST CHART

NATIONAL BUREAU OF STANDARDS-1963-A

3.3.3 Conceptual Design of the MBA Power Supplies

3.3.3.1 General

The power supply conceptual design review was held at NRL in December 1982. The review pertained mainly to the megajoule VF and TF capacitor banks, however it did also cover in a more general form the few hundred joule pulse generators for the recently defined CF and ICF coils.

The VF coil configuration is shown in Figure 3.3.1. The VF power supply is also required to drive three trimmer coils. Ballast inductors in series with each of the trimmer coils allows for adjustment of the individual trimming coil current. Each series combination of trimmer coil and ballast inductor is in shunt with the vertical field coils. A matrix analysis was performed satisfying the various combinations of trimmer coil connections and mutual couplings. Seven percent of the VF current was assumed to flow through each of the trimmer coils. Thus a range of "effective" VF capacitor bank load inductance was determined. This effective load inductance was calculated as 458.3 μH plus/minus 9.6 μH. A value of 458 μH was used in subsequent computations.

The TF coil configuration is shown in Figure 3.3.2. Twelve rectangular TF coils are equally spaced azimuthally about the major (vertical) axis. The TF coils are series connected via coaxial buswork which include demountable joints that provide installation and maintenance access to the VF coils, the auxiliary coils, and the vacuum chamber. The TF capacitor bank load inductance was determined to be 90 μH.

C'_L

LOWER COIL ASSEMBLY
CONNECTED IN SERIES

UPPER COIL
ASSEMBLY

C_5

C_4

C_3

C_2

C_1

MIDPLANE
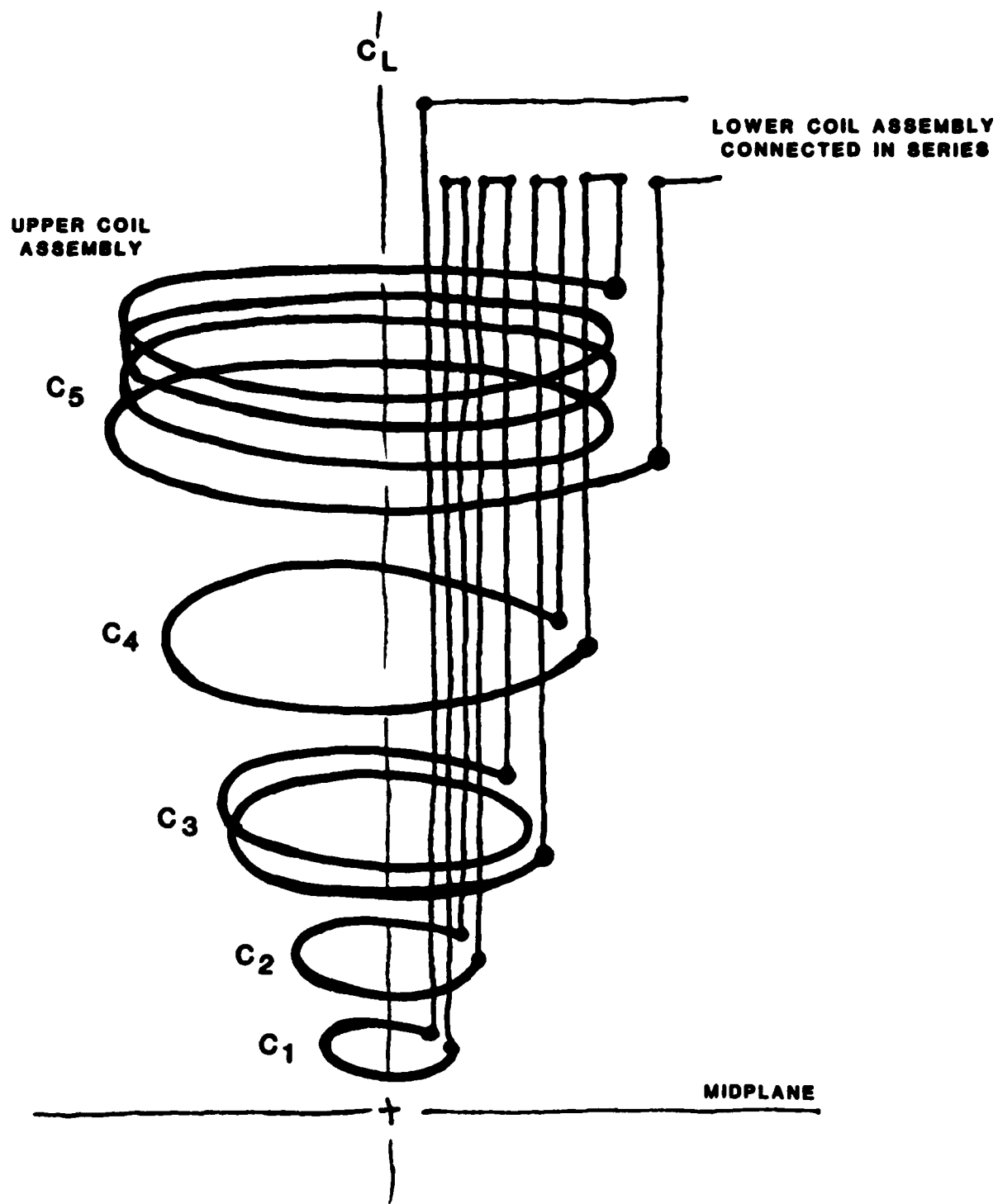
Figure 3.3.1 Vertical field coil configuration
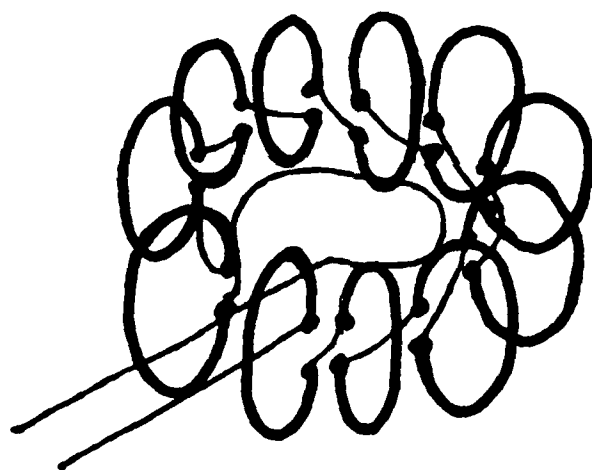
Figure 3.3.2 Toroidal field coil configuration

90

For given VF and TF magnetic fields at injection and at the end of acceleration, sets of required 1/4 sine wave charge times were defined for given acceleration times. Figure 3.3.3 shows the results of these computations based upon the following assumptions:

a) Betatron acceleration times of 1 to 3 ms

b) VF at injection 150 gauss

c) TF at injection 1,400 gauss

d) Peak VF (end of Accel.) 1,850 gauss

e) Peak TF (end of Accl.) 5,000 gauss

f) VF nominal peak current 54 kA (allows for 9 kA in shunt trimmer coils)

g) TF nominal peak current 210 kA

h) Maximum peak currents for both VF and TF capacitor banks to be 1.3 x I nominal

i) VF coils 590 μH, 1.63 mΩ (upper and lower coils in series 1/4" Cu over SST)

j) VF bus 8.7 μH, 2 m

k) TF coils 85 μH, 0.86 m

l) TF bus 4.1 μH, 0.44 m

Use of Figure 3.3.3 shows for example that for an acceleration time of 3 ms, the time to peak current (54 kA) of the VF capacitor bank should be 3.2 ms, and the time to peak current (210 kA) of the TF capacitor bank should be 3.6 ms.

91
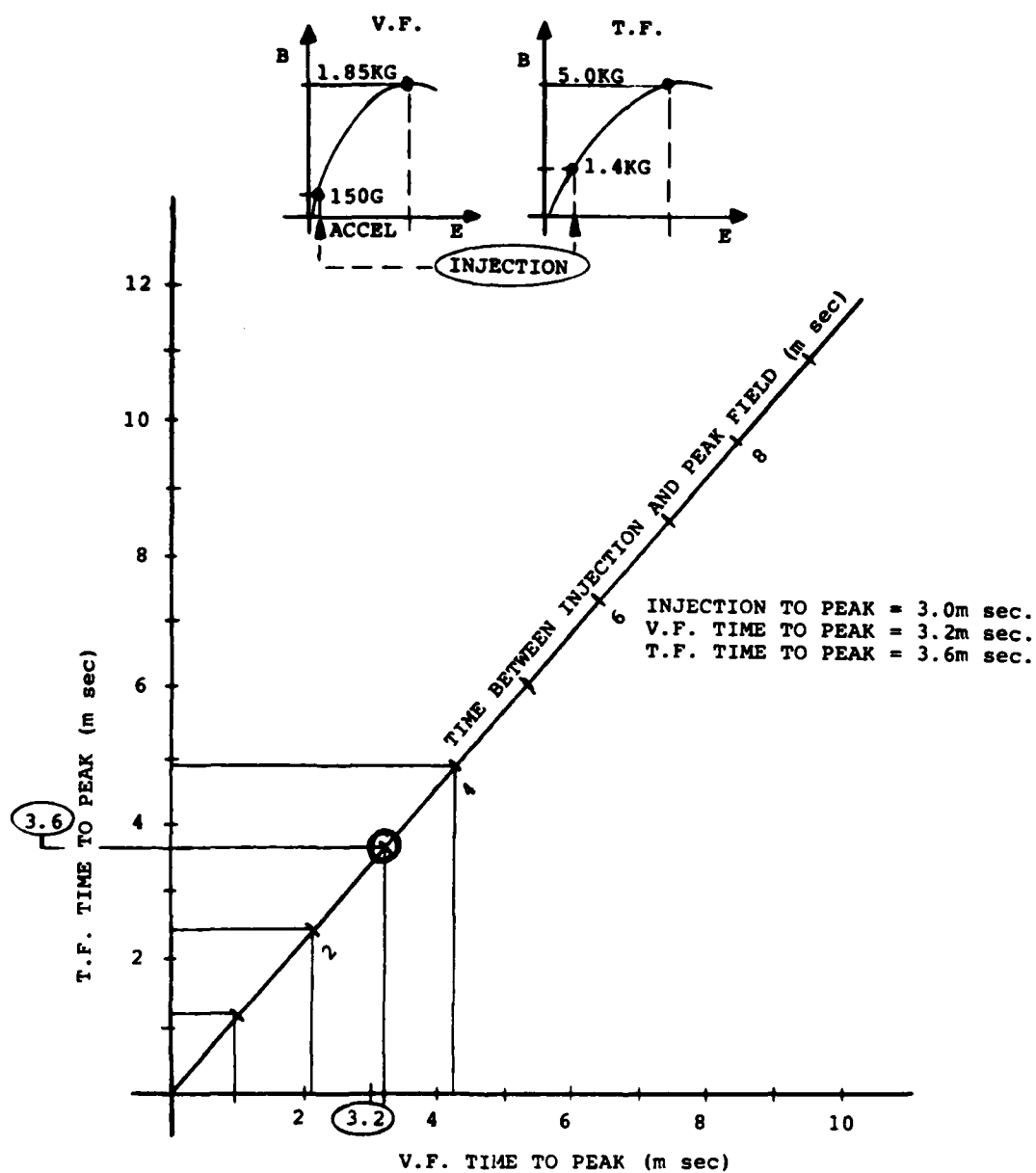
Figure 3.3.3 Vertical and toroidal field risetimes

The capacitor banks were initially designed on the basis of roughly optimized resistors placed in series with each capacitor and in series with capacitor groups (modules) to limit fault mode capacitor reversal. NRL guidance was followed in the likely location of the VF and TF capacitor banks, with 200 ft. and 135 ft. allowed respectively between the VF and TF capacitor banks and the load coils. In order to provide voltage insulation and reduce series resistance losses, 10 and 50 parallel RG-220 coaxial cables were assumed respectively between the VF and TF capacitor banks and load coils.

Under these assumptions the VF capacitor bank capacitance/nominal voltage/maximum voltage calculated to be 0.91 mF/40.6 kV/46.7 kV, 4.01 mF/19.3 kV/22.2 kV, and 9.19 mF/12.7 kV/14.6 kV for betatron acceleration times of 1 ms, 2 ms, and 3 ms respectively.

Similarly, the TF capacitor bank calculated to be 6.66 mF/25.7 kV/29.6 kV, 27.8 mF/12.6 kV/14.5 kV, and 61.6 mF/8.7 kV/10.0 kV for betatron acceleration times of 1 ms, 2 ms, and 3 ms respectively.

The bank operating voltages associated with the 1 ms acceleration time are considered high for safe operation in air. The 2 ms acceleration time maximum VF bank voltage of 22.2 kV is considered to be acceptable for operation in air. The 3 ms acceleration time operating voltages are considered to be very safe for operation in air. Initially, following the NRL desire to minimise the Betatron acceleration time, capacitor bank designs compatible with 2 ms were pursued.

Finally, NRL selected a 3 ms acceleration time. The required VF and TF capacitor bank firing sequence is shown in the two upper curves of Figure 3.3.4. The same TF capacitor bank design was adopted after NRL requested that the TF be kept roughly constant (plus/minus about 10 percent) during acceleration, by firing the TF bank earlier (about 2.2 ms before injection). The two lower curves of Figure 3.3.4 show the modified time phasing of the VF and TF capacitor banks.

The basic switching circuit for both the VF and TF capacitor banks is straight forward as shown in Figure 3.3.5. A capacitor bank is dc-charged and discharged into the inductive load to produce a 1/4 sine wave. The capacitor bank is then crowbarred at peak current to minimise capacitor voltage reversal. Ignitron switching is employed in both the discharge and crowbar circuits because of the large quantities of charge transferred (a few $10^2 - 10^3$ coulombs).

3.3.3.2 Circuit Selection

Figure 3.3.6 shows the parameters used in modeling the VF and TF capacitor bank/load coil circuits. The parameters selected allowed for damping resistance as well as inherent resistance and inductance associated with the capacitor bank and buswork, the series output switch, the crowbar circuit, the parallel cable connection between the capacitor bank and load, and the load.

Figure 3.3.7 shows examples of a large parameter scan which was made to assist in the selection of an optimum set of component values. The

94
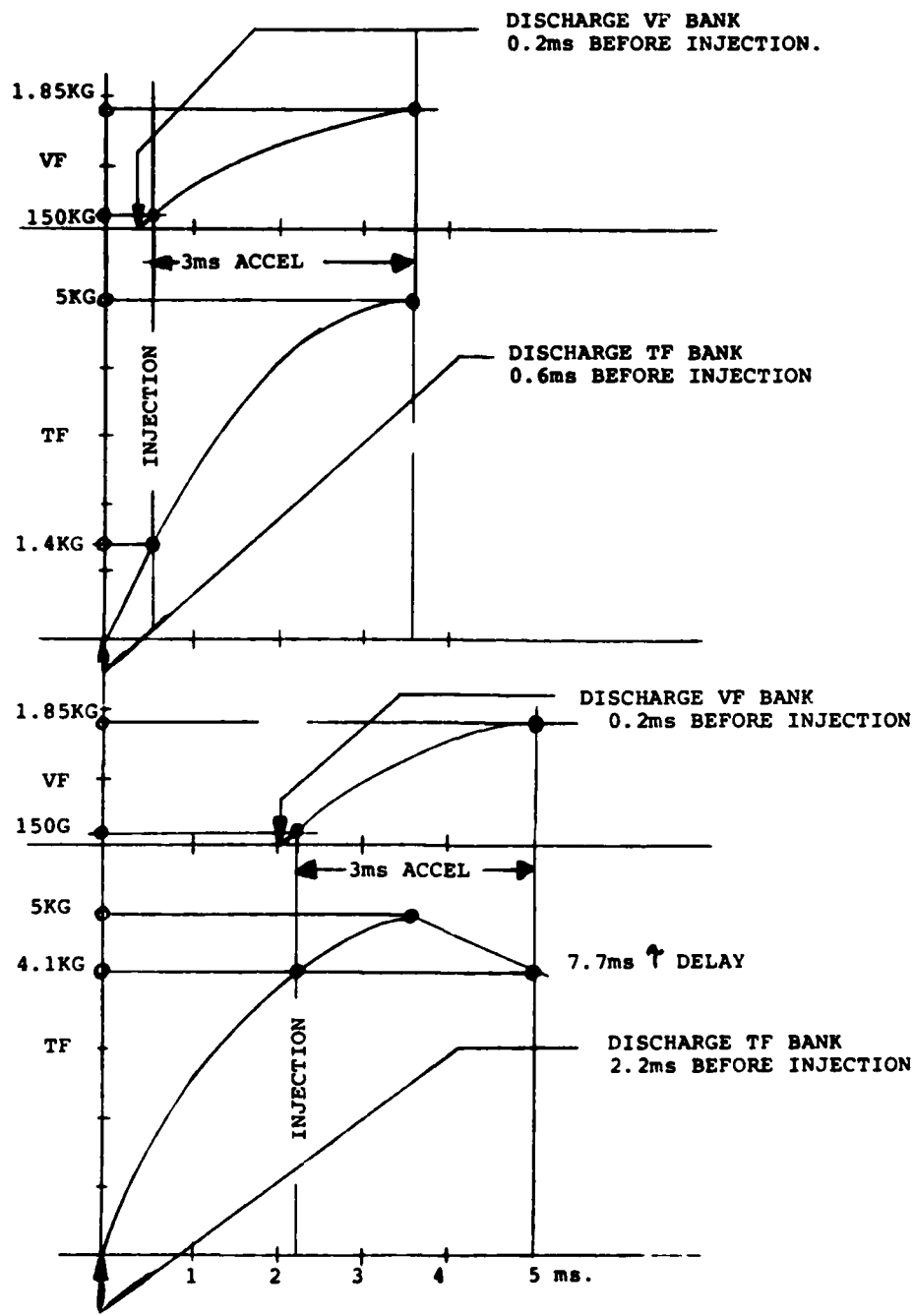
Figure 3.3.4 Vertical and toroidal field timing

Labels within figure:

DISCHARGE VF BANK
0.2ms BEFORE INJECTION.

1.85KG

VF

150KG

3ms ACCEL

5KG

DISCHARGE TF BANK
0.6ms BEFORE INJECTION

TF

1.4KG

INJECTION

DISCHARGE VF BANK
0.2ms BEFORE INJECTION

1.85KG

VF

150G

3ms ACCEL

5KG

4.1KG

7.7ms ↑ DELAY

TF

INJECTION

DISCHARGE TF BANK
2.2ms BEFORE INJECTION

1   2   3   4   5 ms.
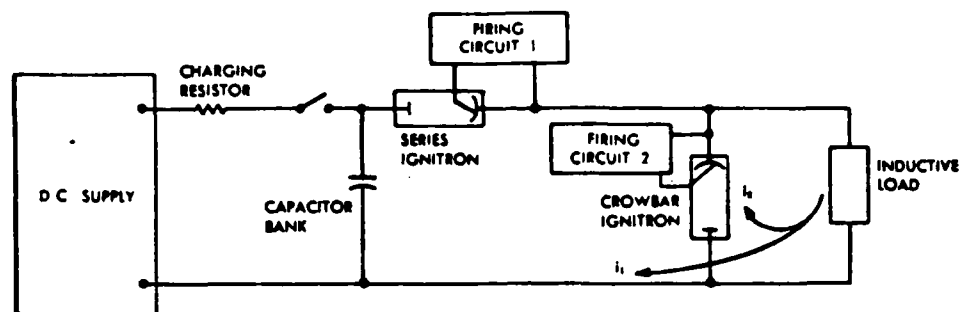
Discharge Circuit with Ignitron Crowbar
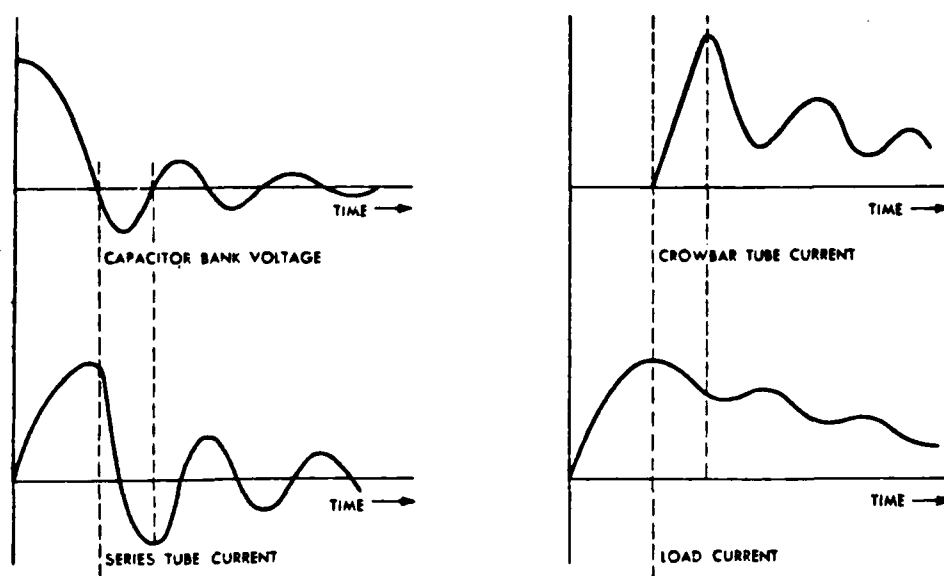
Capacitor Voltage and Currents in Complex Discharge Circuit

Figure 3.3.5 Capacitor bank switching circuits

VERTICAL/TRIMMER FIELDS

SERIES OUTPUT SWITCH   12 CABLES, 200'

2mΩ   0.25µH   6.47mΩ   1.25µH

1.36µH   0.83µH   498.9µH

CAPACITOR
BANK   CROWBAR
CIRCUIT

8.12mΩ   83.5mΩ

COMBINED
VF AND
TRIMMER
COILS

17.3mΩ

8.23mF

TOROIDAL FIELD

SERIES OUTPUT SWITCH   48 CABLES, 135'

0.5mΩ   0.25µH   1.09mΩ   0.21µH

2.12µH   1.0µH   89.1µH

CAPACITOR
BANK

2.39mΩ   9.0mΩ

TF
COILS

1.57mΩ

57mF

* INCLUDES ALLOWANCE FOR: BANK BUSWORK,
                            MODULE RESISTORS,
                            CAPACITOR RESISTORS,
                            CAPACITORS, & FUSES

Figure 3.3.6 Capacitor bank/load coil circuits

	VERTICAL FIELD		TOROIDAL FIELD			
C BANK	8.23	8.23	57	57	57	mF
V BANK	14.8	14.8	9.33	9.33	9.33	kV
E BANK	0.9	0.9	2.48	2.48	2.48	MJ
C REVERSAL	23.1	15.5	26.6	19.6	15.6	%
S_1 { IpK	54	54	209	209	209	KA
QT	178	159	815	739	697	Cb
$\int i^2 dt$	6.2	5.9	110	105	103	MA^2 sec
S_2 { IpK	41	46	160	189	224	
QT	250	363	1052	1580	2315	b
$\int i^2 dt$	6.4	9.5	106	164	252	sec
Coil { IpK	54	54	209	209	209	
R	17.3	17.3	1.57	1.57	1.57	
L	499	499	89	89	89	μH
		(with trimmers)				
R DISCHARGE CIRCUIT	33.9	33.9	5.6	5.6	5.6	mΩ
R CROWBAR CIRCUIT	107	74	17.7	11.7	7.7	mΩ
T IpK	3.2	3.2	3.6	3.6	3.6	m sec
T DELAY	4.7	6.8	5.1	7.7	11.7	m sec

● TENTATIVE PARAMETER SELECTION

Figure 3.3.7 Capacitor bank parameters

differences in the columns of VF and TF parameters are associated with differences in the crowbar circuits. Making the crowbar decay constant larger by decreasing the value of the crowbar circuit resistance increases the charge the crowbar switch must carry, and decreases the capacitor voltage reversal. Crowbar circuit decay constants of 4.7 ms and 7.7 ms were chosen respectively for the VF and TF capacitor banks, consistent with allowable capacitor voltage reversals, commerical ignition ratings, and the desire to hold the toroidal magnetic field approximately constant during acceleration.

3.3.3.3 Energy Dump and Shorting Systems

The capacitor bank charging discharge (energy dump) and shorting scheme is shown in Figure 3.3.8. The capacitor/load circuit is insulated from ground. Individual fuses and resistors are put in series with each capacitor. Capacitors are grouped into modules, with the modules connecting to a common output bus via module resistors. Two independent discharge systems operate a) via the common output bus, and b) via lateral intermodule resistors.

Because of symmetry the lateral resistors do not carry current during either a normal pulse or a bank output fault. Moreover, if the connection of a module resistance to the common output bus should fail, or if the module resistor should fail, there are two lateral paths to discharge the disconnected module(s). In addition, by connecting the second discharge circuit and the second shorting and grounding switches to the lateral resistor ring, the safety of the bank is further increased.

99
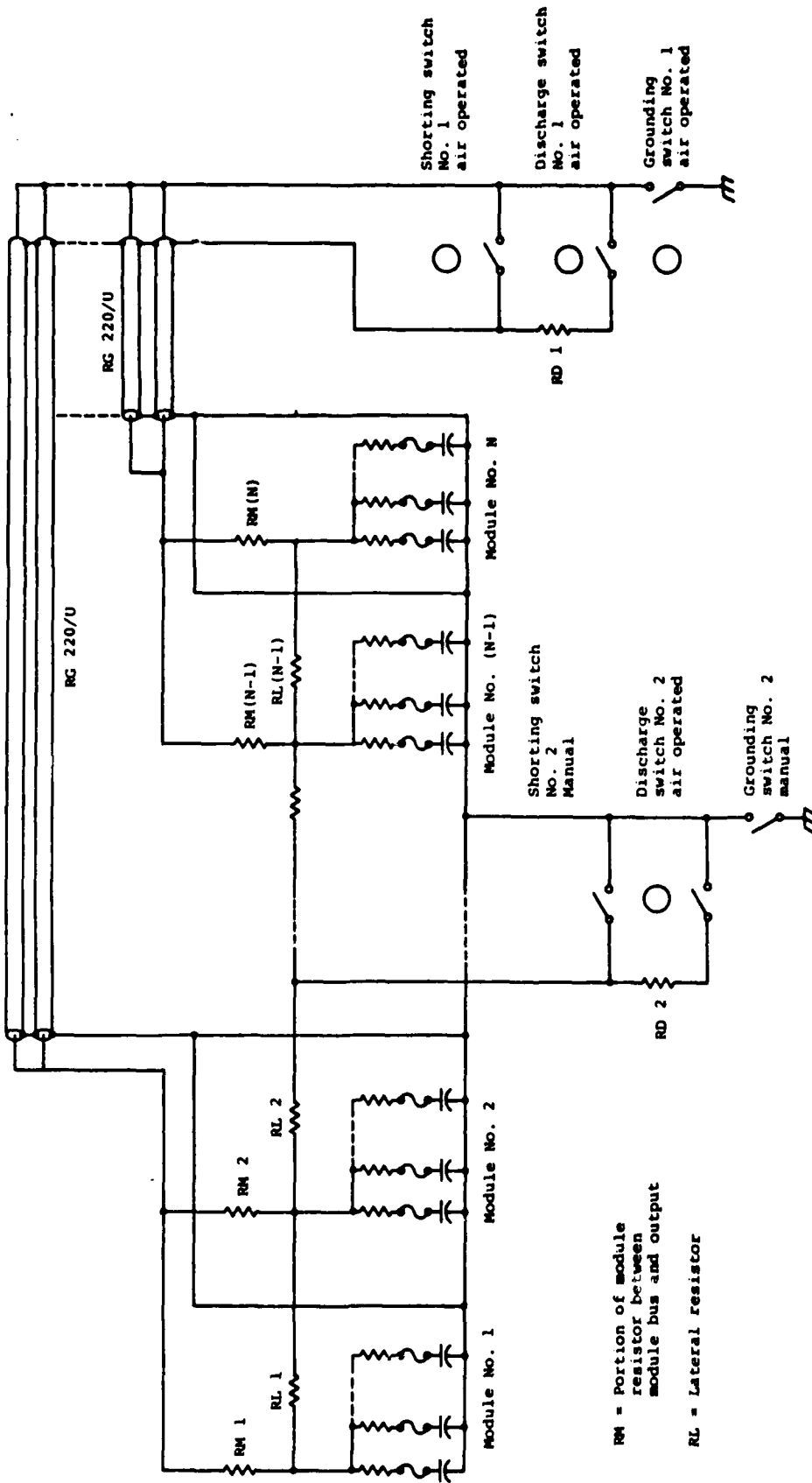
Figure 3.3.8 Protection resistors, discharge, and shorting switches

RM = Portion of module resistor between module bus and output

RL = Lateral resistor

Charging of the capacitor bank is accomplished via the primary discharge resistor (RD1). By this means the continuity of the primary discharge circuit is checked during the capacitor bank energisation process.

3.3.3.4 System Layout

Figures 3.3.9 and 3.3.10 show conceptual isometrics of the VF and TF capacitor banks respectively, including the output and crowbar switching system cabinet, and the bank and module discharge system cabinet. In the case of the VF bank 8 modules of capacitors are mounted symmetrically (four on each side) on a common metal support rack insulated from ground. Six 170 μF, 17 kV capacitors comprise each module for a total of 48 capacitors in the bank. In the case of the TF bank, 12 modules of capacitors are mounted symmetrically (six on each side) on a common metal support rack insulated from ground. Twelve 396 μF, 10.6 kV capacitors form each module for a total of 144 capacitors in the bank.

The rack structure serves as both the capacitor case bus and the mechanical support for the capacitors. The back-to-back arrangement of capacitors mounted to the rack ensures a very compact design, and easy visual and mechanical access to all components. The capacitors have their mounting brackets on the opposite end to the bushing. The capacitors are then cantilevered out on both sides of the case bus structure. The photograph shown in Figure 3.3.11 employs a similar capacitor bank layout. This 15 MJ capacitor bank forms part of the Doublet III system located at General Atomic, La Jolla, California.

101

TOROIDAL FIELD CAPACITOR BANK: 57mF

normal operating level: 9.33KV, 2.48MJ stored

maximum capability: 10.6KV, 3.23MJ stored

BANK AND MODULE
DISCHARGE SYSTEM CA
- BANK DISCHARGE   S\
- BANK SHORTING   S\
- BANK GROUNDING   S\
- MODULE DISCHARGE S\
- MODULE SHORTING   S\
- MODULE GROUNDING S\

OUTPUT AND CROWBAR
SWITCHING SYSTEM CABINET
- OUTPUT IGNITRON
- 2 PARALLEL INDEPENDENTLY
TRIGGERED CROWBAR IGNITRONS
EACH WITH SERIES RESISTOR ASSEMBLY
(ALL IGNITRONS, TRIGGER CIRCUITRY
AND SERIES CROWBAR RESISTORS
ISOLATED FROM GROUND)

CABLE TRAY
TO TOROIDAL
FIELD COILS

8 FT.

M
B

EXTREN IN

Figure 3.3.10 Toroidal field capacitor bank

BANK AND MODULE
DISCHARGE SYSTEM CABINET
BANK DISCHARGE . SWITCH NO. 1 AIR OPERATED
BANK SHORTING SWITCH NO. 1 AIR OPERATED
BANK GROUNDING SWITCH NO. 1 AIR OPERATED
MODULE DISCHARGE SWITCH NO. 2 AIR OPERATED
MODULE SHORTING SWITCH NO. 2 MANUAL
MODULE GROUNDING SWITCH NO. 2 MANUAL

10 FT.

28 FT.

LATERAL MODULE RESISTOR (STEEL

396 MICROFARAD CAPACITOR (1 OF 144)
NORMAL OPERATING LEVEL: 9.33KV, 17.2KJ S
MAXIMUM CAPABILITY: 10.6KV, 22.2KJ STORED

MODULE SERIES RESISTOR ASSEMBLY (1 OF 12)

CAPACITOR MODULE BUS (1 OF 12)

SERIES CAPACITOR FUSE (1 OF 144)

SERIES CAPACITOR RESISTOR (1 OF 144)

METAL CAPACITOR CASES MOUNTED VIA
BRACKETS TO COMMON METEL FRAME

EXTREN INSULATING SUPPORTS

pacitor bank

2

R OPERATED
R OPERATED
R OPERATED

R OPERATED
ANUAL
ANUAL

10 FT.

28 FT.
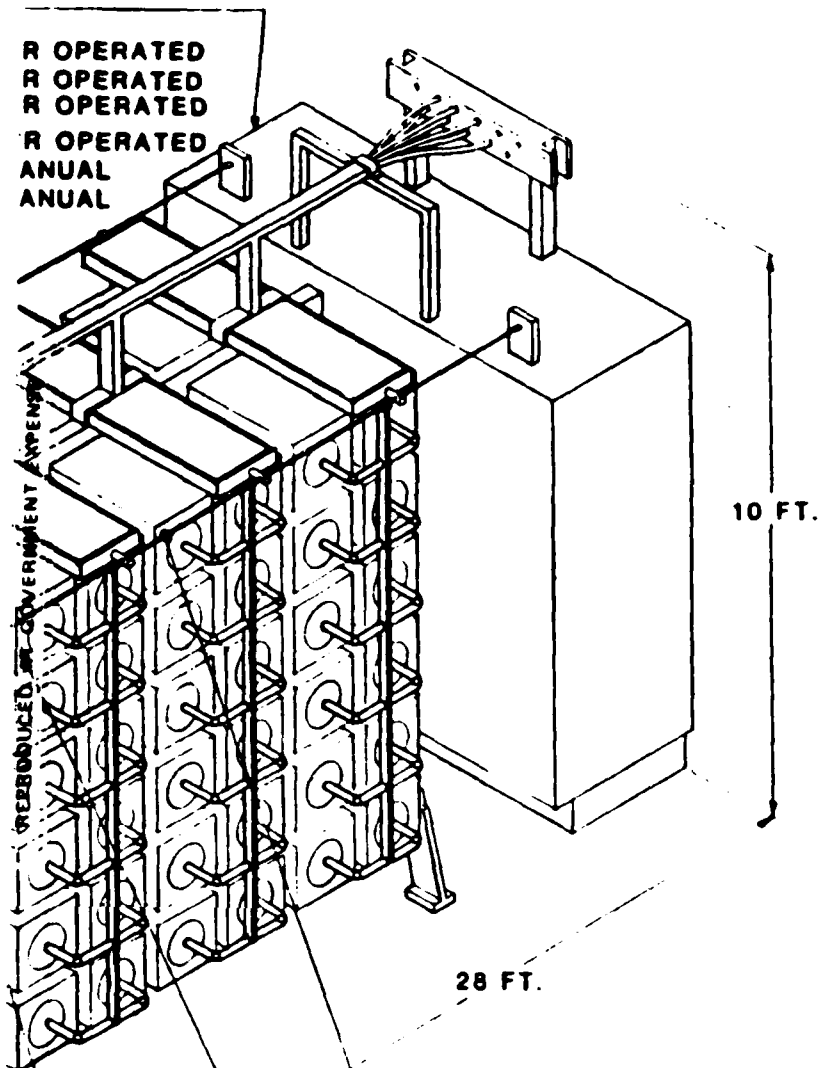
LATERAL MODULE RESISTOR (STEEL TUBE 1 OF 2)

396 MICROFARAD CAPACITOR (1 OF 144)
NORMAL OPERATING LEVEL: 9.33KV, 17.2KJ STORED
MAXIMUM CAPABILITY: 10.6KV, 22.2KJ STORED

MODULE SERIES RESISTOR ASSEMBLY (1 OF 12)

– CAPACITOR MODULE BUS (1 OF 12)

RIES CAPACITOR FUSE (1 OF 144)

APACITOR RESISTOR (1 OF 144)

OR CASES MOUNTED VIA
COMMON METEL FRAME

PORTS

QTY REQD	IDENTIFYING NUMBER		DESCRIPTION		ZONE	ITM NO
			LIST OF MATERIALS			

NEXT ASSY NO		BY	DATE			
UNLESS OTHERWISE SPECIFIED DIMENSIONS ARE IN INCHES	DR			PULSE SCIENCES INC		
✓ MAX ALL MACHINED SURFACES	CHR					
BREAK ALL SHARP EDGES 1/64 MAX REMOVE ALL BURRS	DES			NRL		
	ENGR	P. HANLING		BETATRON POWER SUPPLIES		
TOLERANCES				TOROIDAL FIELD CAPACITOR BANK		
DECIMALS	FRACTIONS			CODE IDENT NO	SIZE	DWG NO	REV
.X					D	10311	
.XX	ANGLES						
.XXX				SCALE		SHEET	
DO NOT SCALE THIS DRAWING							

3

VERTICAL FIELD CAPACITOR BANK: 8.23mF

normal operating level: 14.8KV, 900KJ stored
maximum capability: 17KV, 1.17MJ stored

102

CABLE TRAY

OUTPUT AND CROWBAR
SWITCHING SYSTEM CABINET
• 1 PARALLEL OUTPUT IGNITRON
• 3 PARALLEL INDEPENDENTLY
  TRIGGERED CROWBAR IGNITRONS
  EACH WITH SERIES REGISTOR ASSEMBLY
  (ALL IGNITRONS, TRIGGER CIRCUITRY
  AND SERIES CROWBAR RESISTORS
  ISOLATED FROM GROUND)

CABLE TRAY
TO VERTICAL
FIELD COILS

8 FT.

EXTR
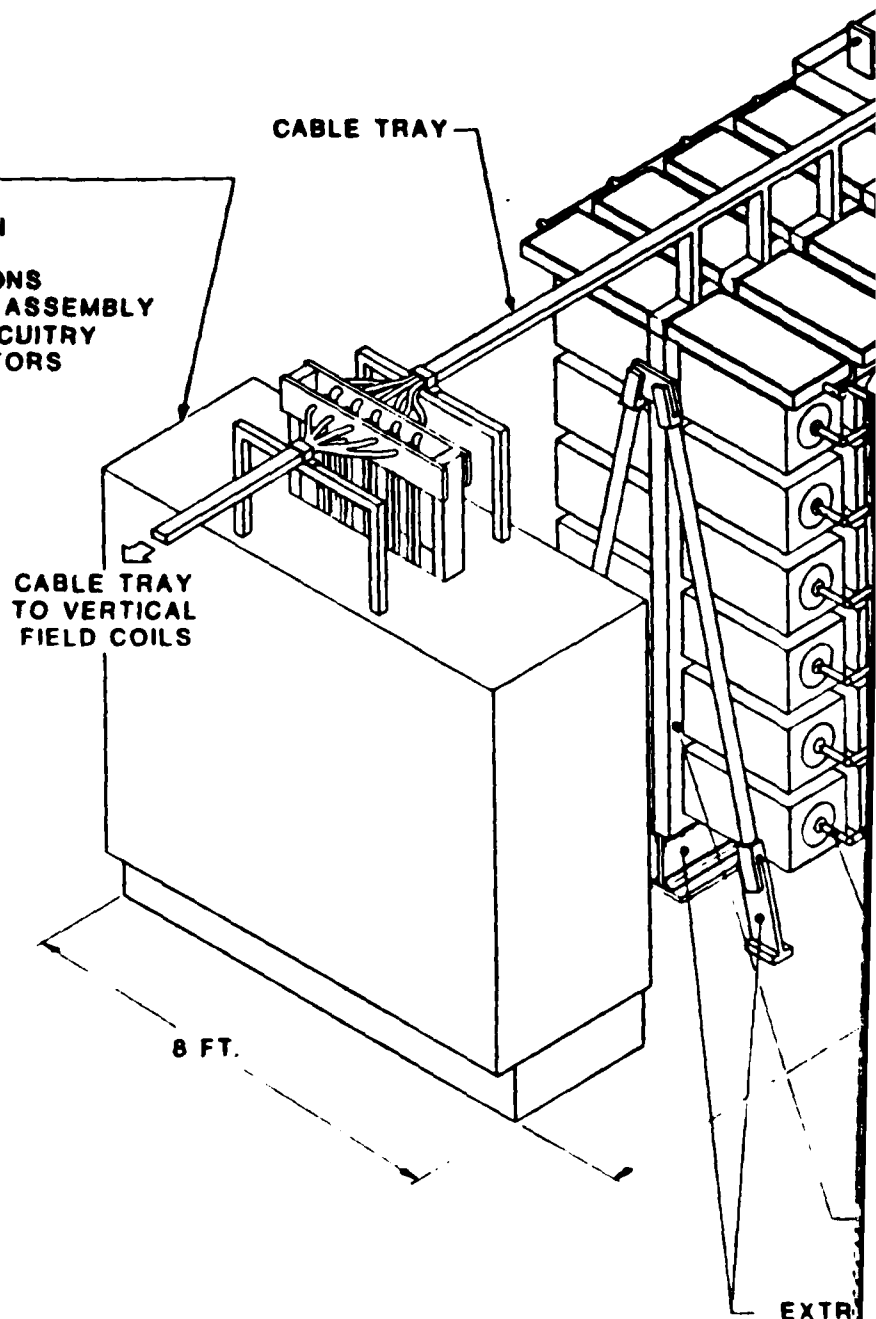
Figure 3.3.9 Vertical field capacitor

BANK AND MODULE
DISCHARGE SYSTEM CABINET
- BANK DISCHARGE   SWITCH NO. 1 AIR OPERATED
- BANK SHORTING   SWITCH NO. 1 AIR OPERATED
- BANK GROUNDING   SWITCH NO. 1 AIR OPERATED
- MODULE DISCHARGE SWITCH NO. 2 AIR OPERATED
- MODULE SHORTING   SWITCH NO. 2 MANUAL
- MODULE GROUNDING SWITCH NO. 2 MANUAL

10 FT.

16.5 FT.

LATERAL MODULE RESISTOR (STEEL TUBE

172 MICROFARAD CAPACITOR (1 OF 48)
NORMAL OPERATING LEVEL: 14.8KV, 18.8KJ STOR
MAXIMUM CAPABILITY: 17KV, 24.9KJ STORED

MODULE SERIES RESISTOR ASSEMBLY (1 OF 8)

CAPACITOR MODULE BUS (1 OF 8)

SERIES CAPACITOR FUSE (1 OF 48)

SERIES CAPACITOR RESISTOR (1 OF 48)

METAL CAPACITOR CASES MOUNTED VIA
BRACKETS TO COMMON STEEL FRAME

EXTREN INSULATING SUPPORTS

:apacitor bank

2

BANK AND MODULE
DISCHARGE SYSTEM CABINET

- BANK DISCHARGE   SWITCH NO. 1   AIR OPERATED
- BANK SHORTING   SWITCH NO. 1   AIR OPERATED
- BANK GROUNDING   SWITCH NO. 1   AIR OPERATED

- MODULE DISCHARGE   SWITCH NO. 2   AIR OPERATED
- MODULE SHORTING   SWITCH NO. 2   MANUAL
- MODULE GROUNDING   SWITCH NO. 2   MANUAL

10 FT.

5 FT.

LATERAL MODULE RESISTOR (STEEL TUBE 1 OF 2)

172 MICROFARAD CAPACITOR (1 OF 48)
NORMAL OPERATING LEVEL: 14.8KV, 18.8KJ STORED
MAXIMUM CAPABILITY: 17KV, 24.9KJ STORED

MODULE SERIES RESISTOR ASSEMBLY (1 OF 8)

CAPACITOR MODULE BUS (1 OF 8)

SERIES CAPACITOR FUSE (1 OF 48)

S CAPACITOR RESISTOR (1 OF 48)

ITOR CASES MOUNTED VIA
COMMON STEEL FRAME

SUPPORTS

2
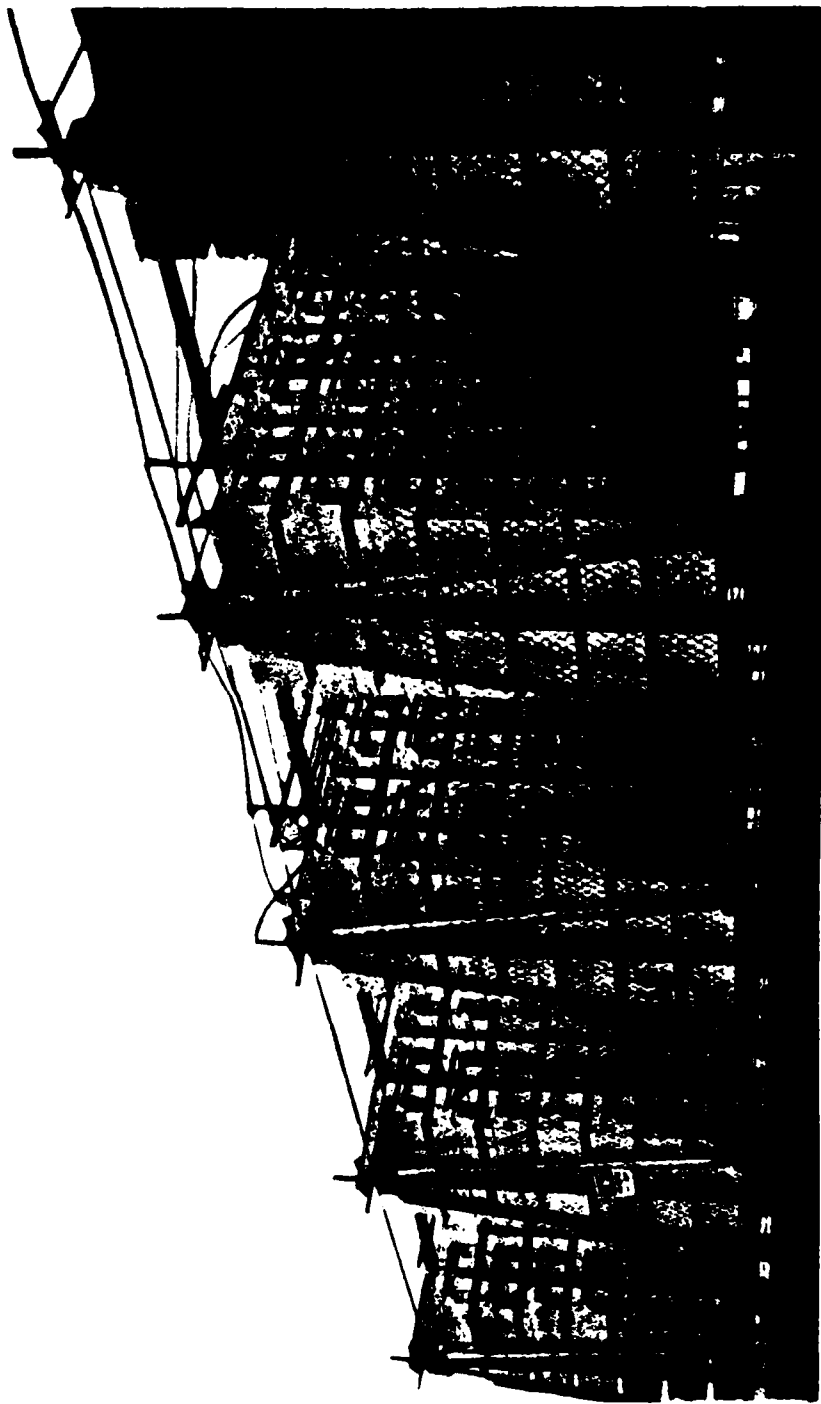
Figure 3.3.11 15 MJ bank at general atomic installation La Jolla, California

3.3.3.5 Energy Audit

Figure 3.3.12 shows an energy audit for the VF and TF conceptual designs, a) assuming a lossless discharge circuit, b) actual unavoidable losses, c) the energy required as a result of the fault protection circuitry, and d) the additional energy required to provide a 30 percent safety factor to ensure higher reliability at the specified peak output current and/or provide an energy reserve for potential future requirements.

3.3.3.6 Capacitors

The characteristics of the capacitors selected for the VF and TF conceptual bank designs are 172 μF, 17 kV and 396 μF, 10.6 kV units respectively (as shown in Figure 3.3.13. The VF and TF capacitors are required to operate at a nominal dc charge voltages of 14.8 kV and 9.33 kV and nominal peak discharge currents of 1-1/8 kA and 1-1/2 kA respectively, with a normal capacitor reversal voltage of about 20 percent. For VF and TF banks comprising 48 and 144 capacitors operating at the nominal voltage and 20 percent voltage reversal, the mean time between capacitor failure (MTBF) will be approximately 3400 shots and 2200 shots respectively. This is provided that only the capacitors be used which survive an individual 'burn-in' of 25 shots at full rated voltage and 40 percent reversal. Maxwell Laboratories estimated that the MTBF number will still be realised, if during the course of operation at the nominal voltage, ten's of fault modes occur resulting in peak currents and reversals of up to 50 kA and 60 percent respectively.

VERTICAL FIELD	TOROIDAL FIELD

NO LOSSES

VERTICAL FIELD	TOROIDAL FIELD
8.27mF 13.3kV } 731KJ	57.3mF 8.4kV } 2.02mJ

ESSENTIAL RESISTIVE LOSSES

coils/cables/ignition/bank bus work/capacitors

26.1mΩ 8.25mF } 860KJ 14.4kV	3.41mΩ 57.18mF } 2.30MJ 8.97kV

PLUS PROTECTION RESISTORS/FUSES

33.9mΩ 8.23mF } 900KJ 14.8KV	5.55mΩ 57.0mF } 2.48MJ 9.33KV

ESSENTIAL R + PROTCTION R
+ 30% ENERGY SAFETY FACTOR

1.17MJ	3.23MJ

Figure 3.3.12 Capacitor bank losses/safety factor

Figure 3.3.14 shows that the protection resistors limit the capacitor reversals in the various fault mode situations to less than 60%, providing the crowbar circuit operates. Crowbar closure is assumed by means of parallel auto-triggered switches.

3.3.3.7 Ignition Switching

Figure 3.3.15 shows the capacitor bank switching circuitry. A single triggered series output ignitron is used, and parallel auto-triggered crowbar ignitrons are used. Current sharing in the ignitrons is assured by means of the individual crowbar resistors. Figure 3.3.16 shows the firing delay and jitter versus the ignitor pulse voltage for a typical 2" ignitron with approximately 10 kV on the anode. Figure 3.3.17 shows firing delay versus anode voltage for the same 2" ignitron with about a 3 kV ignitor pulse.

The characteristics of General Electric ignitrons in the range of interest are given in Figure 3.3.18. It is extremely important to be aware of the fact that ignitrons in general may only be reliably operated at voltages up to approximately one half of the manufacturer's rating. For this reason nominal 25 kV rated ignitrons are selected for the nominal VF and TF bank voltages of 14.8 kV and 9.33 kV respectively. Figure 3.3.19 shows the tentative ignitron selection for each capacitor bank. Note that this selection also ensures the peak rated capability is not exceeded, even when one of the parallel crowbar ignitrons fails to fire.

MAXWELL $\left\{\begin{array}{l}\text{HIGH QUALITY PAPER -}\\ \text{ALUMINUM FOIL -}\\ \text{CASTER OIL.}\end{array}\right.$

	VERTICAL FIELD	TOROIDAL FIELD
C	172µF	396µF
Vmax	17.0KV	10.6KV
Vnom	14.8KV	9.33KV
Emax	25KJ	22.2KJ
Enom	18.8KJ	17.2KJ
N	48	144
MEAN TIME BETWEEN FAILURE 20% REVERSAL	>3400 shots @ 14.8KV	>2,200 shots @ 9.33KV
FAULT MODE 10's SHOTS IpK	50KA	50KA
REVERSAL	60%	60%

Figure 3.3.13 Capacitors

VERTICAL FIELD   TOROIDAL FIELD

LOAD BUS FAULT

25%   40%
_____|_____

FAULT AT INPUT TO CABLES

33%   50%
_____|_____

CAPACITOR BANK BUS FAULT

35%   58%
_____|_____

MODULE BUS FAULT

27%   46%

Figure 3.3.14 Capacitor bank fault modes
capacitor reversal

TRIGGERED SERIES OUTPUT IGNITRON

BANK
OUTPUT
CABLES

LOAD INDUCTOR

CROWBAR
RESISTORS

POSITIVELY
CHARGED
CAPACITOR
BANK

AUTO TRIGGERED PARALLEL
CROWBAR IGNITRONS

CABLE MATCHING
NETWORK
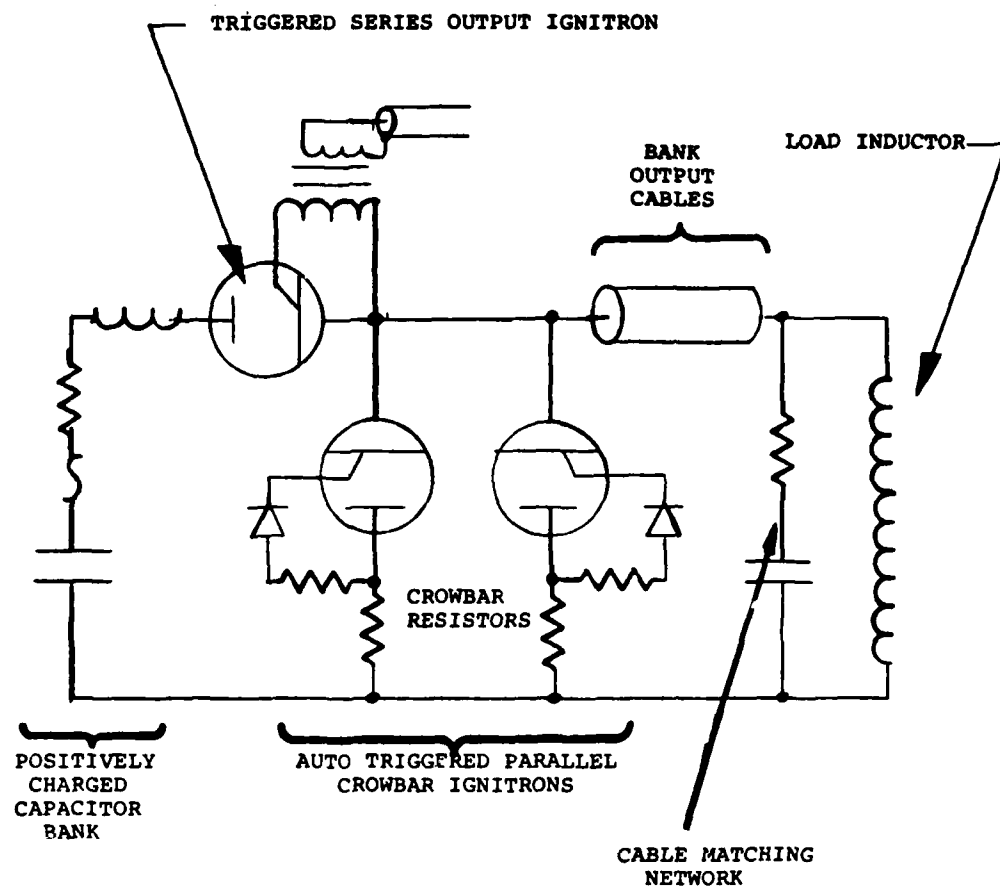
Figure 3.3.15 Capacitor bank switching

110
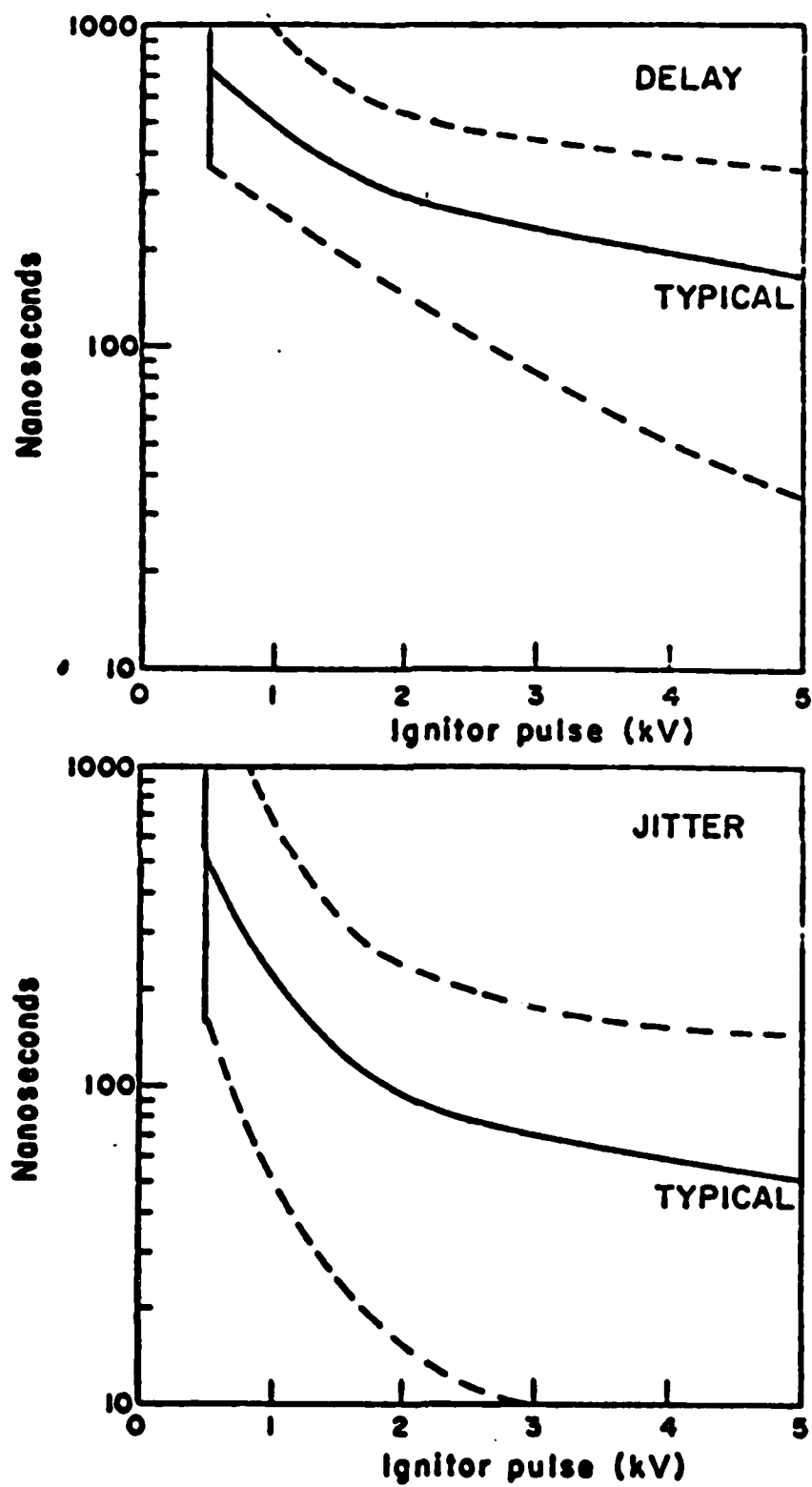
Figure 3.3.16 Delay and jitter of 2″ ignitrons with
approximately 10 kV on anode

111
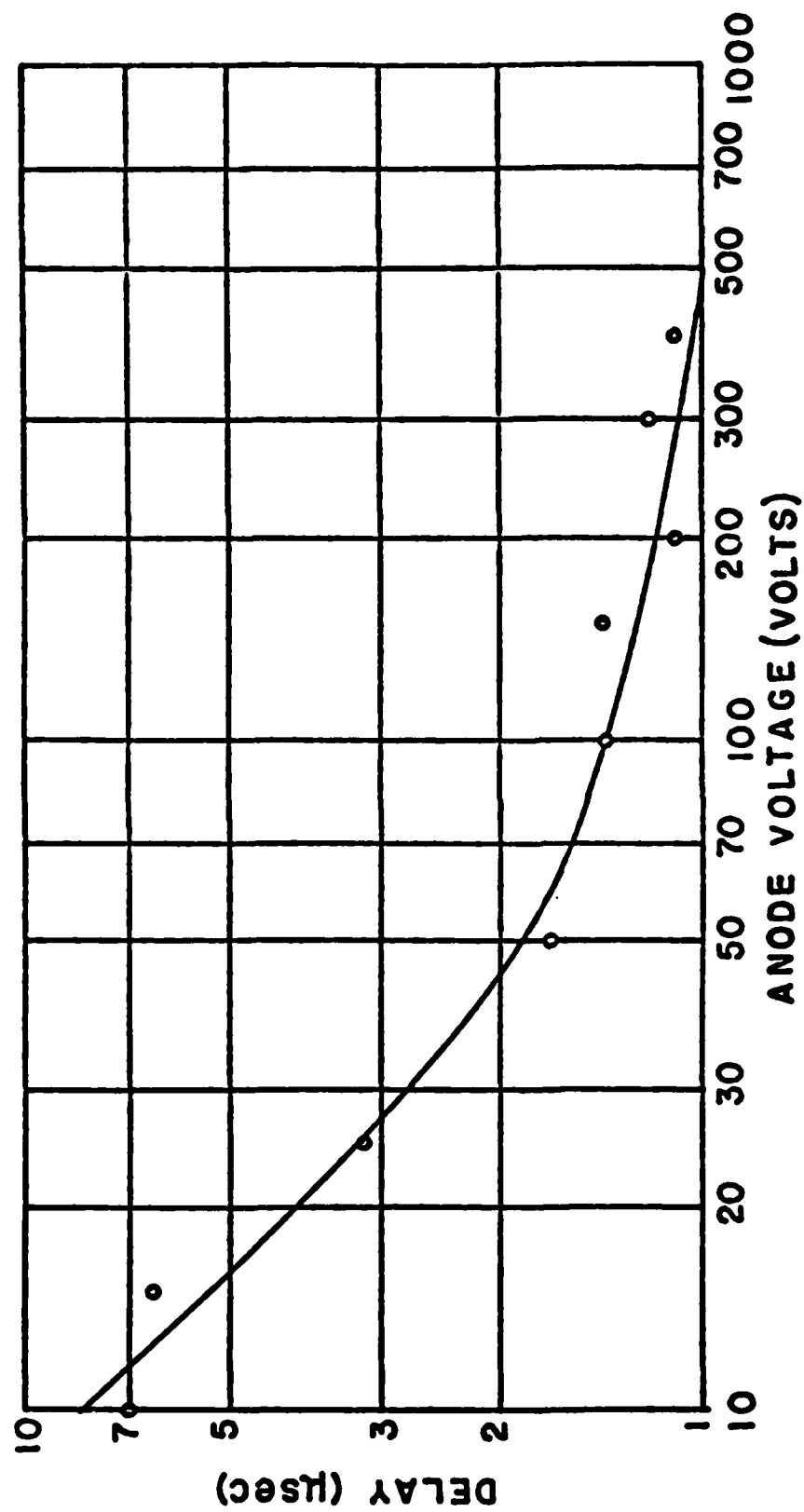
Figure 3.3.17 Firing delay of 2" ignitron with about 3 kV ignitor pulse

	MAX KV	PEAK KA	TOTAL Cb
GL 7171	10	35	30
GL 7703	25	100	30
GL 37207	25	300	200
GL 8205	25	600	1500
GL 87248	50	15	15
GL 35391	50	100	30

Figure 3.3.18 Ignitrons

113

	KV	KA	Cb
VERTICAL FIELD OUTPUT SWITCH Requirement	14.8	54	178
Capability using single GL 87207	25	300	200
VERTICAL FIELD CROWBAR SWITCH Requirement	14.8	41	250
Capability using 3 parallel GL 87207	25	900	600
If only 2 fire	25	600	400
TOROIDAL FIELD OUTPUT SWITCH Requirement	9.33	209	739
Capability using single GL 8205	25	600	1500
TOROIDAL FIELD CROWBAR SWITCH Requirement	9.33	189	1580
Capability using 2 parallel GL 8205	25	1200	3000
If only 1 fires	25	600	1500

Figure 3.3.19 Capacitor bank ignitron selection

3.3.3.8 Fuses

The VF and TF circuits used to calculate the action through the individual capacitor fuses are shown in Figures 3.3.20 and 3.3.21 respectively. In each figure, the limb on the left represents a single capacitor/fuse/resistor element. The central limb represents the remaining parallel capacitor/fuse/resistor elements in that module. The limb on the right represents all the remaining modules in parallel coupled to the first module resistor. The action was computed through the fuses under various fault modes. Inductance was introduced into each limb, consistent with the fault mode under consideration.

Fuse selection is based upon the desire for the fuse to blow only in the event that the capacitor to which it is connected fails. The fuse, a) considerably reduces the energy deposited into the failed capacitor, b) conveniently takes the failed capacitor out of circuit for continued bank operation, and c) provides an indication of the location of the damaged capacitor.

As shown in Figure 3.3.22, a basic current-limiting fuse consists typically of one or more silver wire or preformatted ribbon elements suspended in an envelope filled with sand. To make the fuse as short as possible, it is normally spirally wound on a high-temperature-resistant, nontracking form called a spider. When operating against a high-fault current, the fusible element melts over the full length. This energy melts or fuses the sand surrounding the element. The rapid loss of heat energy and the confinement of

MODULE RESISTORS { 50mΩ $\frac{50}{7}$ = 7.14mΩ

INDIVIDUAL CAPACITOR RESISTORS { 100mΩ $\frac{100}{5}$ = 20mΩ $\frac{100}{42}$ = 2.38mΩ

FUSES { 7.1mΩ $\frac{7.1}{5}$ = 1.4mΩ $\frac{7.1}{42}$ = 0.17mΩ

ENERGY STORAGE CAPACITORS { 172μF   172 x 5 = 860μF   172 x 42 = 7.22mF
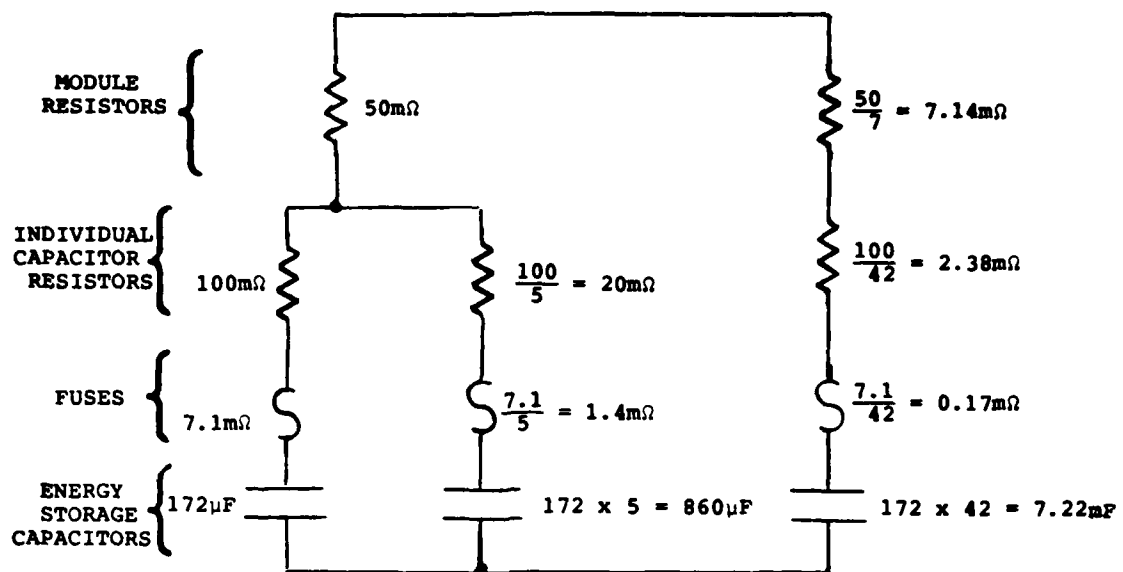
INDUCTANCES WERE SELECTED TO
SUIT FAULT MODE.

Figure 3.3.20 Vertical field capacitor bank fault circuit

116

Figure 3.3.21 Toroidal field capacitor bank fault circuit

Clip-Style Current-Limiting Fuse

STANDARD CONSTRUCTION   MAGNIFORMED CONSTRUCTION

END FITTINGS (CONTACTS)
Silver- or tinplated as required. Copper or red brass provides excellent current- and heat-conducting properties.

SILVER RIBBON ELEMENT
High-purity silver with ±5% tolerance assures accurate melting characteristics.

SPIDER
Gas-evolving support element to cool heat dissipated during fuse operation and aid low current clearing.

AUXILIARY CONTACTS
Cause the arc length to triple during low fault currents, thus dissipating circuit energy more rapidly.

SAND-FILLED
Silica sand (99.5% pure) fuses into a glass-like tunnel structure (fulgurite) during fuse *operation dissipating arc heat* energy rapidly.

INDICATOR BUTTON
Indicates a blown fuse when protuding.

END CAP
Seated to the fuse tube using a magnetic formation technique where high-energy capacitors discharge into a magnetic core to provide consistent force around the cap circumference.

EPOXY BOND
For added cap-retention strength.

NOTE: All 8.3, 15.5 and 23 kv 2-inch-diameter NX fuses have magniformed end fittings.

AUXILIARY ELEMENT
Silver wire melts rapidly to aid in low-current operation.

M SPOT (SOLDER)
Reduces melting temperature of silver element at low fault-current operation.

HIGH-TEMPERATURE-RESISTANT TUBING
contains internal pressures during fuse operation.

Figure 3.3.22 Basic components of the McGraw-Edison NX current-limiting fuse

the arc by the molten glass-like cylinder chokes off the current at a relatively small value know as the let-through current.

Figure 3.3.23 shows the characteristics of McGraw-Edison 15.5 kV C-rated NX current-limiting fuses. Action (amp.^{2} sec) is plotted versus the ampere rating of the fuse. For the higher ampere ratings two fuses are operated in parallel. For a given ampere rating the top of the black band indicates the minimum action required to melt the fuse. Action below this value will not blow the fuse. The top of the white band indicates the maximum action required to ensure blowing the fuse.

Figure 3.3.24 presents the action per fuse assembly for both VF and TF capacitor banks under normal operation, a load fault (short circuit), a fault at the input to the cable feed, and a bank bus fault. Note that the most demanding fault for the fuse to service is that of a module bus fault.

Figure 3.3.24 shows that an initial selection of one 15.5 kV/100 amp fuse per VF bank capacitor, and two 15.5 kV/80 amp fuses per TF bank capacitor insures that the fuses will not blow under load fault, or bus fault conditions. Moreover the selection of these fuses ensures that following a capacitor failure, the extra energy delivered into the capacitor is less than 0.7 kJ (assuming a 50 volt drop per capacitor series section in the failed capacitor).

The desire to avoid blowing all the fuses in a shorted module requires a high ampere fuse rating. Figure 3.3.25 shows that allowing the fuses (six in the case of the VF capacitor bank and twelve in the case of the TF capacitor

119
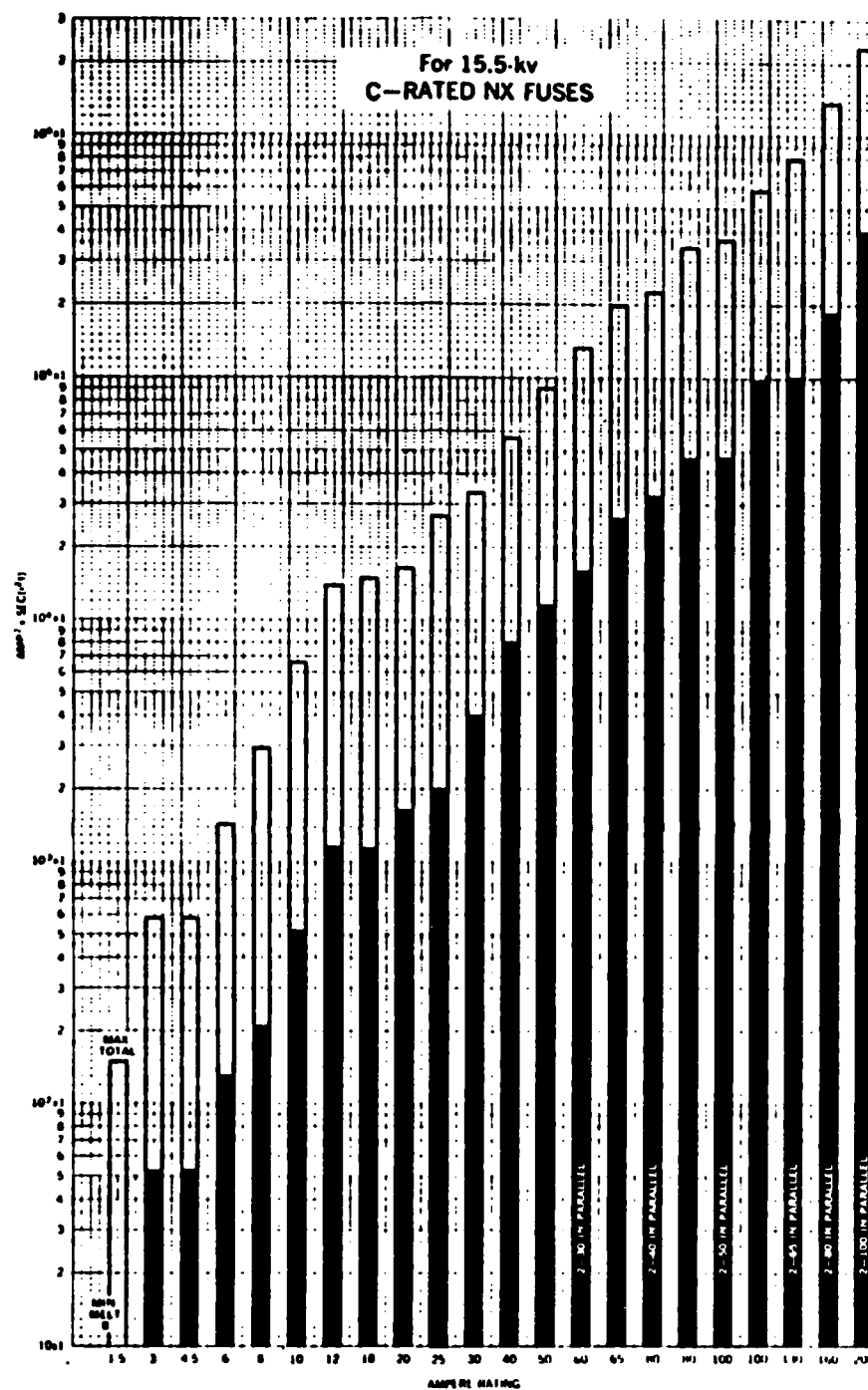
Figure 3.3.23 McGraw-Edison current-limiting fuses

120

VERTICAL FIELD	TOROIDAL FIELD

$$\int i^2 dt/\text{fuse assembly}$$

NORMAL

2.7×10^3 AMP^2. sec	5.1×10^3 AMP^2. sec

LOAD FAULT

2.35×10^4 AMP^2. sec	3×10^4 AMP^2. sec

FAULT AT INPUT TO CABLES

3.86×10^4 AMP^2. sec	4.14×10^4 AMP^2. sec

BANK BUS FAULT

4.8×10^4 AMP^2. sec	5.0×10^4 AMP^2. sec

MODULE BUS FAULT

$8.1 - 8.8 \times 10^4$ AMP^2. sec	1.3×10^5 AMP^2. sec

McGRAW EDISON C-RATED NX FUSE

15.5KV 100 A/capacitor	2 x 15.5KV 80 A/capacitor

FUSE SURVIVES ABOVE CONDITIONS

Fuse blows at	Fuse blows at
6×10^5 AMP^2. sec	1.3×10^6 AMP^2. sec

EXTRA ENERGY INTO FAILED CAPACITOR ASSUMING
50 V/CAPACITOR SECTION VOLTAGE DROP

(2 x 50 = 100V)	(1 x 50 = 50V)
< 700 joules	< 700 joules

Figure 3.3.24 Fuses

121

The desire to avoid blowing the fuses residing in a shorted module sets the high value of $\int i^2 dt$ for fuse blowing.

Two options are open:

a) Accept blowing the fuses residing in a shorted module.

VERTICAL FIELD	TOROIDAL FIELD
6 FUSES	12 FUSES

McGRAW EDISON C-RATED NX FUSE

15.5KV 80 A/capacitor Fuse blows at 3.2×10^5 AMP^2. sec	15.5KV 100 A/capacitor Fuse blows at 5.9×10^5 AMP^2. sec

EXTRA ENERGY INTO FAILED CAPACITOR

157 JOULES	657 JOULES

b) Maintain same overall series bank resistance, but lower module resistance value & raise individual capacitor series resistance.

Rm 50mΩ ⟶ 33mΩ Rs 100mΩ ⟶ 200mΩ	Rm 24mΩ ⟶ 18mΩ Rs 57mΩ ⟶ 130mΩ

Figure 3.3.25 Fuses continued

bank) to blow in the event of a module bus short, lowers the extra energy delivered into a failed VF capacitor to about 157 joules but barely influences the energy delivered into a failed TF capacitor. An alternate approach to lowering the ampere rating of the fuses was recognised as lowering the value of the module resistance and raising the individual capacitor series resistance (i.e., maintaining the same overall series bank resistance) as shown in Figure 3.3.25. This approach was pursued in the preliminary design of the TF power supply.

Failure of a capacitor when operating the bank at reduced voltage is addressed in Figure 3.3.26. Lower voltage capacitor bank operation results in more energy being deposited into the failed capacitor before the fuse blows. However, the likelihood of a capacitor failing at these lower voltage is much less (capacitor life varies roughly as the capacitor voltage raised to the seventh or eighth power). Deposition of 12 to 25 kJ extra (as in the case of no fuses) is likely to cause catastrophic rupture of the case with the risk of blowing off the insulating bushing.

Also included in Figure 3.3.26 is the maximum energy available to be deposited into a failed capacitor in the case of not using fuses. Deposition of an extra 1 or 2 kJ into a failed capacitor already storing in the region of 25 kJ is not considered sufficient to rupture the capacitor.

EXTRA ENERGY INTO FAILED CAPACITOR

VERTICAL FIELD	TOROIDAL FIELD
HALF VOLTAGE OPERATION	
< 1.4KJ	< 1.3KJ

QUARTER VOLTAGE OPERATION

< 2.7KJ   < 2.5KJ

NO FUSES

MAXIMUM ENERGY AVAILABLE INTO FAILED CAPACITOR

25KJ   12KJ

Figure 3.3.26 Fuses continued

3.3.3.9 Resistors

The required capacitor bank resistors are listed in Figure 3.3.27. Since the inductance of the resistors in this application is not critical the choice is based largely on obtaining energy-absorbing mass in the most effective form.

An economical and reliable form of resistance is the low resistance Vitreous-enameled and bare rib-wound type of resistor. Resistance alloys can be operated up to 600 degrees C without loss of mechanical properties.

Vitreous-enameled rib-wound resistors of the type shown in Figure 3.3.28 were selected for use in the individual capacitor resistor and crowbar resistor assemblies. Although the normal operating currents that the capacitor resistors are required to handle are modest (~ 1 kA) capacitor bank fault mode currents can however be considerably higher (~ 100 kA). The Vitreous-enameled resistors are relatively small in diameter, and consist of multiple parallel ribbon sprials providing an inductance of the order of 1μ H or less. Thus the magnetic forces tending expand the spiral radially, and compress the sprial longitudinally are minimised. In previous tests run on two 1-ohm, 300-watt units with a 0.96 msec RC time constant a dull red glow could be seen (in a darkened room) at a level of 1.45×10^{-5} J/lb of resistance ribbon. Only moderate flaking was absorbed in 100 pulses. The resistance ribbons remained tight with no permanent damage detected.

Bare rib wound resistors were selected for use in the discharge resistor assemblies. These resistors are of the type shown in Figure 3.3.29. As these

INDIVIDUAL CAPACITOR
RESISTORS

CROWBAR RESISTOR
ASSEMBLIES

DISCHARGE RESISTOR
ASSEMBLIES

● OHMITE MANUFACTURING
CORPORATION

● COMBINATION OF BARE
AND VITREOUS-ENAMELED
RIBWOUND RESISTORS

● RATED FPR 600°C TEMP.
RISE

● TYPICALLY 0.6lb OF
METAL/RESISTOR

● CAPABLE OF ABSORBING
∿ 150KJ EACH

MODULE RESISTOR
ASSEMBLIES

LATERAL RESISTORS

● STAINLESS STEEL TUBING

Figure 3.3.27 Resistors
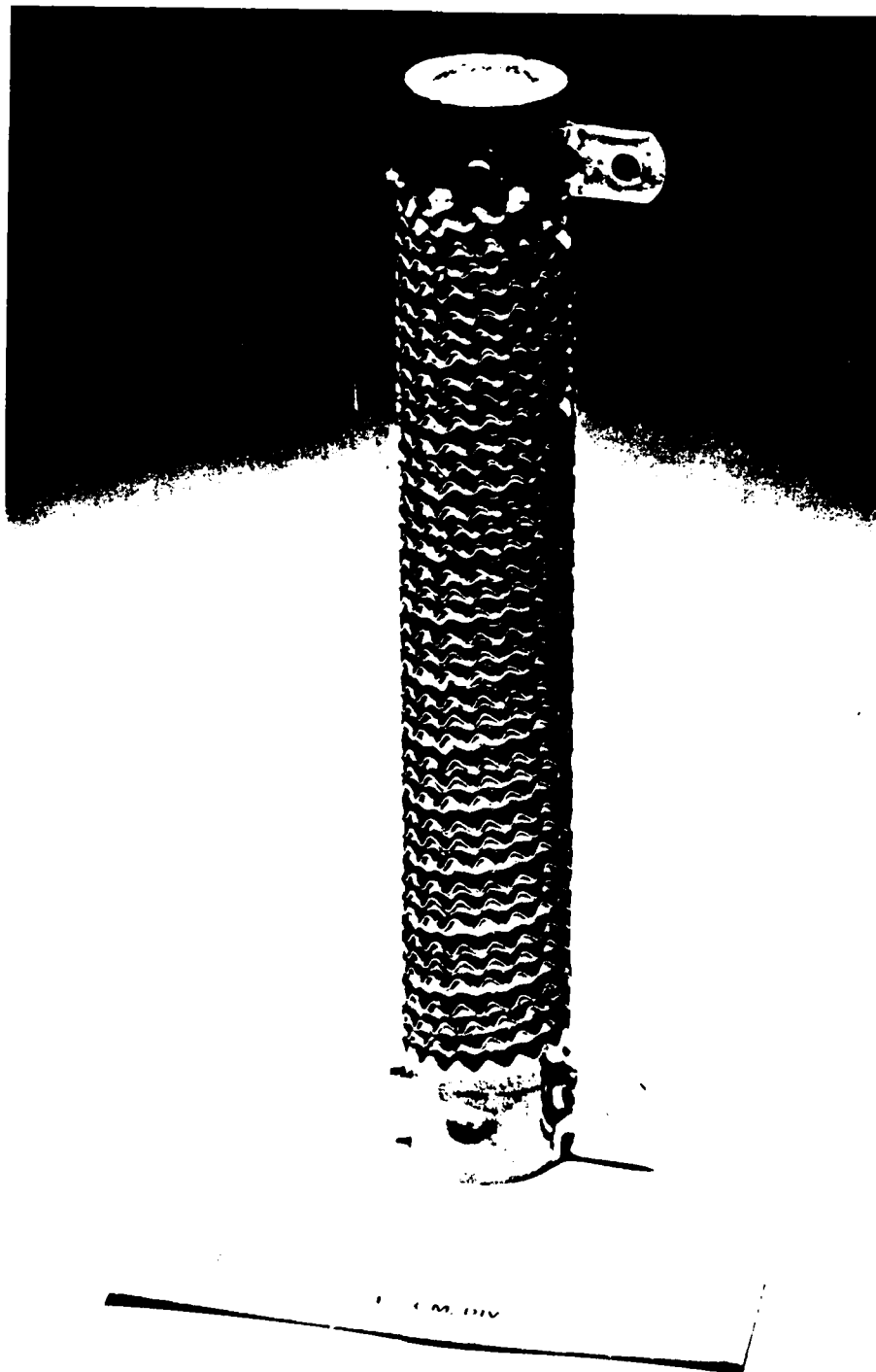
Figure 3.3.28 300 watt ribwound resistor used in
module resistor assemblies
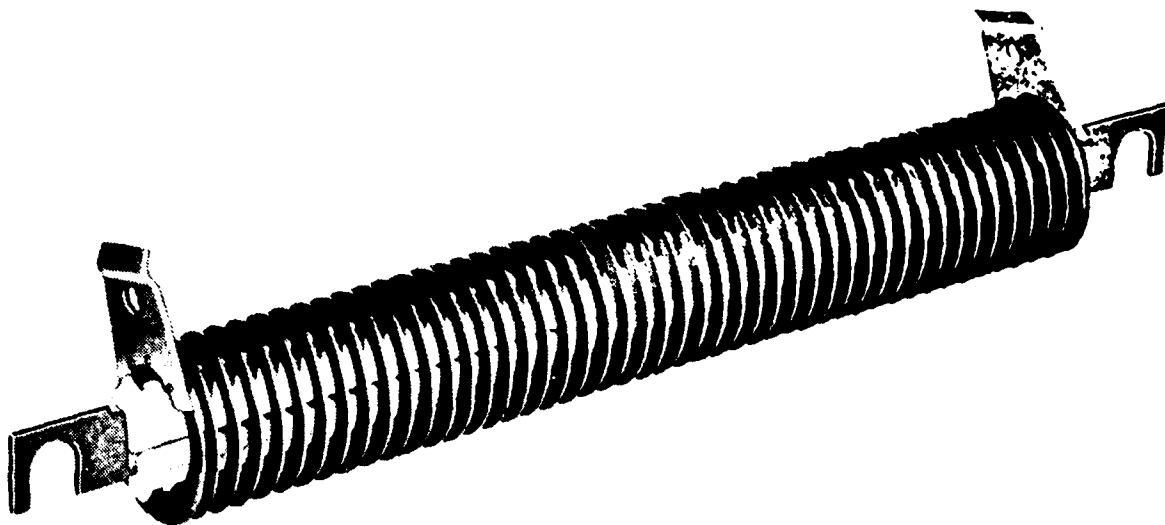
Figure 3.3.29 1600 watt bare ribwound resistor to be
used in discharge resistor assemblies

128

resistors must handle only a few kiloamperes, the larger diameter unsupported resistive windings can be used. This type of resistor typically provides a few pounds of energy absorbing metal per unit.

In the case of the module and lateral resistor assemblies the associated inductance and resultant magnetic forces are of more concern. For this reason stainless steel tubing is used to provide the energy absorbing mass. In each application the stainless steel tube is bent into a zig-zag above the modules. This arrangement provides adequate mass, reduces the inductance and size of the assembly and is very economical.

3.3.3.10 Energy Discharge (Dump and Shorting) Switches

Two redundant bank discharge systems are incorporated in the conceptual design. The essential features are listed in Figure 3.3.30. The bank discharge (energy dump) switch selected is air actuated with electrical control and spring return of the type shown in Figure 3.3.31. The air actuation permits complete isolation of the switch from ground by using plastic air line. The switches are arranged to be fail-safe in the event of a power failure. The second or back-up discharge (dump) switch has a slow air bleed incorporated so that the primary discharge switch operates first in the event of a power failure.

Figure 3.3.32 shows an example of the primary discharge circuit shorting and grounding switch type. This switch is also air operated first shorting the capacitor bank ground to laboratory ground and then shorting the main bank output bus to ground. A manual knife switch in the secondary discharge (dump)

129

●2 REDUNDANT BANK DISCHARGE SYSTEMS.

●EACH SYSTEM CONSISTS OF:
　　　 Discharge Switch & Resistor
　　　 Shorting Switch
　　　 Grounding Switch

●SWITCHES ARE COMBINATION OF:
　　　 Air Operated
　　　 Manual
　　　 Air Actuated with Electrical Control

●FAIL SAFE.
　　　 Slow air bleed so air operated primary
　　　 discharge switches operate first in event
　　　 of power failure.

Figure 3.3.30 Discharge switches
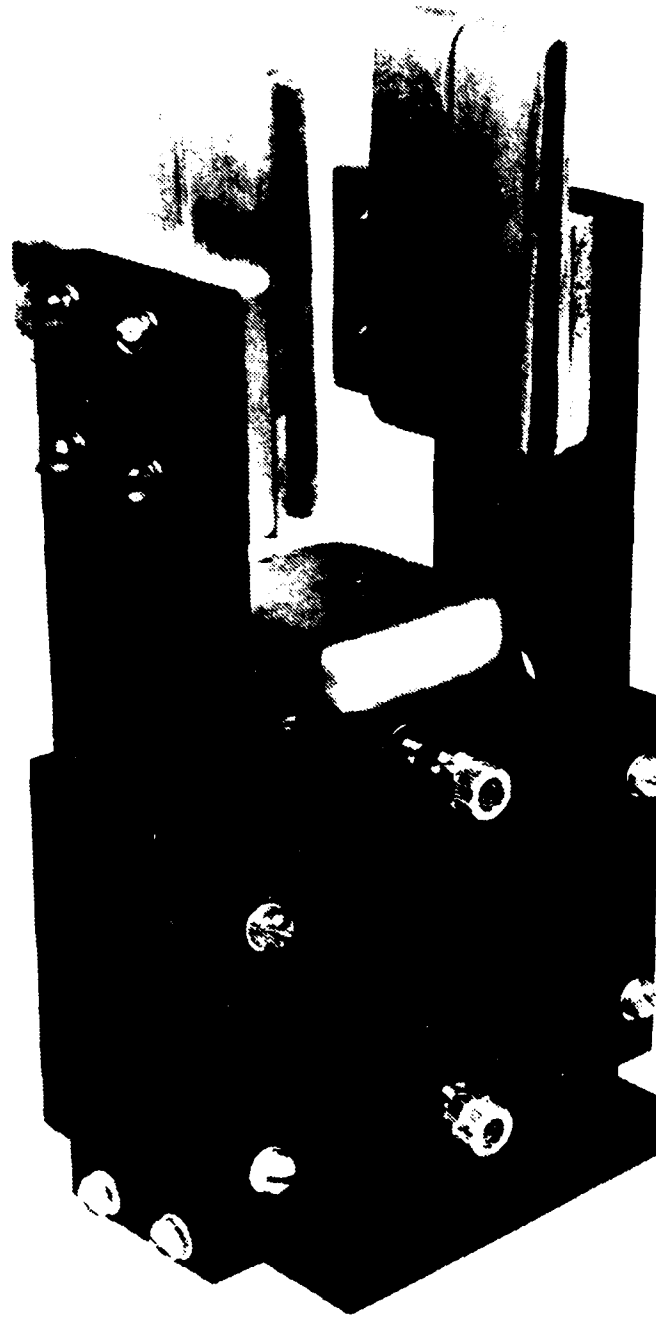
Figure 3.3.31 Bank discharge switch
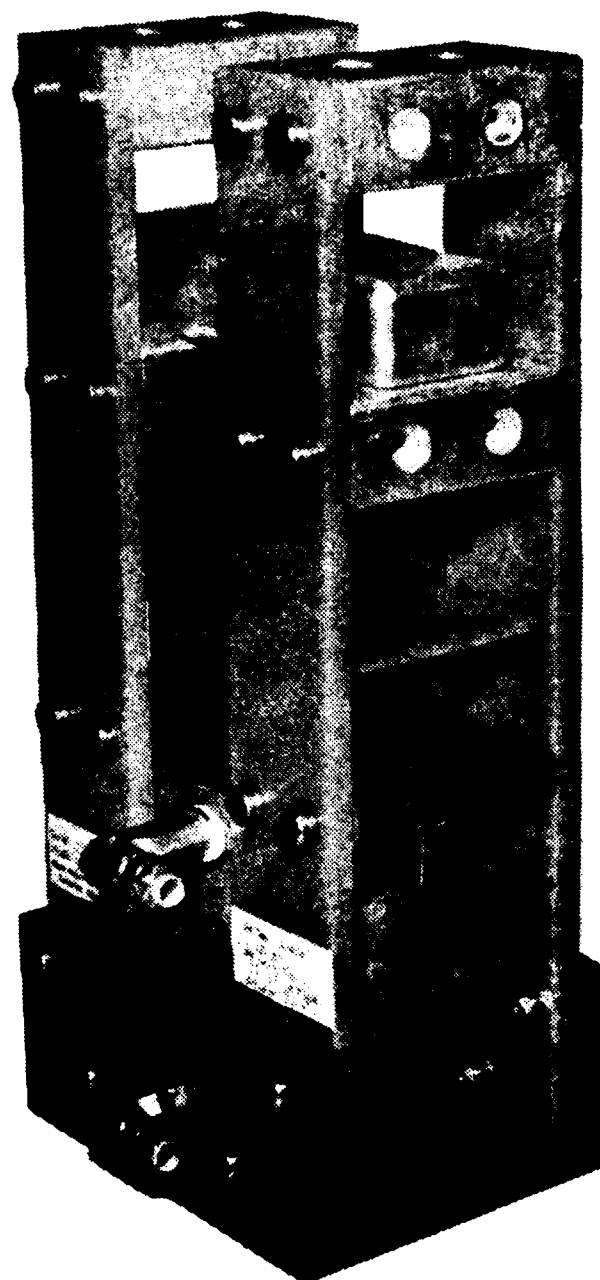
Figure 3.3.32 Shorting and grounding switch type

circuit first shorts the capacitor bank ground to laboratory ground and then
shorts the connection to the capacitor bank lateral resistors to ground. Thus
the sequence of events to discharge (dump) the capacitor bank is as follows:

Step (1) Dump Switch 1 is closed pneumatically

Step (2) Dump Switch 2 is closed pneumatically a few seconds after
Dump Switch 1

Step (3) Grounding Switch 1 is closed pneumatically a few seconds
after Dump Switch 2

Step (4) Shorting Switch 1 is closed pneumatically a few seconds
after Grounding Switch 1

Step (5) The manual knife switch is closed, first grounding the
capacitor bank then shorting the bank.

3.3.3.11 High Voltage Charging Supplies

The power supply charges the capacitor bank essentially at constant
current until the required set-point is reached. Thereafter the power supply
regulates the charge voltage at the set-point voltage. The power supply is
designed to be disconnected from the capacitor bank (high voltage and ground
terminal) immediately before the capacitor bank energy is command delivered
into the load. The disconnect action is also designed to discharge the power
supply through resistors in the high voltage power supply. The tentative
power supply rating requirements are given in Figure 3.3.33.

a) ● CONSTANT CURRENT CHARGING

	VERTICAL FIELD	TOROIDAL FIELD
1 MIN CHARGING	TO 14.8kV 2.3 AMPS @ 17.0kV	TO 9.33kV 10 AMPS @ 10.6kV
2 MIN CHARGING	TO 14.8kV 1.2 AMPS @ 17.0kV	TO 9.33kV 5 AMPS @ 10.6kV

b) ● COAXIAL CABLES
50 Ω RG 220

VERTICAL FIELD	TOROIDAL FIELD
200' x 12 CABLES IN PARALLEL. EQUIVALENT TO 1.25µH, 6.47mΩ	135' x 48 CABLES IN PARALLEL. EQUIVALENT TO 0.21µH, 1.09mΩ

Figure 3.3.33 a) Capacitor bank power supplies
b) Capacitor bank/coil connections

134

3.3.3.12 Capacitor Bank/Load Transmission Lines

The module bus consists of a metal rod or bar located in front of the capacitor bushings. The individual capacitor fuses and resistors connect to the common vertical module bus.

The main capacitor bank output bus consists of an air-insulated parallel plate transmission line located above the modules, running the full length of the capacitor bank. The main output bus connects at one end to the ignitron switching circuitry, and at the other end to the two redundant bank discharge systems. The module busses connect to the main output bus at intervals along the bus, and at either side of the bus, via the module resistors.

An effective way to connect between the capacitor bank ignitron switching circuitry and the distant load is with coaxial cables. The advantages are, a) flexibility, b) generous internal electrical insulation, c) ample external insulation to prevent arcing between adjacent cables, and between cables and racks, d) no forces between cables, e) adequate strength to resist internal magnetic pressure under fault conditions, f) no joints except at the ends, g) experience of use in large capacitor banks.

As shown in Figure 3.3.33 the design uses 12 parallel cables for the VF capacitor bank, and 48 parallel cables for the TF capacitor bank.

3.3.3.13 Mechanical Design of the TF Capacitor Rank

The conceptual design of the toroidal field capacitor bank shown in Appendix 3F consists of a frame structure which supports the cantilever mounted capacitors, a bank and module discharge system cabinet, and an output and crowbar switching system cabinet. The concepts were reviewed by NRL on August 1982. The PSI response to Conceptual Design Review entries, included in Appendix 3G, was sent to NRL on September 1982.

3.3.3.14 CF and ICF Power Supplies

Figure 3.3.34 shows the approximate location of the CF coils with respect to the vacuum chamber. The CF coils provide the few gauss required to move the equilibrium position of the electron beam immediately after injection. Note the opposite sense of the currents.

Figure 3.3.35 shows the approximate location of the ICF coils with respect to the vacuum chamber, and the required distribution of currents to compensate for the decay of the beam induced currents. Note also that the ICF coils are interspaced between the CF coils.

The required CF and ICF total current profiles & time histories are shown in Figure 3.3.36. Figure 3.3.36 shows the total CF and ICF currents relative to each other and relative to the time of injection. The CF current comprises a ¼-sine wave of 40 ns half-period, 350 amperes peak current. The ICF current would rise to peak current in 4 μsec, but is crowbarred at 3 μsec to produce a peak current of 10.4 kA. Through the use of a suitable series resistance the

136
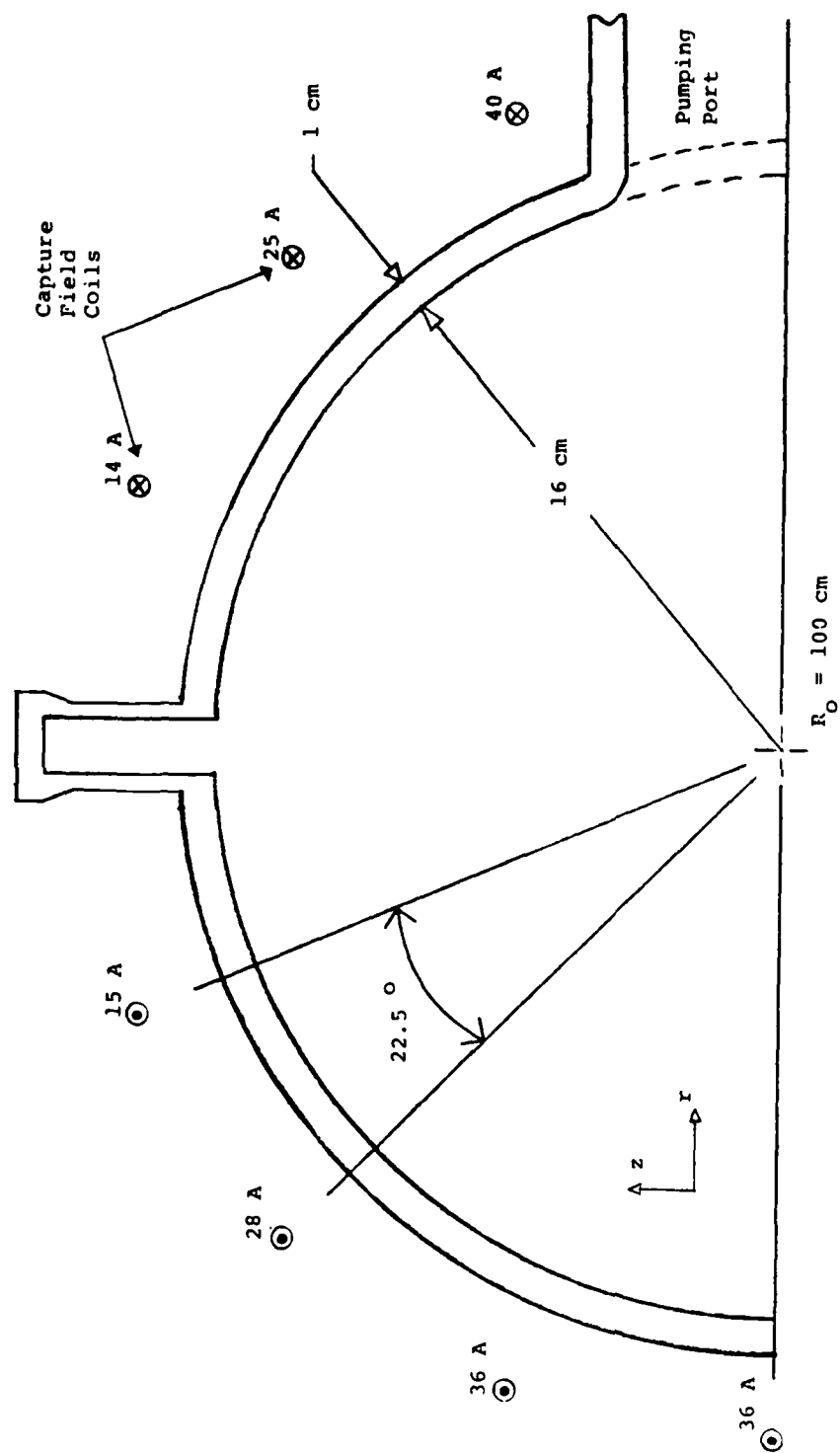
Figure 3.3.34 Vacuum chamber showing CF coils
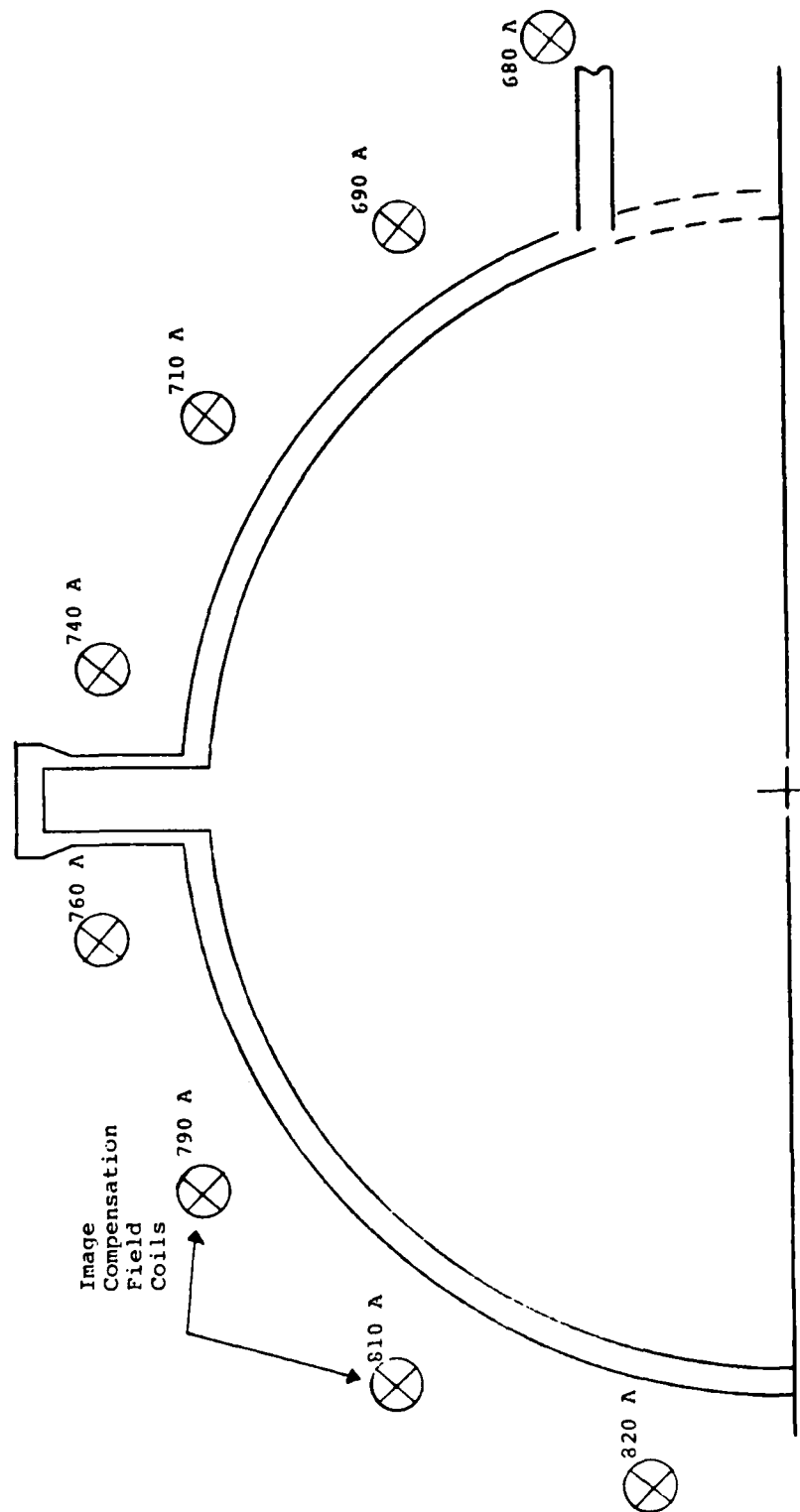
Figure 3.3.35 Vacuum chamber showing ICF coils

680 A

690 A

710 A

740 A

760 A

Image
Compensation
Field
Coils

790 A

810 A

820 A

138

CF CASE

time of injection

I_{TOTAL} (A)

350

time (ns)

0   100   200   300   400

ICF CASE

$I = 10.4e^{-t/3ms}$

$I = 12(1 - e^{-t/3\mu s})$

I_{TOTAL} (kA)

10.4

time (µs)

0   1   2   3   4
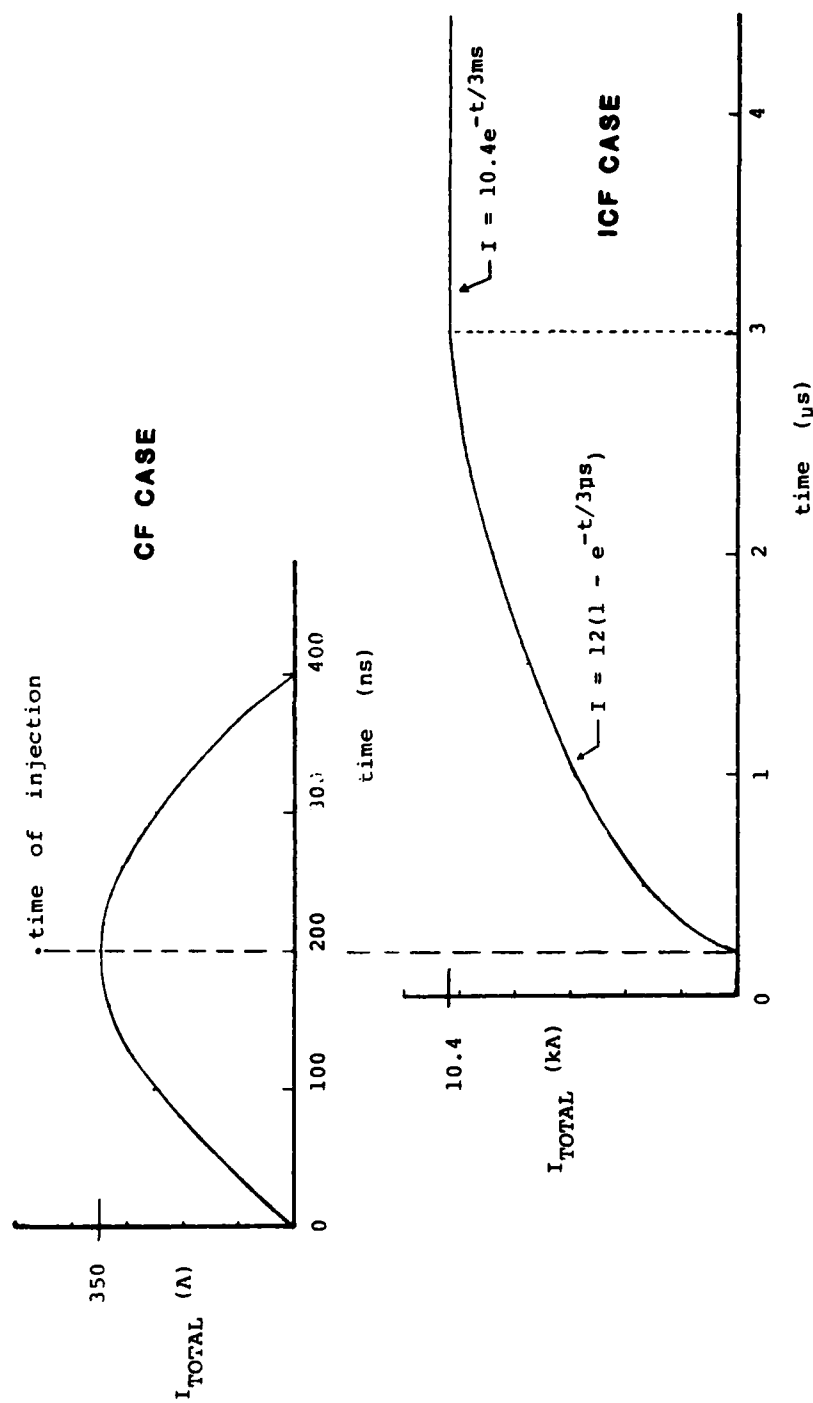
Figure 3.3.36 Current histories in auxiliary coils

required exponential current rise is produced. The desire is to maintain the
10 kA for the remaining 3 ms acceleration time.

The auxiliary CF and ICF coil drive circuits are shown in conceptual form
in Figure 3.3.37. Considerable mutual coupling exists from coil to coil in a
given circuit, and from circuit to circuit.

In the case of the CF circuit, resistors are shown distributing the coil
currents as desired. Inductors would be better suited; however, slightly
different zero-crossing times would result for the individual coil currents.
The coil resistance helps to reduce self-coupling. A common series diode
clamps the current at about 400 ns.

Series resistance in the ICF circuit tailors the current risetime and
aids in minimising coupling from the CF circuit. Diodes are inserted in
series with each coil again to minimise coupling from the CF circuit.
Appropriately chosen inductors enable the required individual coil current
distribution to be obtained.

The conceptual design phase did not address a full interactive circuit
analysis. Moreover, this would have been premature as the CF and ICF coil
requirements were not at all firm. The design effort concentrated more upon
ensuring the general circuit philosophy was sound and that the circuit
components likely to be required were available.

Figure 3.3.38 shows an approximation of the CF circuit. The load
inductance of 3 μH includes a first order estimate of mutual coupling. A
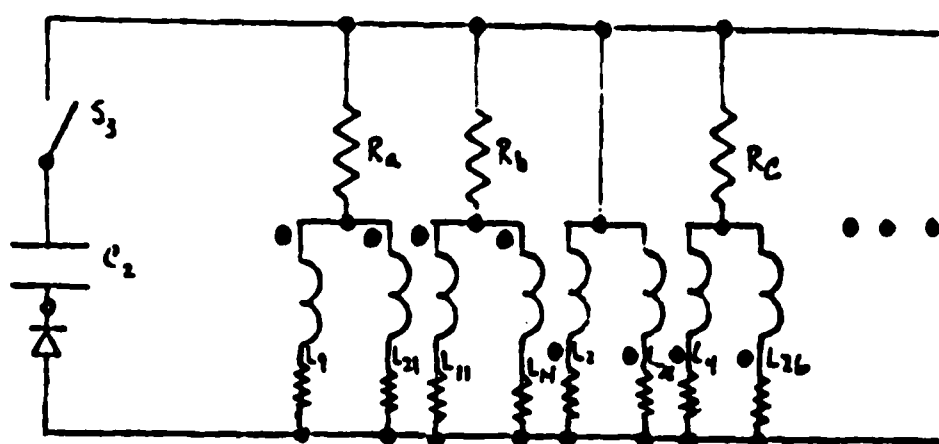
CAPTURE FIELD CIRCUIT
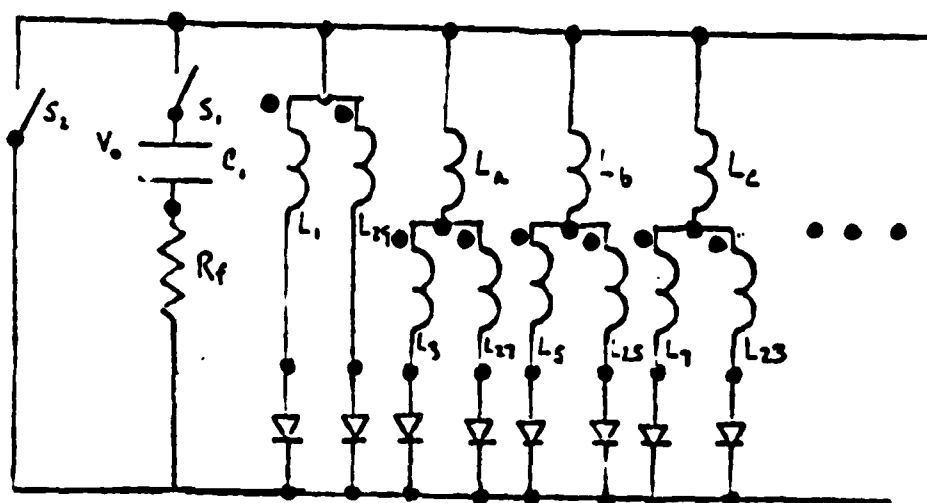
IMAGE COMPENSATION FIELD CIRCUIT

Figure 3.3.37 Auxiliary coil drive circuits

141
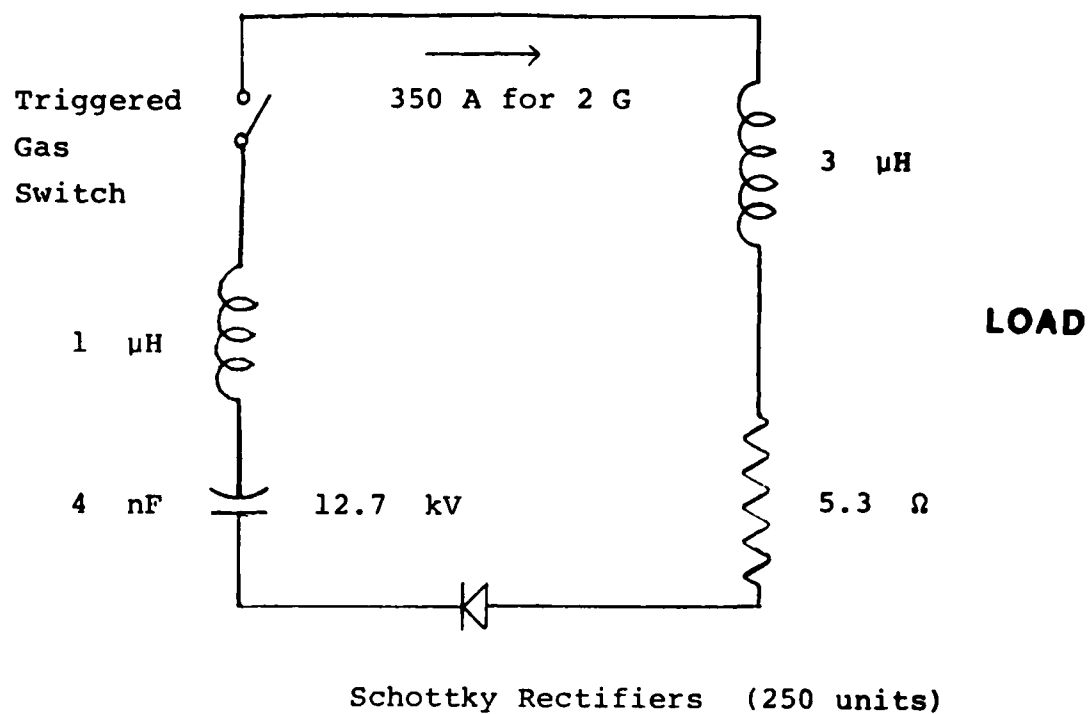
Figure 3.3.38 Approximate capture field circuit

triggered gas spark gap discharges the very modest (<1 joule) amount of energy stored in the 4 nF capacitor at 12.7 kV. A series stack of fast acting Schottky rectifiers (250 units) provides current clamping, with a recovery time of 10-35 ns from the peak forward current of 350 amps.

Figure 3.3.39 shows an approximation of the ICF circuit. The first and second circuit limbs from the left, represent the ICF power supply and ICF load coils respectively. A triggered gas spark gap discharges the few hundred joules stored in the 1.6 μF capacitor charged to 25 kV.

Eight series silicone rectifiers are required for each ICF coil. The parallel combination of 16 load coil/rectifier elements is estimated to have a forward impedance of about 1.1 mΩ.

An ignitron is used to crowbar to ICF coil current. Figure 3.3.40 shows an approximate relation between ignitron current, voltage drop across the ignitron, and ignitron impedance. The 1.1 mΩ load coil/rectifier impedance in combination with the ignitron impedance would not enable a long enough current decay constant. An ancillary crowbar circuit is used to overcome the limitation by increasing the L/R current decay constant. The L/R decay constant is increased by raising L (the crowbar circuit inductance) substantially, at the expense of raising R (the crowbar circuit resistance) only slightly.

A second ignitron is used to discharge a 16 μF capacitor charged to 26 kV into a 30 μH load (chosen somewhat arbitrarily to be ten times the ICF coil inductance). The ancillary crowbar circuit parameters are chosen, and the

143

1 μH

16 μF

1 Ω

26 kV; 5.4 kJ

30 μH

Ignitron

ANCILLARY CROWBAR

Ignitron

Crowbar
(50 kV, 15 Cb)

10 kA   10 kA

10 kA

Silicon
Rectifiers
(8 in series
for each coil)

Triggered Gas Switch

3 μH

26 kV; 540 J

ICF

1 μH

1.6 μF

1 Ω
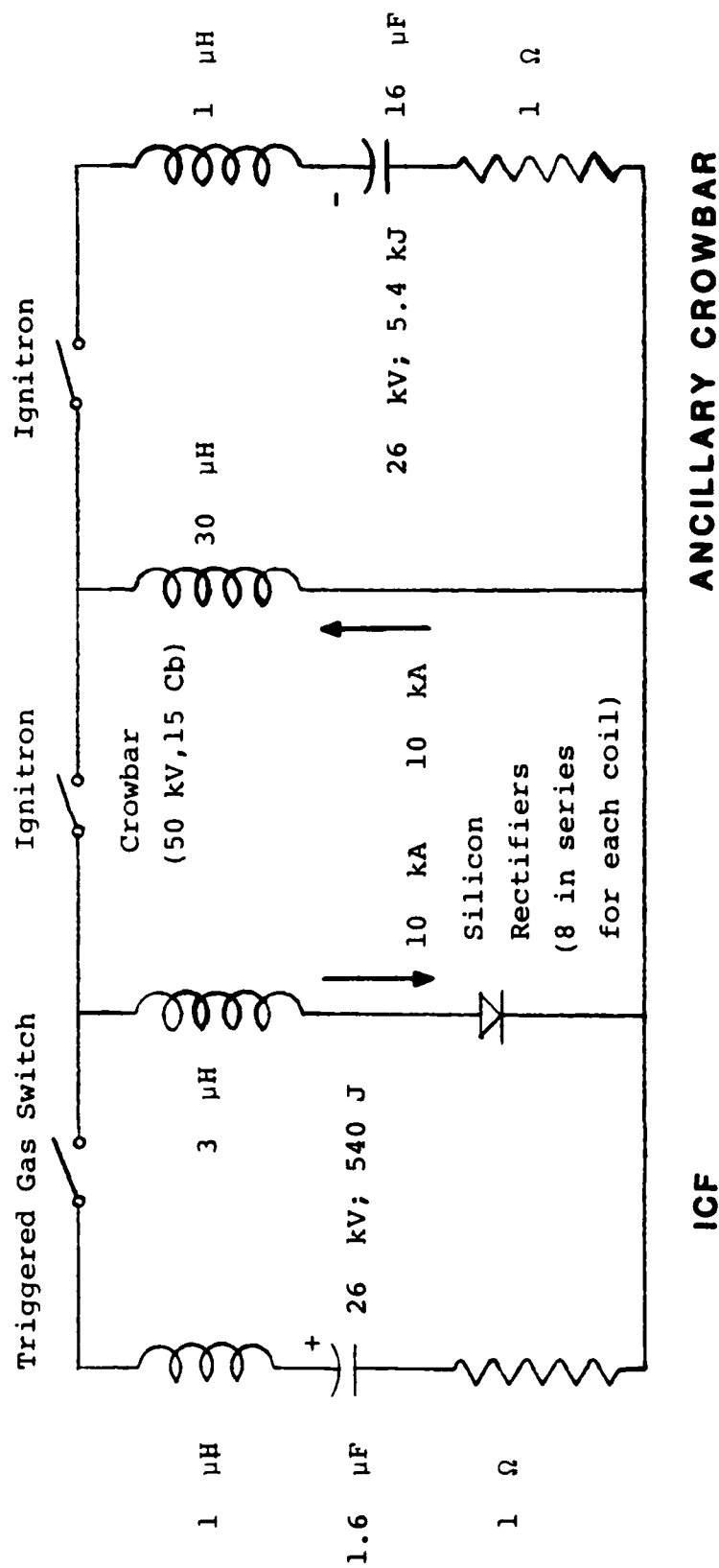
Figure 3.3.39 Approximate image compensation field circuit
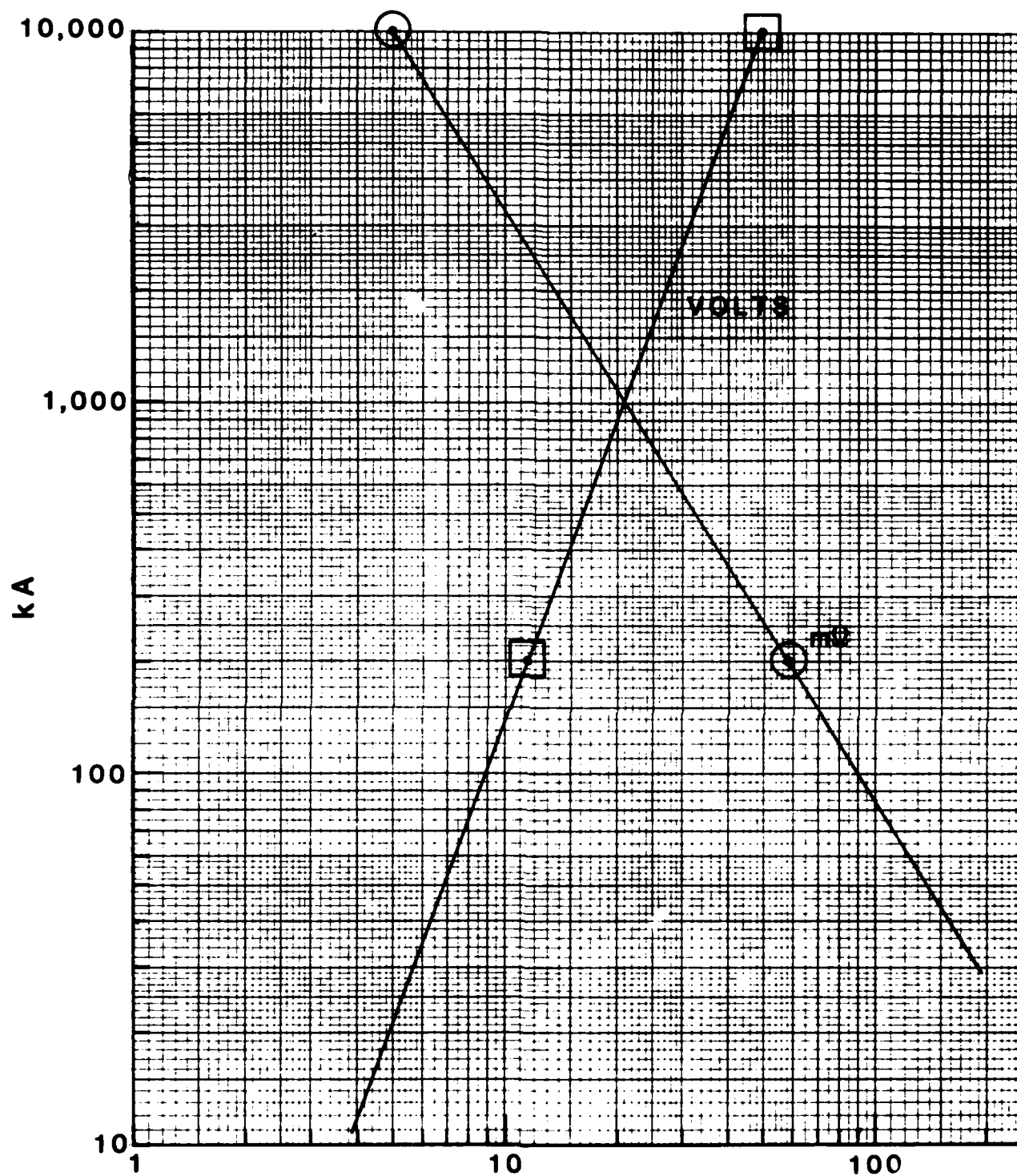
Figure 3.3.40 Ignitron current vs. voltage drop/impedance

145

second ignitron crowbar fired, such as to achieve a peak current of 10 kA in the 30 μH inductance at the same time the 10 kA is reached in the ICF load coils. The ancillary crowbar circuit requires about ten fold the time required by the ICF power supply/load coil circuit to reach peak current. The ancillary crowbar circuit is therefore fired before the ICF circuit. The ICF crowbar ignitron is then fired as the ICF and ancillary crowbar circuit currents coincide at 10 kA. The ICF crowbar ignitron now crowbars eleven times the original circuit inductance, with the circuit resistance increased only by that of the additional resistance of the 30 μH ancillary crowbar inductor. By this means, the requisite current decay constant of 3 ms is achieved. It is also interesting to note that because the resistance of the ICF crowbar ignitron increases with decreasing current (as shown in Figure 3.3.40) the actual ICF load coil current decay will be more linear than exponential.

Figure 3.3.41 summarises future work required on the CF and ICF circuits once the coil geometries and required current time histories are confirmed by NRL.

3.3.4 Preliminary Design of the Toroidal Field Power Supply

3.3.4.1 General

The preliminary design of the TF capacitor bank was conducted between September 1982 and May 1983. A Preliminary Design Review (PDR) was held at PSI on May 26, 1983.

- CONFIRM SUITABILITY OF ICF CROWBAR CIRCUIT

- WRITE DIFFERENTIAL EQUATIONS FOR EACH CIRCUIT (INCLUDING CIRCUIT MUTUALS)

- USE A NUMERICAL DIFFERENTIAL SOLVER TO OBTAIN A SOLUTION FOR EACH CIRCUIT

- INTRODUCE REAL COMPONENT VALUES

- FIND APPROPRIATE VALUES OF L_S/R_S FOR DESIRED CURRENT DISTRIBUTION IN THE ICF/CF CIRCUIT

- INCLUDE THE EFFECTS OF MUTUALS BETWEEN IC, ICF, AND VF COILS

Figure 3.3.41 Further work required on CF and ICF circuits

147

The preliminary design effort consisted initially of circuit analyses to define the required specifications of the energy storage capacitors, ignitrons, capacitor banks/load transmission line, protection/discharge/dump resistors, fuses, and discharge/dump/shorting switches. Preliminary mechanical design effort was then pursued in parallel with development of circuit schematics leading to preliminary specification sheets for major components.

3.3.4.2 Capacitors

A capacitor specification was developed recognizing that there is no such thing as designing for a given life with zero failures. A specific failure level is introduced to give a realistic goal for the manipulation of failure statistics. Although a different number may be selected during the final design, a target was considered important to get vendors designing to a common standard.

A life scaling paragraph was incorporated since most systems are not operated at full rated voltage much of the time. In this way pulses use up rated life per the vendor's life scaling formula.

Finally, rather than asking that the final acceptance of the capacitors be in the assembled TF capacitor bank (where the capacitor vendor cannot control possible voltage transients which might damage his units), acceptance is proposed in part on the basis of a 25 shot full voltage elevated reversal test per capacitor.

The preliminary specification for the TF bank high voltage energy discharge capacitors is given in Appendix 3I.

3.3.4.3 Ignitrons

The TF capacitor bank output ignitron is required to pass a peak current of 210 kA, and a total charge of 713 Cb, for the nominal capacitor bank charge voltage of 9.33 kV. A single General Electric GL 8205 ignitron is used rated at 25 kV, 600 kA peak current, and 1500 Cb total charge.

The TF capacitor bank crowbar circuit is required to pass a peak current of 175 kA, and a total charge of 1560 cb for the nominal capacitor bank charge voltage of 9.33 kV. Two parallel General Electric GL 8205 ignitrons are used to provide a combined capability of 25 kV, 1200 kA peak current, and 300 Cb total charge.

In the unlikely event of only one crowbar ignitron firing, the 600 kA, 1500 Cb capability is considered sufficient to handle the anticipated 175 kA, 1500 Cb.

The physical layout of the output and crowbar ignitrons is shown in Figure 3.3.42 and in Appendix 3M. The output circuit comprises a) a coaxial air-insulated feed from the parallel plate bank output bus to the single output ignitron, and b) a parallel plate air-insulated feed from the output ignitron to 32 symmetrically located RG 220 coaxial cables forming the load output feed. The resistance and inductance of this region is estimated to be 0.5 mΩ, and 105 μH respectively. The crowbar circuit comprises two

149

Figure 3.3.42 Output and crowbar ignitron layout

150

ignitron/series resistor elements located symmetrically on either side of the output ignitron. The crowbar ignitrons are mounted into the parallel plate air-insulated transmission line formed by the crowbar resistors and electrode feed. The resistance and inductance of the two ignitron/series resistor regions inparalel is estimated to be 9 m Ω, and 168 μH respectively. Auto closure of the two crowbar ignitrons is anticipated before a voltage reversal of minus 300 volts is attained at a time of 3.57 ms after firing the output ignitron.

The ignitron trigger generator schematic, bank output switching schematic, delay generator and trigger amplifier schematic controls operation discussion and timing diagram are included in Appendix 3M.

3.3.4.4. Capacitor Bank/Load Transmission Line

The design uses 32 parallel RG 220/V coaxial double braid cables. The center conductors of RG 220/V has a solid copper wire of 0.66 cm diameter. The cross section is 0.343 cm^2. The double braid of RG 220/V consists of 864 strands of 0.025 cm^2 diameter copper wire with a total area of 0.438 cm^{2}s.

The required cable run between the ignitron switch region and the MBA TF coil distribution feed through the building wall was estimated to be 64 feet. This results in a cable resistance of 0.55 mΩ. The normal temperature rise would be 0.6^0 C and 2.1^0 C for the inner conductor and braid respectively. For a bank load fault resulting in a 34 percent reversal, the braid temperature rise would be 80^0 C PVC jacket softening temperature.

The peak magnetic pressure within the coaxial cable for a normal pulse would be 0.3 psi, which is trivial. The peak magnetic pressure for a bank fault would be 0.5 psi, which is still inconsequential considering the pressure limit of 780 psi based on a yield strength of 20,000 psi for copper wire.

A cable matching network is provided at the MBA end of the cables. This matching network also serves as the interface connection between the 32 capacitor bank/load feed cables and the four special, large-diameter cable distribution feeds to the TF coils.

The cable matching network consists of an RC filter where R and C are selected to be 1 ohm and $2\,\mu F$ respectively. This results in an RC time constant eight times that of the anticipated ignitron switching risetime. The inductance of the matching network is made much less than $2\,\mu H$ to ensure the L/R risetime is substantially less than the anticipated $2\,\mu sec$ ignitron switching time.

3.3.4.5 Resistors

In the conceptual design, the resistance in series with each capacitor (Rs) and in series with each module of twelve capacitors (Rm) was $57\,m\Omega$ and $24\,m\Omega$ respectively. Optimization of the individual protection resistors allowed the maximum action that the fuses must withstand (as a result of a module short) to be lowered while maintaining the overall series bank resistance. This optimization process included consideration of the current flowing in the resistors in series with each capacitor and the resultant magnetic forces. Typically, the higher resistances are obtained by the use of

152

smaller x-section resistive ribbons. These smaller x-section ribbons are more fragile, and less able to withstand the magnetic forces, tending to axially compress and radially expand the spirally wound ribbon(s). The desire to use compact commercially available resistors for Rs, together with the objective of limiting capacitor voltage reversals under the various fault modes to less than 40 percent led to a choice of Rs = 60 mΩ , and Rm = 18 m Ω. This choice enables the use of two parallel 120 m Ω Ohmite resistors for Rs, and a length of stainless steel tubing for Rm.

Figure 3.3.43 shows fault currents resulting from the failure of one capacitor. For a maximum fuse let-through action of 1.38 x 10^6 amp.^{2} sec, a nominal charge voltage of 9.33 kV and a 1 m Ω effective resistance for the capacitor short, 1.38 kJ additional energy will be deposited in the failed capacitor before the fuse opens at approximately 125 μsec. Thus, each of the two parallel resistors forming Rs must pass a peak current of 61 kA for tens of μsec, or somewhat less, if the capacitor short is lower resistance. The component parameters used in performing these computations were:

Individual capacitance	= 396 μF
Capacitor inductance	= 45 μH
Capacitor resistance	= 26 mΩ
Fuse inductance	= 0.5 μH
Fuse resistance	= 6.4 mΩ
Rs inductance	= 0.98 μH
Rs resistance	= 60 m Ω
Module bus inductance	= 0.67 μH
Module bus resistance	= 0.2 m Ω
Rm inductance	= 1.0 μH
Rm resistance	= 18 m Ω
Bank bus inductance	= 0.63 μH
Bank bus resistance	= 0.08 m Ω

Computations were also performed (using the circuit shown in Figure 3.3.44) to determine the optimum ratio of resistance of the module and lateral

153

$I_{pk} = 122$ kA

Failed Capacitor
Current

Remaining Module
Current

Remaining Bank
Current

1380 kJ
1 mΩ
(119 volts)

690 joules
0.5 mΩ
(60 volts)

kA

usec
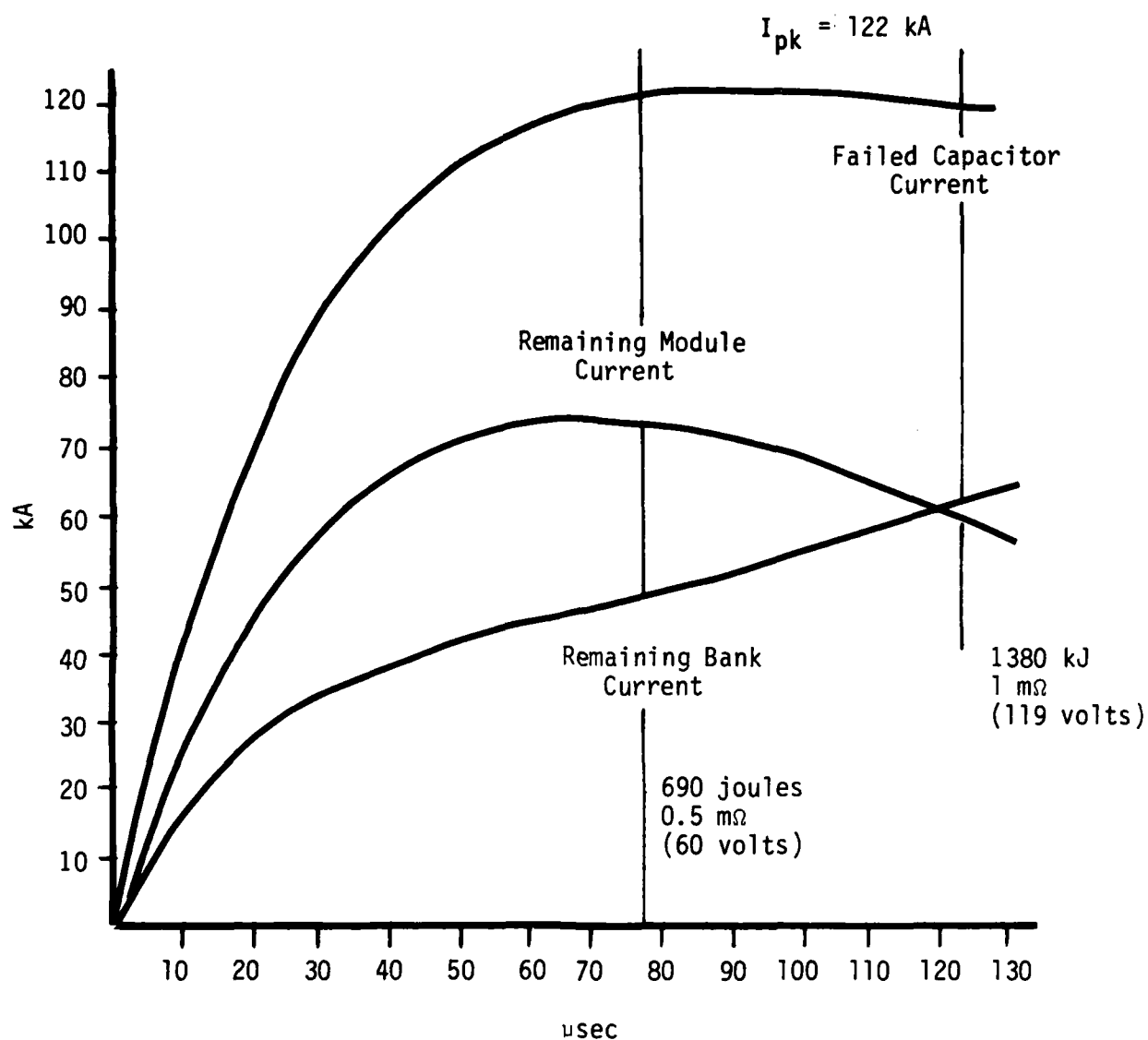
Figure 3.3.43   Currents resulting from a capacitor failure.
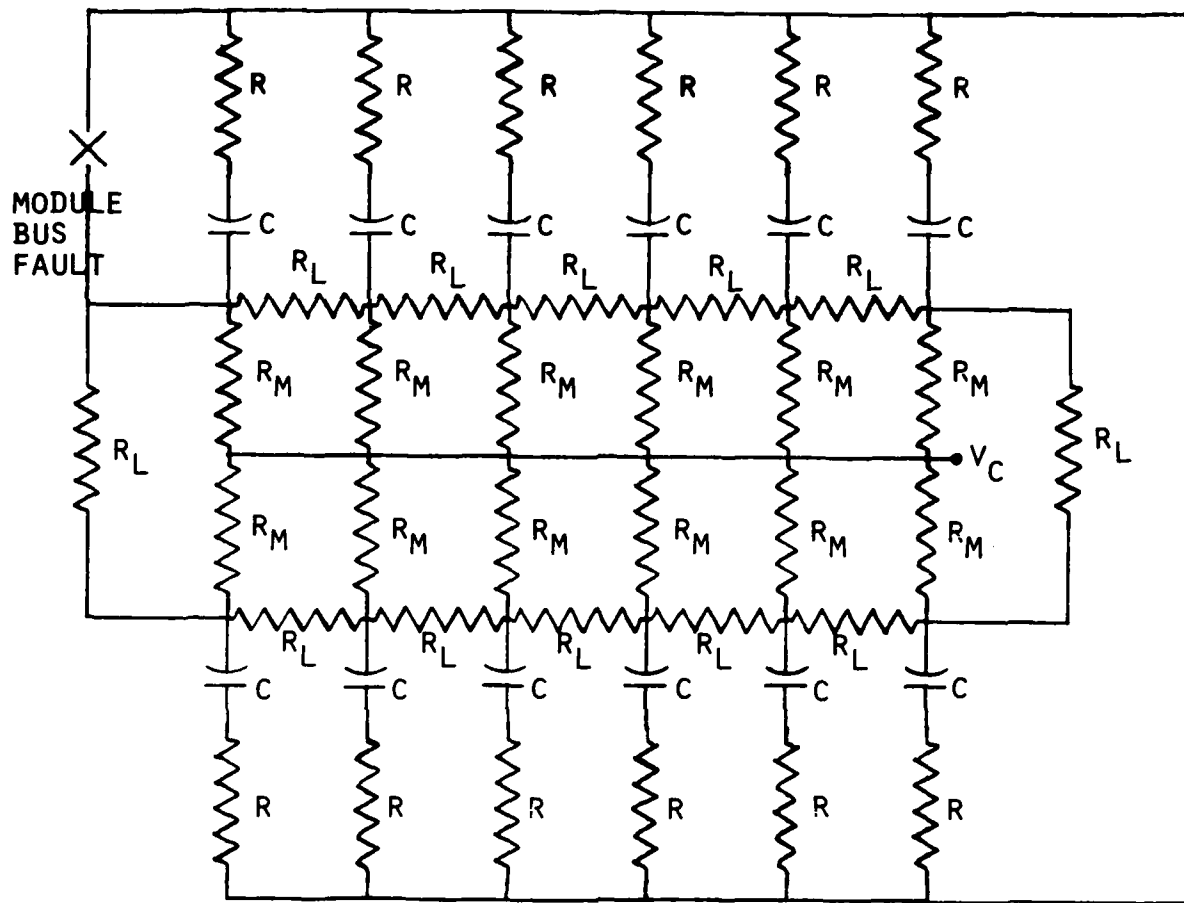
C = MODULE CAPACITANCE
R = MODULE INHERENT RESISTANCE
R_M = ADDITIONAL MODULE SERIES RESISTOR
R_L = INTERMODULE LATERAL RESISTORS

Figure 3.3.44   Analysis circuit for module bus fault

resistors to result in approximately equal energies being deposited in these resistors in the event of a module bus fault. Under normal operating conditions no current is passed by the intermodule lateral resistors, either during capacitor bank charge, discharge, or energy dump. However, in the event of a module bus fault, current flows from the remaining modules into the fault through the various paths offered by the combinations of module and lateral resistors.

For a module capacitance of 4.75 mF, an inherent module resistance of 7.67 mΩ, a module resistance (Rm) of 18 mΩ, a lateral resistance (Rl) of 8.9 mΩ results in approximately equal energies being deposited in each of the two lateral resistors and one module resistor connected to the failed module. Figure 3.3.45 shows the energies deposited in each resistor (in kJ) for a nominal charge voltage of 9.33 kV.

Figure 3.4.46 shows a plan view of a portion of the capacitor bank. The required resistances of 18 mΩ and 8.9 mΩ for the module and lateral resistors, and the capability of absorbing non-destructively, fault mode energies approaching 1/2 MJ are obtained through the use of stainless steel tubing and rod respectively. Fault mode temperature rises are held to 560° C for Rm and 350° C for Rl, and the requisite resistances obtained by using 10 feet of 0.625 inch O.D., 0.385 inch I.D. stainlesss steel tubing for Rm, and 8.2 feet of 0.625 inch O.D. stainless steel rod for Rl. The stainless steel is bent in a zig-zag manner to minimize inductance and conserve space. The assemblies are wrapped with fiber-glass in discrete sections to restrain motion due to magnetic forces.

156
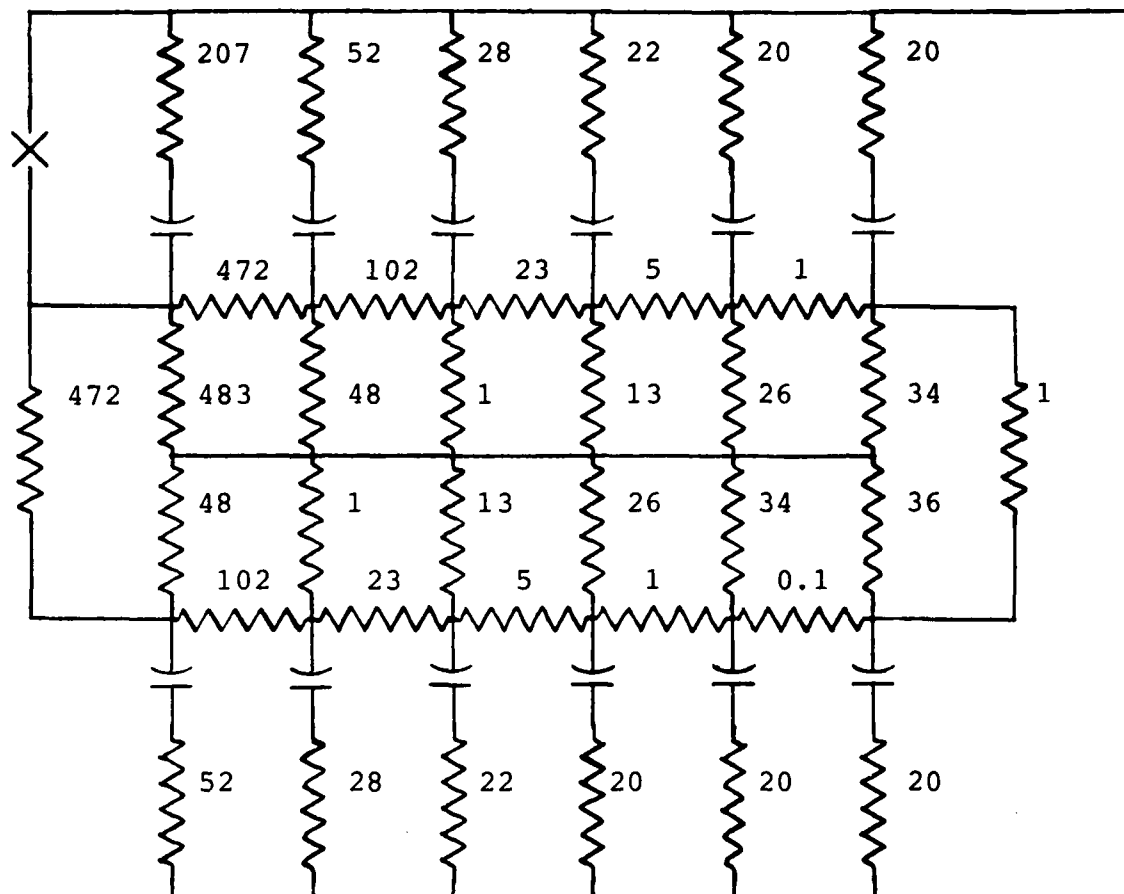
Figure 3.3.45 Fault energies deposited in module and lateral resistors
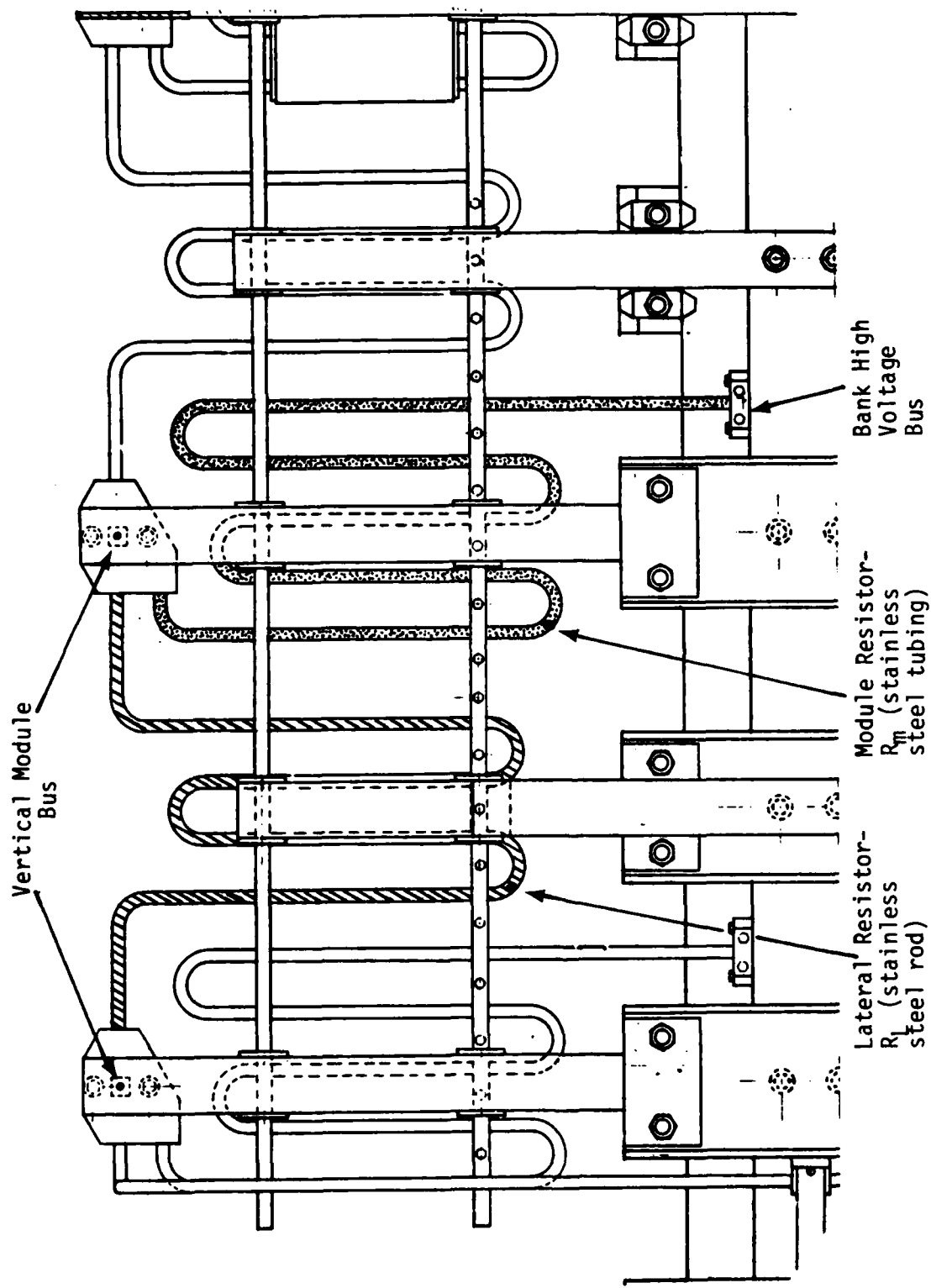
Figure 3.3.46 Plan view of a portion of TF capacitor bank showing R_m and R_L resistors

Vertical Module Bus

Module Resistor-R_m (stainless steel tubing)

Lateral Resistor-R_L (stainless steel rod)

Bank High Voltage Bus

158

The crowbar resistor value is optimized by consideration of the late time energy storage capacitor voltage reversal and the total charge passed by the crowbar switch circuit. Figure 3.3.47 shows how the total charge passed by the crowbar circuit can be diminished at the expense of voltage reversal on the energy storage capacitors. A crowbar resistor value of 9 m was chosen giving a crowbar circuit decay constant of 7.7 ms, and resulting in a normal capacitor reversal of 17%, and a total charge of 1560 Cb being passed by the two parallel crowbar ignitrons.

Through the use of 200 mΩ Ohmite resistors (4 in series, 44 in parallel, arranged in two layers as shown in Figure 3.3.42), a resistance of 18 mΩ is obtained. Two of these resistor assemblies are used in parallel, one connected in series with each crowbar ignitron. The two crowbar resistor assemblies a) ensure reliable auto-closure of both ignitrons, and b) result in a lower crowbar switch circuit inductance which aids in diminishing capacitor voltage reversal.

The total complement of 352 crowbar resistors (0.96 μH, 0.164 lb of metal per resistor) will rise in temperature under normal operating conditions of 9.33 kV capacitor charge voltage to 228° C. Under extremely unlikely fault mode conditions of only one crowbar ignitron firing, the temperature rise will be 456° C (or 590° C for 10.6 kV charge the maximum capacitor voltage rating). The manufacturer's maximum allowable temperature is 600° C.
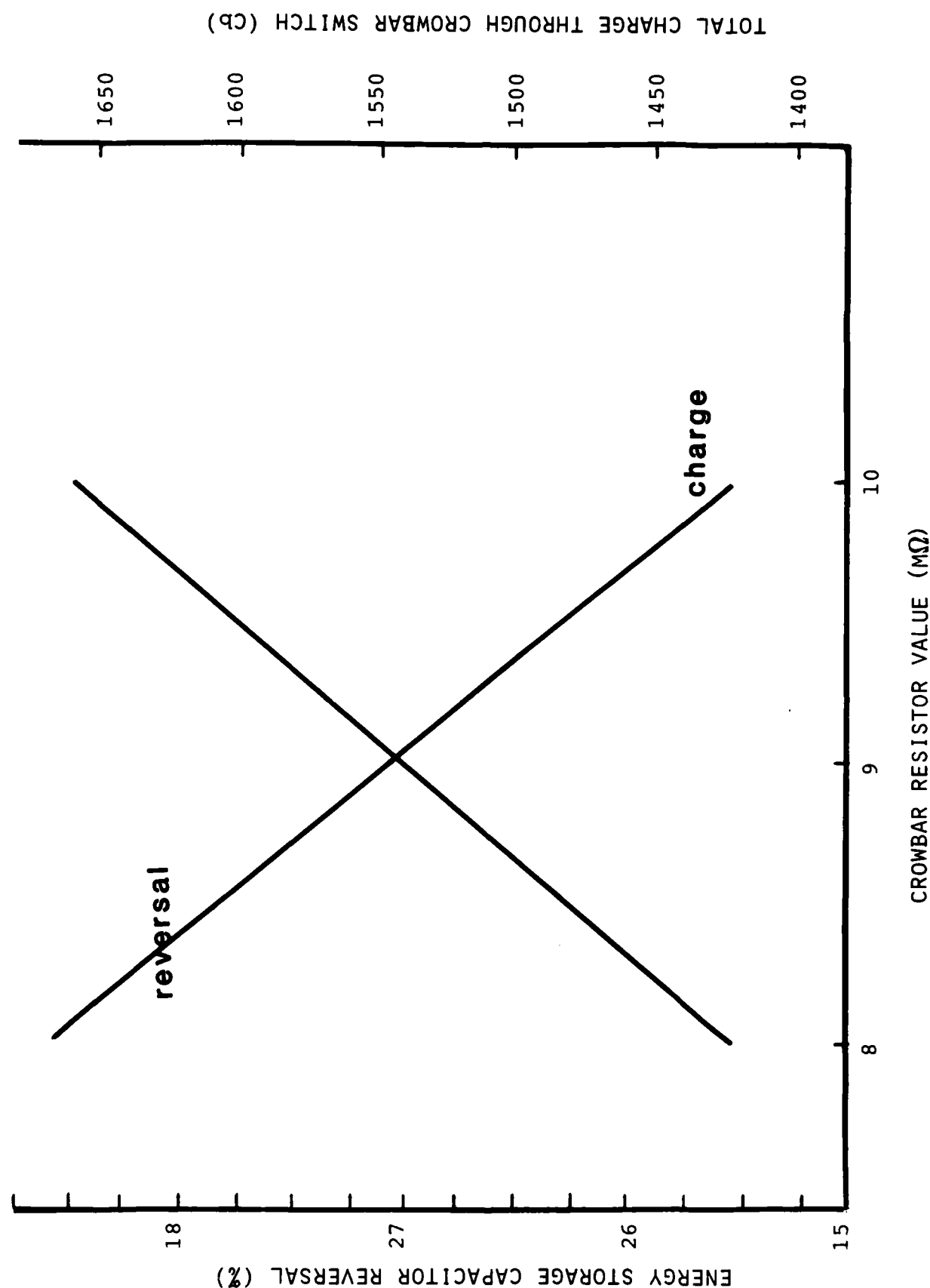
Figure 3.3.47 Capacitor reversal and crowbar coulombs versus crowbar resistance

3.3.4.6   Fuses

McGraw Edison C-rated NX 15.5 kV, 80 A fuses were selected for use on the TF capacitor bank. Two parallel fuses are used in series with each capacitor and capacitor resistor assembly (Rs). The parallel combination of two 80 A fuses limits the maximum let-through action to 1.38×10^6 amp^2 x sec. Thus, all fuses will survive a load fault, a bank bus fault, and a module bus fault. However, in the event of a capacitor fault, the fuse pair in series with the failed capacitor will blow, and clear (taking the capacitor out of the circuit) before a significant (< 2 kJ) amount of additional energy is deposited into the failed capacitor.

Figures 3.3.48 and 3.3.49 show front and side views respectively of the fuse pairs in series with each energy storage capacitor. The fuses are easily inserted and removed through the use of commercial clips. A clearly visible red button protruding from the top of the fuse indicates a blown fuse and a failed capacitor.

3.3.4.7 Energy Discharge, Dump, and Shorting Resistors/Switches

An energy dump cabinet is located at the end of the capacitor bank remote from the output/crowbar ignitron assembly. The protection switch cabinet electrical schematic and protection switch pneumatic schematic are shown in Appendix 3M. Two redundant energy dump systems are incorporated in this cabinet. Each energy dump system comprises a remotely activated switch and series resistor assembly. Each series resistor assembly is sized capable of absorbing the full capacitor bank energy. Charging of the capacitor bank is

161
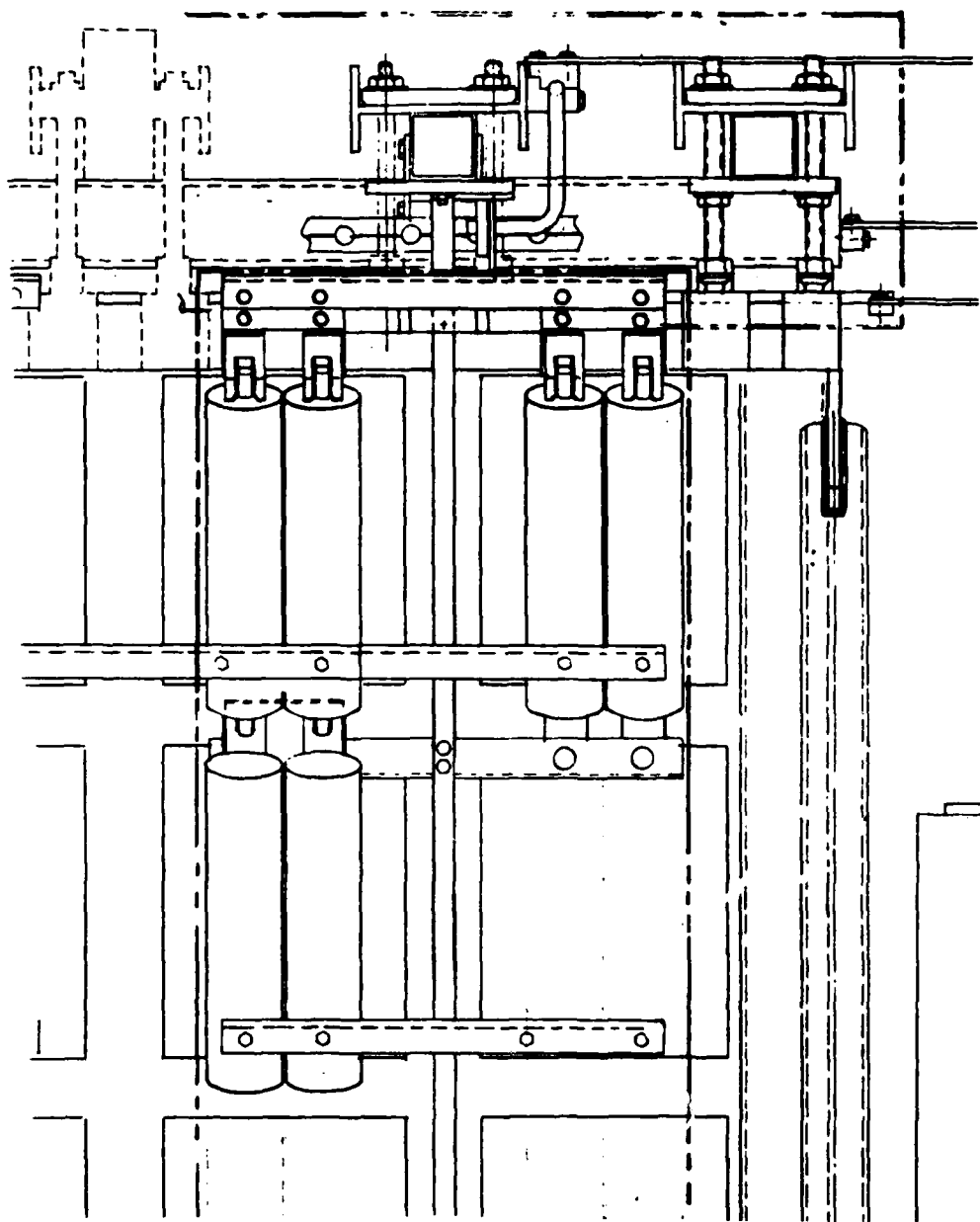
Figure 3.3.48 Front view of fuse pairs in series with each energy storage capacitor
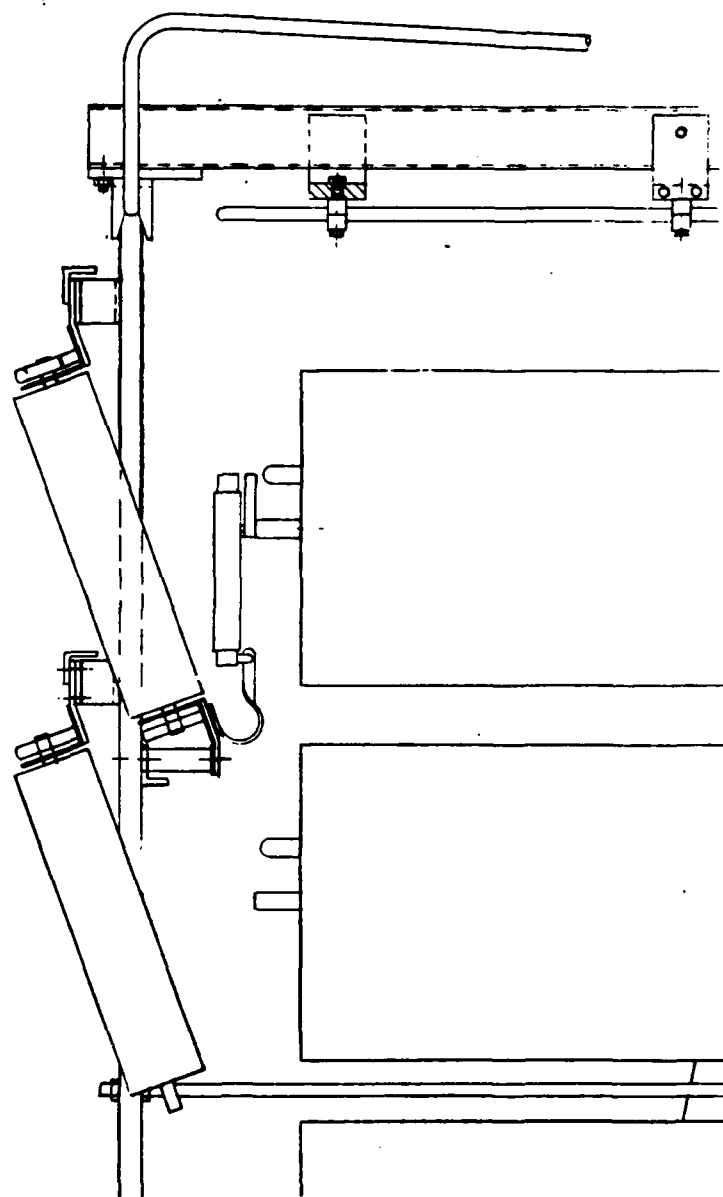
Figure 3.3.49 Side view of individually fused energy storage capacitors

accomplished through one of the series resistor assemblies. This provides a safety continuity check each time the capacitor bank is charged.

Each energy dump resistor assembly consists of ten series 0.25 ohm Ohmite power rib 8-segment resistors. Each resistor contains 3.84 pounds of metal, enabling the 3.23 MJ (10.6 kV maximum charge voltage) to be dissipated with a resistor maximum temperature rise of 370° F. The resistors are rated at 375° F continuous operation.

The 2.5 ohm resistance of the energy dump resistor assembly gives a 0.14 sec time constant. Thus, the capacitor bank voltage decays to less than 50 volts from a maximum charge voltage of 10.6 kV in 0.75 seconds. Recommendations from Ross Engineering required keeping the TF capacitor bank (10.6 kV maximum voltage) peak dump switch current to no more than 5-6 KA, and keeping the VF capacitor bank (17 kV maximum voltage) peak dump switch current to not more than 3-4 kA.

For a nominal charge TF bank voltage of 9.33 kV, the peak dump current is 3.73 kA. Closing the energy dump switch under current requires a high pressure pneumatic assist to minimize electrode wear. Thus, wear is minimized by reducing the peak current.

3.3.4.8 High Voltage Power Supply

The capacitor bank control schematic, panel layout, and controls operation information are provided in Appendix 3H.

As most of the power supply requirements were common to both the TF and VF capacitor banks, a specification was developed combining the two supplies with a few technical performance requirements listed under separate headings. The preliminary specifications for both the TF and VF power supplies are presented in Appendix 3J.

3.3.4.9 Mechanical Design of the TF Capacitor Bank

The preliminary design of the toroidal field capacitor bank concluded with the preliminary design review held at PSI in May 1983. Drawings and a preliminary materials list were reviewed during the design review are included in Appendix 3H.

The TF capacitor bank design consists of capacitor assemblies, module bus assemblies, H.V. output and crowbar switching assembly mounted on a welded steel frame assembly. A charging and energy dump cabinet is mounted on the floor at one end of the frame assembly.

The structural frame is a welded assembly of square structural steel tubing and channels. The square tubing forms a rectangular perimeter oriented vertically with cross beams on each end braced by struts to stabilize the entire assembly. Steel channels are welded between the top and bottom rails of the perimeter frame for cantilever mounting of the capacitor assemblies. The entire TF bank assembly with the exception of the charging and energy dump cabinet is mounted on ceramic insulators which are positioned under the lower rail of the rectangular frame and under the cross pieces at each end the frame.

165

Additional square structural tubes are mounted crossways below the bottom rail of the frame to support the module bus and resistor assemblies. Other brackets are welded to the top of the frame assembly for attachment of the H.V. (high voltage) bus and resistor assemblies.

The capacitors are supplied with three brackets welded to the capacitor case on the end opposite the output bushing. The capacitors are cantilevered mounted on both sides of the brackets to the channel by studs installed in the channel. With capacitors cantilever mounted on both sides of the structure, the torque produced by capacitors on one side of the frame balances the torque produced by capacitors mounted on the opposite side. The three point attachment of the capacitors serves the additional purpose of diagonally bracing the frame against forces in the lateral direction.

The capacitors are mounted 6 high, in modules of 12 capacitors each, 6 modules on each side of the frame for a total of 144 capacitors.

The resistors and fuses for each capacitor are electrically connected to the module bus assembly which also supports the fuses. The module bus is supported on an insulator attached to a crossbeam which is welded to the lower frame rail. The other end of the bus is connected to the high voltage bus and resistor assembly at the top of the structural assembly.

The module and lateral resistor assemblies are fastened to a beam system which holds the resistors in place and also resist severe impact loads in the event of a fault mode during the bank operation. The resistors themselves are

166

wrapped with fibreglass insulation, then overwrapped with fibreglass reinforced epoxy to restrain the resistor in the event of a fault mode.

Fault mode forces from module and lateral resistors in addition to the effective repulsive pressure between bus bars dictated the welded and bolted structural configuration at the top of the frame assembly. The structure is designed to withstand a module bus fault, consequently the forces and torques applied to the structure are not balanced by similar forces on the opposite side of the frame.

The output and crowbar switching assembly are hung from the cantilevered end of the bus bar assembly on the end of the frame opposite the charging and energy dump cabinet. The assembly consists of 3 ignitrons and 352 resistors mounted and supported by a system of parallel plates stiffened with extren beams. The assembly is designed to withstand repulsive forces between the plates of the assembly as indicated in the criteria of section 500 in Appendix 3M.

The charging and energy dump cabinet is located at the opposite end of the bank assembly and contains circuitry required for energy dump and charging. The electrical components in the cabinet are connected to the main bus on the top of the structure by small busses which pass through the top of the cabinet.

A mechanical analysis for the TF bank was performed and is included in Appendix 3M. The analysis report is a collection of design criteria, design notes and stress calculations for the bank design. The report is arranged in

eight sections as listed in the table of contents. Some of the sections have a separate table of contents to make it easier to find worksheets for a specific part of the assembly. Section numbers are shown on the worksheets in the upper right hand corner of the page along with the page numbers for sheets within a specific section.

Section 100 includes a brief written summary and a tabular calculation summary for calculations performed. The written summary was kept as brief as possible and is meant to complement the tabular summary. In some parts of the written summary no comment was made, implying that stress and deflections were within acceptable levels and needed no further discussion. Where comments are made, the design may have been more involved or results may be interpreted as being marginal. In these cases the additional comments were included to express our feelings about the practicality and acceptability of the design.

The tabular calculation summary includes the item description, material used, the allowable and actual stress, and calculated factor of safety. Also included are the sections and page numbers on which backup calculations can be found.

Appendix 3K is a list of material required for fabrication of the complete toroidal field capacitor bank. Included in the list is a small forklift for handling capacitors during initial bank assembly and for removal and replacement during maintenance when required. The forklift will travel in front of the capacitors on either side of the capacitor bank with the forklift center axis and forks oriented parallel to the face of the capacitors. A lifting fixture which incorporates a table that moves at right angles to the

forks of the forklift will have to be designed and fabricated. The table will have to fit between the capacitor being lifted and the one just below it.

During capacitor removal, the capacitor would be lifted once the nuts securing it to the structural framing were loosened and the capacitor withdrawn until it is positioned over the forks. A counterweight will be required on the forklift to counterbalance the overturning moment created by the capacitor when it is extended to the maximum sideways position from the centerline of the forklift.

Final specifications for the forklift and a conceptual design for the lifting fixture, included in Appendix 3L, were sent to NRL in October 1983.

3.4 Electron Beam Injection Into The MBA

3.4.1 General

This subsection describes issues and work performed by PSI relating to a) the interface between the injector accelerator under construction and the MBA, and b) a conceptual design of a possible multi-pulse 5 MV injector accelerator.

3.4.2 Injector-Accelerator/Modified-Betatron Interface

This task developed a conceptual design of the power flow system that is to transport the 3 MV, 50 kA, few 10's nsec, injector-accelerator output pulse to the cathode of the injector located inside the modified betatron.

169

Conceptual design issues and constraints included the following:

1. Pulsed magnetic field "transparancy" of all interface hardware to a distance of 1 m from the minor axis of the modified betatron. Timescale of applied fields (1/4 period) is $\geq$ 3 msec.

2. Low outgas rate of materials exposed to the modified betatron vacuum volume, particularly those forward of the injector-accelerator vacuum pumping port. The vacuum requirement is 1-2 X 10^{-8} torr.

3. Minimization of current losses along the length of the conducting connections between the injector-accelerator output electrode and the cathode tip.

4. A preliminary analysis of cathode-anode geometries near the modified betatron wall, including estimates of electrode plasma formation and impedance collapse.

5. Methods for remote adjustment of the cathode-anode gap spacing, including vertical position adjustment.

6. Diagnostic concepts and monitor locations for monitoring the injected beam voltage and current time histories.

7. Space constraints near the modified betatron, principally
   a) a ~ 10 cm (vertical) X ~ 40 cm (horizontal) rectangular port on the modified betatron torus, b) a ~ 50 cm gap (vertical) between the outer most VF coils, and c) a ~ 80 cm gap (horizontal) between the outermost portion of the TF coils.

Figures 3.4.1, 3.4.2, and 3.4.3 give a schematic representation of the design concept. The central design philosophy is to configure the vacuum transmission line which connects the pulser to the injector diode as a) non-emitting for as long a distance as allowed by the space constraints and 2) self-magnetically insulated in regions where space constraints result in negative electrode fields higher than the electron emission threshold (250 - 300 kV/cm for metal electrodes at a few 10's of nsec pulse durations). The approach allows for a) impedance-matched (60 Ω) operation of the non-emitting vacuum transmission line such that it adds no lumped inductance

170

Figure 3.4.1 Beam injector-side view

Figure 3.4.2 Beam injector—top view
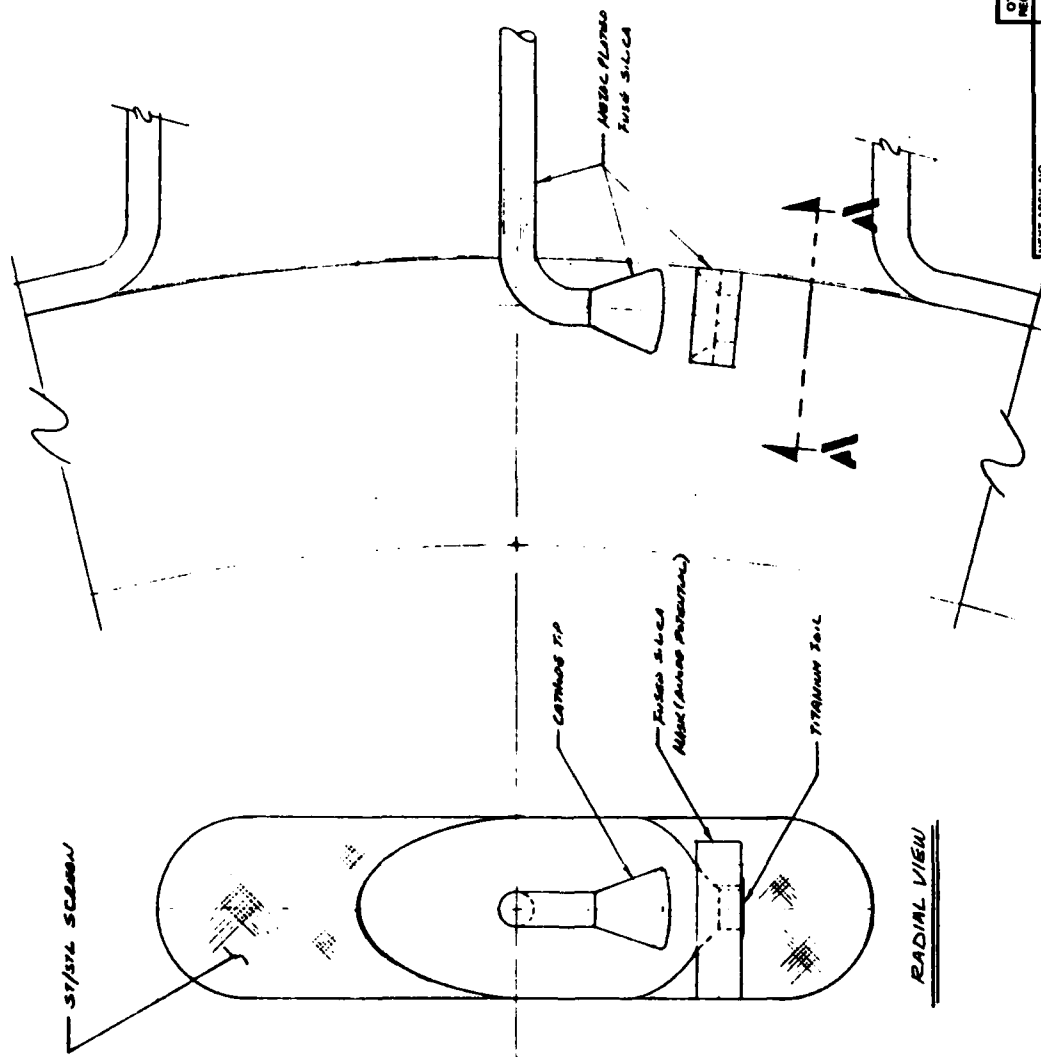
Figure 3.4.3 Beam injector-diode area

to the electrical circuit and b) "conventional" voltage and current diagnostics at≤ 1 meter from the anode-cathode (A-K) gap to monitor the injected pulse.

An additional conceptual design element (Figure 3.4.4) is a cantilevered cathode stalk assembly which is mounted to an adjustable plate located on the high voltage tube endplate. The plate position is remotely adjusted with hydraulic cylinders to allow vertical, horizontal (A-K dimension) and longitudinal adjustments to the cathode tip position. The fluid-filled hydraulic lines can be routed radially across the liquid-dielectric gap in the output line of the pulser or, alternatively, through a transit-time isolator pipe. The latter choice allows for diagnostic cable access to the cathode stalk which could be useful in measuring cathode currents very near the A-K gap.

The injector pulser output vacuum line is chosen to be a stainless steel coax with 70 cm outer and 25 cm inner diameters ending at ~1.1 meters from the torus. Stainless steel was picked for its good vacuum qualities. The diameters give an electric field of 233 kV/cm on the inner conductor, well below the electron emission threshold. A ~10 cm long stainless steel bellows section in the outer is included to allow for minor misalignments between the injector pulser and injector port centerlines. The remaining coaxial vacuum line extending to the A-K gap is designed to be transparent to the few-μsec pulsed magnetic fields. Fused silica with metal plating on the vacuum-side surfaces is chosen for these electrodes under the same rationale as of the torus sections (see following subsection 3.4.3).

174

FLUID-FILLED HYDRAULIC SYSTEM
HOSES OR METAL PIPE CONFIGURED
AS A TRANSIT-TIME ISOLATOR.
(THE LATTER WOULD ALLOW
ROUTING OF CATHODE-POTENTIAL
DIAGNOSTICS)

HYDRAULIC CYLINDER, 3 OR 4 PLCS

LIQUID DIELECTRIC
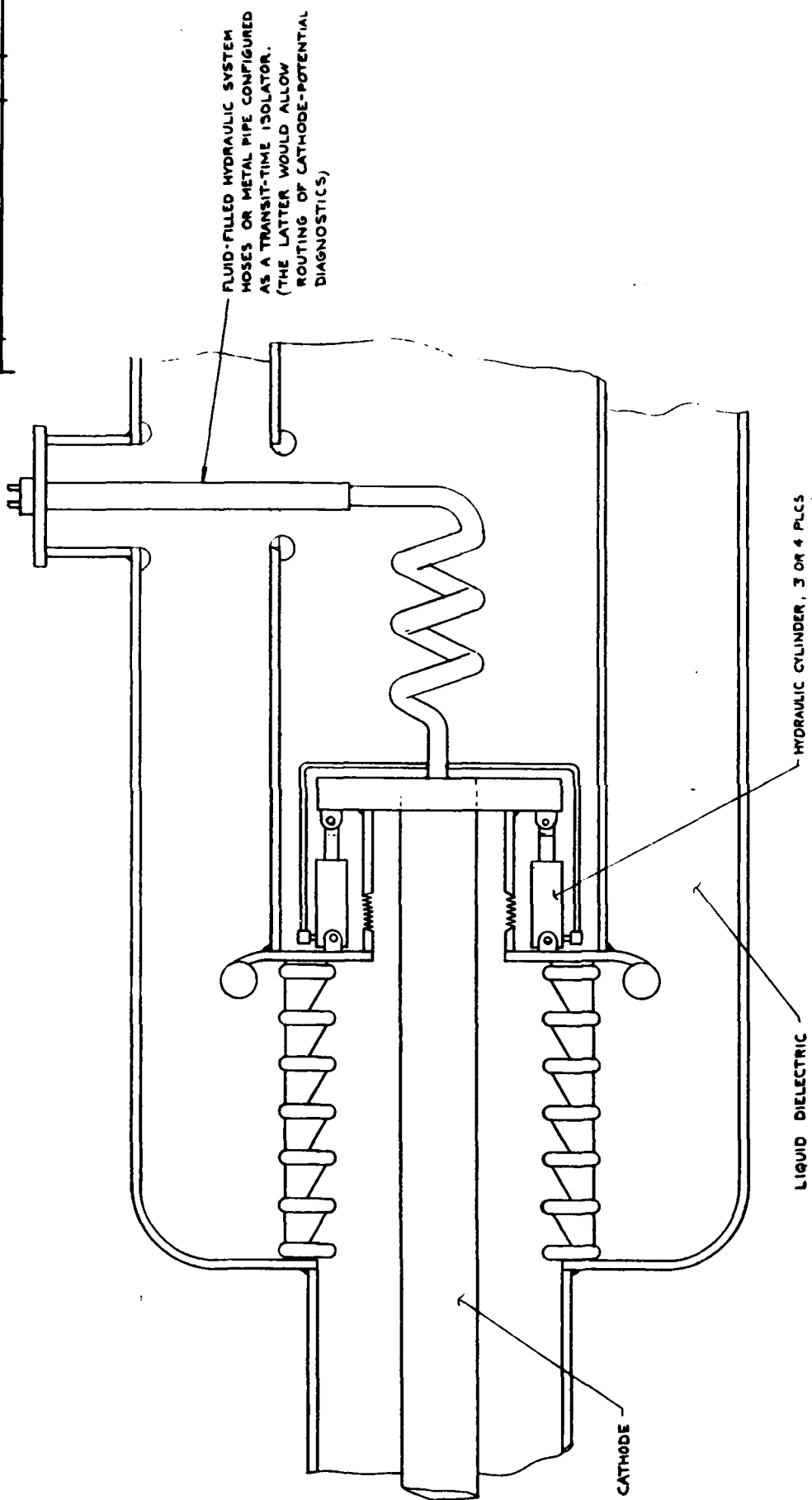
CATHODE

Figure 3.4.4 Beam injector-anode/
cathode adjustment concept

175

The first magnetically transparent coaxial line portion extends at the 60 ohm output line impedance (at 70 cm outer diameter) into the gap between the horizontal field coils until it must taper to clear the vertical field (VF) coils, a distance of roughly ½-meter. Although the inner electrode must start to taper well before the VF coil, the electric fields can likely be kept below 300 kV/cm for all of this first taper section.

The second coaxial line portion with approximately 40 cm and 15 cm inner (dotted line in Figures 3.4.1 and 3.4.2) and outer diameters extends to the entrance of the rectangular port on the side of the torus. Electric fields are roughly 410 kV/cm and it is assumed that this portion of the inner electrode is plated with aluminum which is then hard-anodized to minimize electron emission. Should the hard-anodized surface emit it will be necessary to reduce the inner electrode diameter to roughly 9 cm (solid lines in Figures 3.4.1 and 3.4.2) to achieve self-magnetic insulation in this portion of the transmission line.

The effectiveness of self-magnetic insulation in the presence of VF$\sim$ 0.15 KG and TF$\sim$ 1 KG is not clear. The above design yields $B_{self} \sim$2.2 KG, which should dominate, however a larger impedance mismatch (smaller diameter inner electrode) may be necessary to increase the ratio of B_{self} to the TF & VF fields.

The final portion of the vacuum transmission line (Figure 3.4.3) is a 2 cm diameter rod which slips into the tapered end of the 15 cm (or 9 cm) diameter stalk. Both the rod and the final portion of the taper will emit electrons independent of the coating material. B_{self} will be$\sim$ 10 kG providing

electron losses have so far been minimal. Loss of half the current at this point (25 kA) will still give ~5 kG self-field which should be adequate to provide insulation. Again, use of a $\lesssim 2$ m diameter stalk would give a higher self magnetic field at the expense of added diode inductance. The final portion of the stalk has a 90° bend and ends at the cathode tip which opposes a shaped annular anode block. Termination of the vacuum line by such a diode located on only one "side" of the axis will produce return current asymmetries and tend to lower B_{self} on the other side of the 2 cm cathode stalk. Electron losses to the 10 X 40 cm port walls may result, in addition to the injector of a beam in the opposite direction from the injector diode. J X VF will cause the latter electrons to drift into the torus wall.

An upper limit to the electron losses across the TF can be estimated under the assumption that B_{self} is non-insulating but restricts electrons to make vertical excursions no greater than $r_L = \gamma m V / e \, B_{self}$ (~1 to 2 cm). Under these assumptions electron emission at ~30 A/cm^2 could occur over 3 to 4 cm X 20 cm ≈ 60 to 80 cm^2 per "side" for a loss current of 3.5 to 5 kA, if only the 2 cm shank is emitting. Losses could approach 20 kA if the 9 cm diameter portion of the shank is included. The losses should be considerably lower however since B_{self} appears to be strong enough to provide some measure of insulation.

Under these arguments at least 30 kA will be available to the A-K gap which is required to generate a ~3 cm^2 5-20 kA low emittance beam for internal injector into the modified betatron. Due to the strong self-magnetic fields in the A-K gap, the anode and cathode shapes must be shaped to increase the local electric field, to partially counteract the self-pinching forces.

177

Detailed design of electrode shapes is not considered here. Injection current densities over the ~π cm^2 beam cross-sectional area are 1.6 to 6.4 kA/cm^2.

At 3 MV, the Child-Langmuir current density (relativistic, unipolar flow) is about 8.6 kA/d^2, where d is the anode-cathode gap. The dose/fluence coupling coefficient is~ 1.0 at 3 MV; the 1.6 to 6.4 kA/cm^2 current densities translate to ~100 to ~400 J/g dose levels in the anode foil (if one is used) and surrounding densities (above 200-300 J/g doses) anode plasma will likely form and result in ion currents drawn from the anode and mask back to the cathode tip. At low current densities (2 kA/cm^2), Child-Langmuir unipolar flow will exist and A-K spacings of roughly 2 cm are implied. At current densities above 4-5 kA/cm^2, anode plasma will form at some time into the pulse, resulting in a shift to bi-polar flow and a ~ doubling of the current. This will produce a very non-linear impedance-time history. An option may be to pre-form an anode plasma to avoid any mid-pulse transitions from uni-polar to bi-polar flow. For bi-polar flow, A-K spacings of~ 2 cm will give 4 kA/cm^2 electron current densities.

Impedance collapse (motion of electrode plasmas across the A-K gap) will introduce another non-linearity in the impedance-time history. With the potential for plasma on both electrode, collapse velocities up to 10 cm/μsec can be expected. Thus, the 2 cm A-K gaps could "close" by up to 2 to 3 mm in the 20-30 μsec pulse duration, giving a 20 to 30% diode impedance change during the pulse "flat top". The combination of plasma closure and ion effects may make it difficult to maintain $\leq$ 2% voltage variation during the full 20 ns flat top of the pulse.

Diagnostics include a) a vacuum line voltage monitor (VVM), either capacitive or resistive, located in the final stainless steel section of the injector pulser output line, and b) a dB/dt probe near the the VVM to facilitate accurate inductive voltage corrections, and c) current monitors (self-integrated Rogowski strips or stainless foil current shunts) located at various points along the outer vacuum line electrode. If a transit time isolator is added for cathode stalk adjustment access (Figure 3.4.4), diagnostic cable access to the cathode stalk will also allow placement of current monitors along the stalk.

In summary, the 3 MV injector accelerator/modified betatron interface design is compatible with the space constraints, magnetic transparancy and low outgas rate requirements, and allows for external adjustment of the A-K gap. Loss current reduction techniques consisting of use of non-emitting electrodes, where possible, and self-magnetic insulation in regions of high field appear to limit the loss current to less than 20 kA under the worst case approximations. Questions of time-varying diode impedance behavior and A-K electrode shaping to produce an adequately low emittance and constant voltage beam are not completely resolved. It is strongly recommended that separate diode experiments and diode code calculations be undertaken to answer these questions. It may be found necessary, for example, to increase the toroidal field above the present 1 kG design value in order to increase the level of electron trajectory control in the A-K gap.
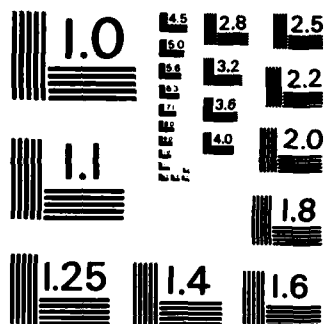
MICROCOPY RESOLUTION TEST CHART

NATIONAL BUREAU OF STANDARDS-1963-A

3.4.3 Injector Conceptual Design

The specifications for the injector are taken to be 5 MV, 30 kA, 50 ns pulse with ± 2% flatness, with a burst of four pulses in about 1 second. The two candidate approaches that can be identified from existing or projected technology are (1) a single full-voltage oil Blumlein with a gas spark gap switch; and (2) a number of lower voltage water lines connected in series with inductive isolation to ground. The second approach is chosen because of its smaller size, better repetitive potential, ease in pulse shaping, and more flexible beam generating capability.

The addition of the voltages from the water Blumleins is shown in Figure 3.4.5. The configuration resembles that of an injector for a linear induction accelerator, with ten 500 kV induction cavities in series driving a central cathode conductor. The latter terminates in a 5 MV diode at or near one end of the vacuum vessel. The ten induction cavities each have a multistage vacuum interface, outside which is an oil filled region that contains the Metglas induction or isolation cores. The whole is enclosed by a cylindrical steel tank about 7 1/2 feet in diameter and 13 feet long.

The over-all layout is shown in Figure 3.4.6. The ten water dielectric Blumleins are about 15 in. in diameter and 4 feet long. They are placed five on each side of the cylindrical tank, and each is connected to two adjacent induction cavities. The Blumleins have output impedances of about 9 ohms and are charged to 400 kV by a five stage Marx generator, shown under the vacuum tank and between the Blumleins. (The charging power supply is not shown.)
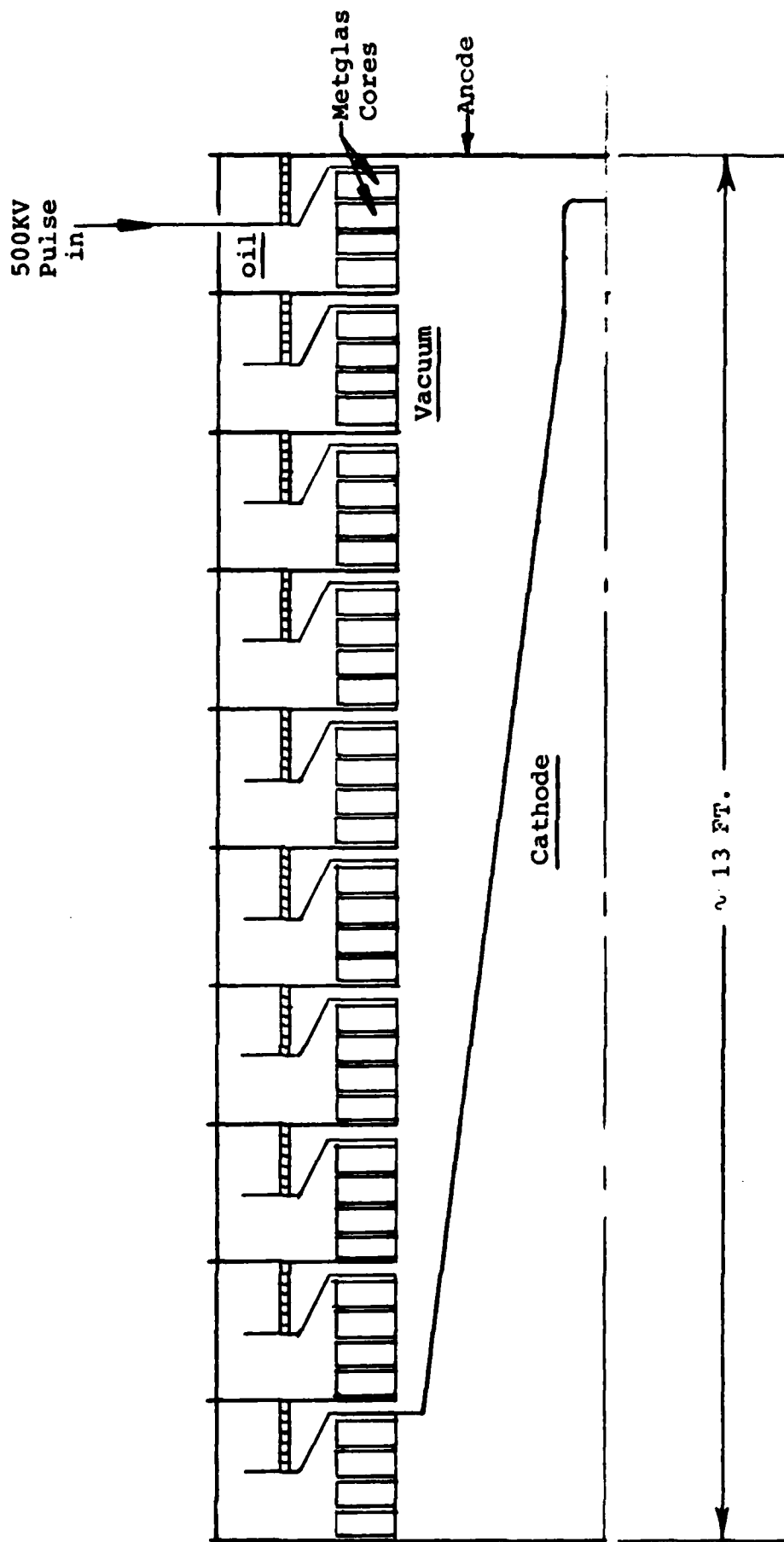
Figure 3.4.5 Internal injection layout
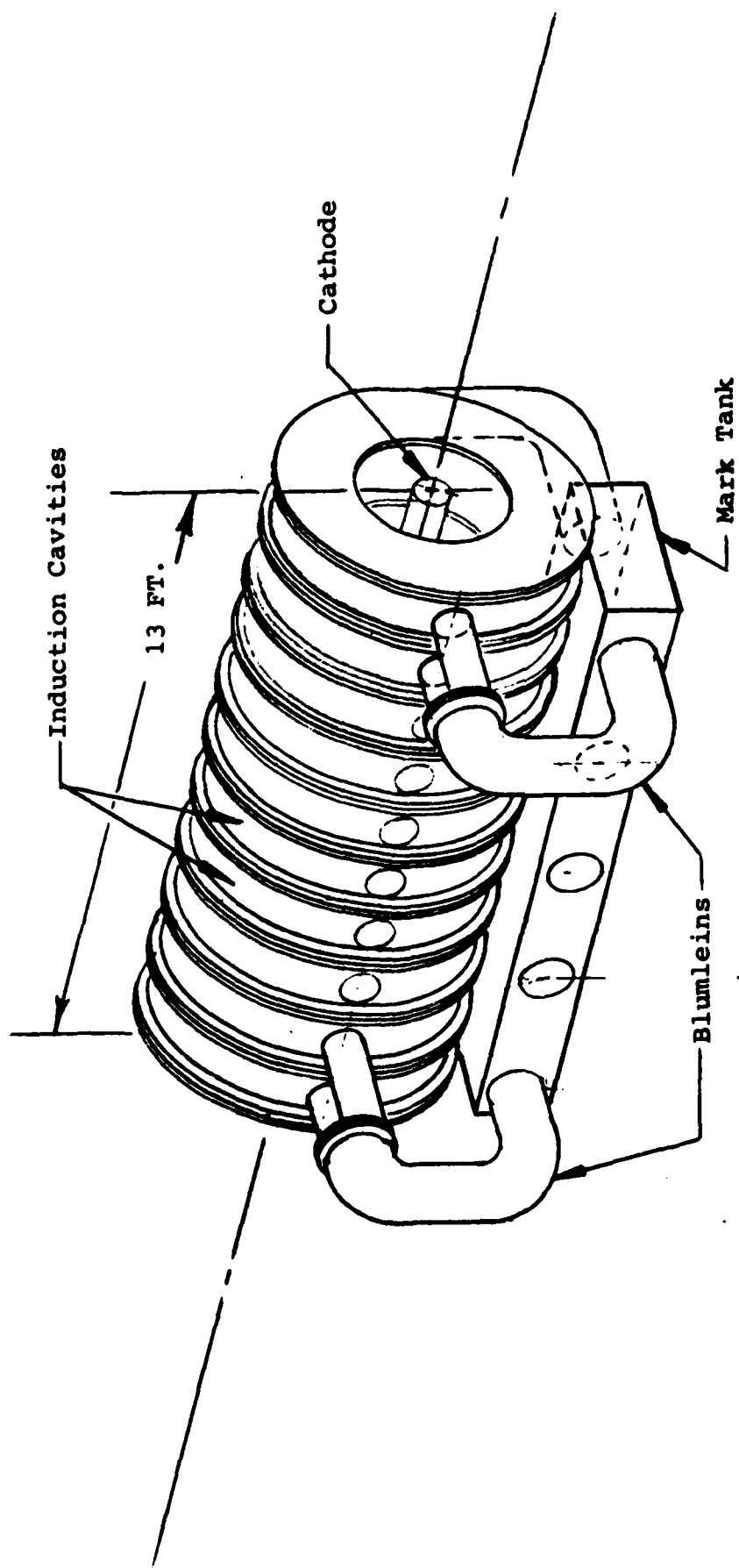
Figure 3.4.6 Injector schematic

Each Blumlein is switched by an SF_6 gas spark gap placed at its lower end. A modest flow of gas through the switch takes place during the pulse burst.

The Blumleins, which are effectively in series, make up a 90 ohm, 4 MV driving circuit for the diode. The vacuum region around the central cathode conductor is designed to keep the pulses impedance-matched until they reach the 167 ohm diode, where the mismatch increases the voltage to 5 MV.

Flexibility in generating the beam and in controlling the diode current is offered by the possibility that fewer than ten of the induction cavities could be connected to the diode, lowering the diode voltage, and the beam post-accelerated to full energy.

The system weighs approximately 80,000 lb. The dimensions of the vacuum region (1.1-1.2 m diameter bore) have been chosen to keep the electric fields on the cathode below emission levels (200-250 kV/cm), since the diode impedance is too high to effect magnetic insulation. A reduction in the size and cost of the vacuum region and consequently the surrounding induction cores would be obtained if emission levels could be raised by treating the cathode surface, or if the central conductor were made positive and the beam extracted by drifting it through this conductor.

The design is somewhat dependent on the diode impedance time-history. A lower impedance could be accommodated without major design changes but with more emphasis on switch development. A time-varying diode impedance, in conjunction with the voltage flatness requirement, could require a

series-switched pulseline (instead of a Blumlein) with a carefully tailored impedance profile, adding to the design and fabrication costs.

The design technology is capable of continuous repetitive operation, though for this it would be desirable to consider magnetic switches rather than gas switches.

In addition to the diode, which is not well defined, areas where development is needed are: in the design are the suppression of electron emission on the central conductor in vacuum (especially for multiple pulse operation), high stress Metglas core insulation, and in the SF_6 spark gap switches, which it is desirable to cause to close with several channels. None of these presents a major problem, and some assistance in the development of cores and switches may be expected from other programs before the injector is finally designed.

We envision a conceptual design phase and a development phase dealing with these technology areas and questions such as load characteristics and type of switch and pulseline, and including some testing. These phases would last a total of 1-1/2 years and are estimated to cost $0.7 M.

Final design, fabrication, assembly and testing are estimated to require about 1-3/4 years and preliminary estimates give a cost of $2 M. This is obviously dependent on load characteristics, and should in any case be considered as a rough budgetary estimate.

184

END

FILMED

10-84

DTIC